Sources de micro-ondes basées sur des résonateurs optiques de haute qualité; Modélisation, optimisation et métrologie

Zeina Abdallah

Université Fédérale
Toulouse Midi-Pyrénées

THÈSE

En vue de l'obtention du

DOCTORAT DE L'UNIVERSITÉ DE TOULOUSE

Délivré par :

Université Toulouse 3 Paul Sabatier (UT3 Paul Sabatier)

Présentée et soutenue par :
Zeina ABDALLAH
le 15 December 2016

Titre :

Microwave sources based on high quality factor resonators; Modeling, Optimization and Metrology

---

École doctorale et discipline ou spécialité :
ED GEET : Photonique et Systèmes Optoélectroniques

Unité de recherche :
LAAS-CNRS

Directeur/trice(s) de Thèse :

M. Olivier LLOPIS
M. Arnaud FERNANDEZ

Jury :

M. Vincent GIORDANO (Président)
M. Marc VALLET (Rapporteur)
Mme. Anne-Laure BILLABERT (Rapporteur)
M. Gilles CIBIEL
M. Benoît BENAZET (Invité)

"It always seems impossible until it's done!"

N. Mandela

Acknowledgements

My three years journey as a Ph.D. candidate has come to an end. There are countless number of people who believed in me and helped me reach this far. Through this humble acknowledgment, I would like to convey my gratitude to specific individuals that made this leg of the journey possible.

These studies were funded by the French national space center (CNES) and the regional council of Midi-Pyrénées, so I would like to take this opportunity to acknowledge them for providing financial assistance.

I would like to thank the committee members, *Prof. Marc VALLET* and *Mcf. Anne-Laure BILLABERT* for their deep review despite the short time provided to them, as well as their insightful comments and questions. My sincere acknowledgments go to *Prof. Vincent GIORDANO*, head of my thesis committee and to *Dr. Gilles CIBIEL*, my technical CNES supervisor, for their helpful comments. I would also thank *M. Benoît BENAZET* for being part of the committee.

And here comes the special acknowledgements…

For all these accomplishments, I am extremely indebted to my supervisor and my advisor *Prof. Olivier LLOPIS*. You encouraged me a lot through these years to overcome many difficulties and you taught me to grow as a self-instructor and as an independent thinker through your guidance, support and encouragement.

I would like to thank also *Mcf. Arnaud FERNANDEZ*, for being helpful and for the deep discussions. In addition, I will never forget the delicious chinese green tea! Thank you again!

I thank all the members of MOST team and of the laboratory LAAS-CNRS in general: *Audrey, Amar, Olga, Oana, Alexandre, Alessandro, David, Napoléon, Adem, Boris, Vincent* and the list goes on and on... Thank you so much for being a great colleagues and a special friends.

I am grateful to all the staff and services at LAAS-CNRS. Many thanks to *Marie ESTRUGA, Marie-Laure PIERUCCI, Ascension DE SOUSA, Marie-Agnès BELLIERES*, and *Virginie HUGUENOT* for their administrative support and for being helpful every time with a sweet smile.

It is extremely hard to convey my deep sense of gratitude to my friends in words: *Serge* (my lovely evil Wati!), *Amani* (Dinner? ice-cream? probably both!), *Florence* (my cutest hostess), *Tarek* (some aricheh?), *Ayad* (no weight gainer!!). Simply, you are part of my family. Thank you for your support and help during the difficult moments.

It is my fortune to gratefully acknowledge the support of my family members. *Mum, Dad,* having you in my life is an honor, I know that you gave up things for me to be here today. *Mariam*, my crazy sister and best friend, thank you for your unlimited support and for always listening to me, mainly thank you for our little Aabous *Lulu*. *Hiba*, thank you for the positive vibes. *Najah*, my sweetest sister-in-law, thank you for always listening to me and never leaving my side when I need. *Alaa, Walid*, my brothers, my backbones! To you all, I am eternally grateful and thankful.

To you all, my precious people, I dedicate this work…

Zeina ABDALLAH

Toulouse, France

December 2016

Table of Contents

Glossary

ADS	Advanced Design System
AM	Amplitude modulation
BAW	Bulk acoustic wave
BGS	Brillouin gain spectrum
COEO	Coupled optoelectronic oscillator
DL OEO	Delay line based optoelectronic oscillator
DR	Dielectric resonator
DRO	Dielectric resonator based oscillator
EDFA	Erbium-doped fiber amplifier
EOM	Electro-optic modulator
F	Finesse
FM	Frequency modulation
FOSO	Fiber-optic stabilized electronic oscillator
FP	Fabry-Perot
FRR	Fiber ring resonator
FSR	Free spectral range
$FWHM$, $\Delta f_{1/2}$	Full-width at half-maximum
FWM	Four-wave mixing
HNLF	Highly nonlinear fiber
IFRR	Immunized fiber ring resonator
$IPEF$	Intra-cavity power enhancement factor
$L(f_m)$	Signal sideband phase noise
LF	Low frequency
LM	Linear modulation
LO	Local oscillator
MZM	Mach-Zehnder modulator
NCR	Noise-to-carrier ratio
OEO	Optoelectronic oscillator
PD	Photodiode
PDH	Pound-Drever-Hall
PI	Proportional-integral
PID	Proportional-integral-derivative
PLL	Phase locked loop

P-M	Polarization-maintaining
PZT	Piezoelectric actuator
Q_0	Intrinsic optical quality factor
Q_e	External optical quality factor
RAM	Residual amplitude modulation
RIN	Relative intensity noise
$S_\emptyset(f_m)$	Spectral density of the phase fluctuations
$S_f(f_m)$	Spectral density of the frequency fluctuations
SAW	Surface acoustic wave
SBS	Stimulated Brillouin scattering
SBST	Stimulated Brillouin scattering threshold
Si BJT	Silicon bipolar-junction transistor
SiGe HBT	Silicon-germanium hetero-junction bipolar transistor
SLC	Sapphire-loaded cavity
SLCO	Sapphire-loaded cavity oscillator
SMF	Signal mode fiber
SNR	Signal-to-noise ratio
SOA	Semiconductor optical amplifier
SRS	Stimulated Raman scattering
SSB	Single sideband
STRS	Stimulated Rayleigh scattering
TE	Transverse electric
TEC	Temperature controller
TM	Transverse magnetic
ULE	Ultra-low-expansion
VCO	Voltage controlled oscillator
VNA	Vector network analyzer
WGM	Whispering gallery mode
WGMR	Whispering gallery mode resonator
YIG	Yttrium iron garnet
α	Intra-cavity losses (or gain)
ρ	Coupler direct transmission coefficient
τ_g	Group delay time

General Introduction

High precision and ultra-stable frequency sources have and undergone tremendous advances from several decades until now, as they are a crucial requirement for many applications. Thanks to the rigorous investigations, oscillators have shown impressive progress and can be used directly if only short-term frequency stability is needed, or coupled to a frequency standard if long-term stability together with short-term frequency stability are both required.

Various type of oscillators have been developed, ranging from simple electronic oscillators to more sophisticated ones, like the microwave oscillator based on sapphire whispering gallery mode dielectric resonator. These oscillators are able to generate low phase noise frequency sources near few gigahertz. However, when higher frequencies are required, their phase noise increases due to the degradation of the resonator quality factor Q.

While trying to circumvent the shortcomings of this type of oscillators, some scientists saw in the photonic devices a strong potential to improve the performance of microwave oscillators thanks to the high Q factors that can be obtained in optical resonators. Besides, optical links are today involved in many applications where they replace advantageously the coaxial cables thanks to their low losses, low size, high bandwidth and their immunity to electrical interference. The development of new optically based microwave sources is thus in good agreement with the development of optics in embedded systems, and particularly in space systems. In 1991, researchers from the NASA's jet propulsion laboratory (JPL) have developed the first fiber-optic stabilized electronic oscillator[1]. It was not until 1994 that the now well-known optoelectronic oscillator[2] has been presented, also by researchers from JPL.

The optoelectronic oscillator can masterly generate highly spectrally pure RF frequencies with excellent short-term stability, while its performance level improves when the frequency of the desire application increases. For that reason, it is used on a large scale for many demanding applications, such as telecommunications systems, space missions, radars, metrology, signal-to-digital converters and so on. Many of these applications have a commonly critical demand, which is very precise timing. For example, to minimize the uncertainty during the tracking process, a Doppler radar necessitates a very low phase noise frequency source[3].

In such an applications, the demand for a low size, low consumption, low cost, higher bandwidth and frequencies and higher performance, especially in terms of phase noise, is worldwide continuously growing. As a result, the pressure is increasing on the RF industries

[1] Logan, R. T., Maleki, L. & Shadaram, M. Stabilization of oscillator phase using a fiber-optic delay-line. *Proc. 45th Annu. Symp. Frequency Contr*., 508-512 (1991).
[2] Yao, X. S. & Maleki, L. High frequency optical subcarrier generator. *Electron. Lett.* **30**, 1525-1526 (1994).
[3] Vig, J. R. Military applications of high accuracy frequency standards and clocks. *IEEE Trans. Ultrason., Ferroelect., Freq., Control* **40**, 522-527 (1993).

and research laboratories to meet these requirements. The optoelectronic oscillator is one of the possible solutions to these problems. However, it has still to be optimized in terms of size, long-term and short-term stability (phase noise). A solution to the problem of size is to replace the optical fiber spool used in conventional delay line optoelectronic oscillators by an optical resonator. However, this solution induces a higher level of system complexity, which must be managed carefully to maintain the performance.

The presented thesis is a continuation of several previous studies that have been made over the past years, and where elegant improvements and solutions have been demonstrated: on one hand, regarding the different coupling processes in high finesse resonators, along with the characterization techniques of these resonators and, on the other hand, regarding the possible solutions to eliminate the different nonlinear noises contributions that could be present in an optical resonator, which affect significantly the short-term stability of oscillator.

This work is part of a collaborative research project between the French National Space Center (CNES, Toulouse), Thales Research & Technology (Paris), and three of the CNRS laboratories: LAAS-CNRS (Toulouse), ENSSAT-FOTON (Lannion) and FEMTO-ST (Besançon). The targets of this research were to identify and overcome some limitations which are imposed by different factors in the optoelectronic oscillator system, such as locking the laser's frequency properly onto the cavity resonance and the noise conversion processes. These steps aim to finally optimize and improve the phase noise performance and the long-term stability of the overall system.

Taking into account the importance of the short-term stability, a clear definition of the phase noise and a presentation of the related measurement techniques are given in the first chapter of this manuscript, along with a review of the noise sources that may occur in an oscillator. In addition, this chapter provides an overview of the several oscillator topologies and types, starting from the microwave oscillators, and moving to the optoelectronic oscillators, while presenting and comparing their phase noise performance. A particular focus has been given to the optoelectronic oscillator based on optical resonator, since it is the one studied in this thesis.

At the heart of many commonly employed optoelectronic oscillator is the high quality factor optical resonator. As a result of many research and developments, the optical resonators can be found in different configurations, form and size. The first section of the second chapter is devoted to the discussion of the most well-known resonators designs: the Fabry-Perot, the whispering gallery mode and the fiber ring resonators. In the second section, a rigorous analytical model of the fiber ring resonator is presented, where it has been demonstrated that almost all the main properties and characteristics of the ring resonator can be computed from its intra-cavity losses and its coupling coefficient, such as the coupling regime, the loaded quality factor, the intra-cavity power enhancement factor and so on. The

third section deals with methods used to characterize an optical resonator, especially the RF spectrum approach, which features a very high precision in frequency, close to 1 Hz.

Contrary to the case of a microwave oscillator, the degradation of phase noise performance of an optoelectronic oscillator is not a specific marker of a particular noise source. In such a complex system, the noise of the various components in the loop, along with some noise conversion processes between them, contribute severely to the short-term stability. After an introduction outlining these noise sources and the conversion processes, an extensive investigation on the nonlinear behavior of the photodiode and its impact on the conversion process of the laser amplitude noise to microwave phase noise are presented in the third chapter. The breakthrough here is achieved with a new nonlinear equivalent circuit model, which is able to describe this specific conversion, and consequently a good computation and prediction of the phase noise performance of an optoelectronic oscillator can be obtained. All these investigations and studies are well described in this chapter.

The final chapter is dedicated to the frequency stabilization techniques that have, as main purpose, to continuously control the frequency difference between the laser and the optical resonator. These techniques are mandatory in the optoelectronic system. However, they could limit its RF phase noise performance. Specific attention has been given to the electronic feedback locking technique, known as Pound-Drever-Hall. The difficulties and the shortcomings of this technique have been addressed deeply and new circuits and configurations have been designed in order to overcome some limitations, such as its bandwidth. Finally, promising results are shown, where a fiber laser and a semiconductor laser were successfully locked onto a very high-Q fiber ring resonator and where the new Pound-Drever-Hall configurations have demonstrated an outstanding stability and performance regarding the locking process.

Chapter I: Optoelectronic Oscillator

I.1 Introduction

Oscillators are considered virtually as a heartbeat supplier for all RF and microwave systems regardless of their applications, such as communications, navigations or test and measurement systems. For example, they allow frequency conversion (up and down) as a local oscillator, generate the carrier in radar systems, and are used as a reference source for system synchronization.

Since 19th century, several types of oscillators have been developed, starting with simple electronic oscillators, and then, around 1920, the microwave oscillator based on a vacuum tube feedback became the basis of radio transmission. Reflex klystrons were a common way to produce power in the X or Ku range right into the 1970s. Then, semiconductor devices oscillators have become very popular, thanks to their low size, low cost and low power consumption. They were amplified by travelling wave amplifiers (TWT) when high power was required, but in many applications their output power were sufficient. It is not until early 1990s that some scientists tend to focus on generating pure microwave signals using microwave-photonic technology, known now as optoelectronic oscillators. The main goal was to take advantages of each technology to deliver higher performance, higher functionality, smaller size and lower cost.

This chapter reviews the different state of the art of the microwave oscillators and the microwave-photonic oscillators. Discussions about their technologies, together with their potentials, limitations and especially their noise performance, are included.

I.2 Microwave oscillators

Basically, all oscillators consist of a passive frequency-determining resonant element along with a feedback active gain element, creating a loop oscillator to generate an oscillating signal. A phase control element is used between the active and passive devices to satisfy a proper phase condition (one of the oscillation conditions). An active device with sufficient gain is used to compensate the feedback loop losses and deliver the signal to the load.

As a response to the growing demand for microwave components with higher performance, lower cost and smaller size, microwave oscillators are classified into many different groups based on frequency bandwidth, type of resonant or active devices used. The resonant element mainly affects the cost, frequency tuning range, stability, sensitivity and noise performance of the oscillator, and is used to designate different types of oscillators. The noise power is inversely proportional to the quality factor (Q) of this element, making the use of high Q resonator the most effective way to achieve a low noise oscillator.

Microwave oscillator are characterized as tunable and/or fixed frequency. Tunable oscillators are essential part of electronic systems, as they are used in phase locked loops (PLL) to synthesize frequency stable signals. These synthesized signals are found in electronic counter measures (ECM), electric support measures (ESM), swept sources for testing and in synthesized sources for communication systems. They are characterized by their tuning bandwidth and linearity, settling time and post tuning drift. Varactor-tuned sources are the most common [1], as this technology can be used with any resonant device. In case of low Q integrated oscillator, wide frequency bandwidths can be obtained with varactors. In some cases, tunable resonators replace the fixed frequency resonator, such as yttrium iron garnet (YIG) spheres [2] which are magnetically tunable.

On the other hand, fixed frequency oscillators offer higher frequency stability and lower phase noise spectral density. They are used as part of frequency converters in telecommunications systems, as the main frequency delivery system in radars or as the high frequency head of precision clocks. The key element of the fixed frequency oscillator is the high quality factor (Q) passive resonant element, such as micro-strip based resonators, piezoelectric surface acoustic wave (SAW) or bulk acoustic wave (BAW) resonators, dielectric resonators (DR), ceramic coaxial resonators, metallic cavity resonators or sapphire-loaded cavity resonators (SLC). Each has its unique features and limitations. Below are some examples of such oscillators with their performances.

Dielectric resonators [3] have made a great strides in microwave oscillator devices due to their compactness, excellent temperature stability and high Q factor which lead to a low phase noise oscillator. The practical frequency range for these resonators lies between 2 and 40 GHz, while the Q factor degrades linearly with increasing frequency [3,4]. A low phase noise performance of -135 dBc/Hz at 10 kHz has been reported at 10 GHz using dielectric ceramic based resonator [5,6]. Another type of low phase noise dielectric resonator oscillator

is the sapphire-loaded cavity resonator oscillator (SLCO). Featuring the lowest dielectric losses, sapphire crystal is used to build a microwave resonator in whispering gallery mode configuration. Excellent phase noise performance of -160 dBc/Hz at 10 kHz offset at 10 GHz has been reported [5].

Bulk acoustic wave resonator oscillators (BAWO) provide an excellent performance in terms of power consumption, long term frequency stability and a low close-to-the-carrier phase noise. The practical frequency range for these resonators is typically between 500 MHz to 5 GHz. One of the best BAW oscillator at 100 MHz has shown a phase noise level of -160 dBc/Hz at 10 kHz. This oscillator has been used to generate a 1 GHz signal through direct frequency multiplication [7].

Typically, wideband tunable oscillators exhibit more noise than fixed frequency oscillators. Hence, when low noise is required, a fixed frequency oscillator can be combined with frequency mixers to build a low noise wideband frequency source.

Figure I-1 presents these different resonators with their loaded quality factors' values and the oscillators in which they are used, along with their phase noise performance.

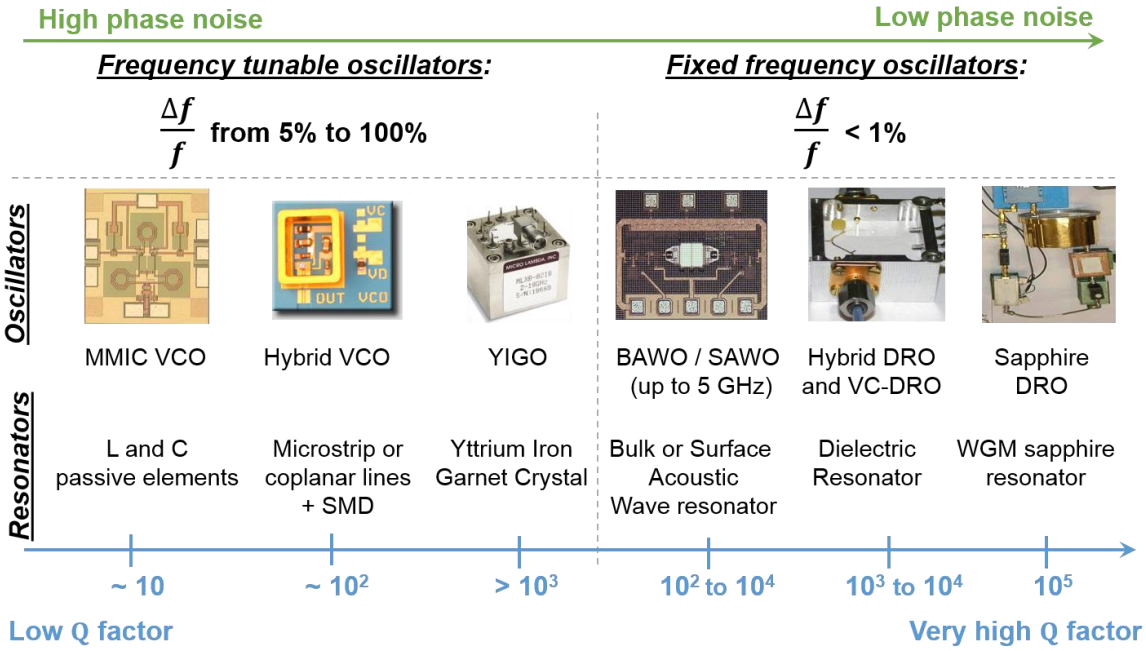

Figure I-1 Microwave oscillators with their respective resonators. MMIC: monolithic microwave integrated circuit; VCO: voltage controlled oscillator; SMD: surface mounted device; WGM: whispering gallery mode.

I.2.a Noise in microwave oscillators

Generally, oscillators are characterized and differentiated by their quality factor, frequency stability and/or their noise. The output of an ideal oscillator would be a pure sinusoidal signal represented in the frequency domain as a single-frequency (f_0) vertical line.

However, the generated signal is not that perfect, since the oscillator includes noise instabilities that cause the output frequency to deviate from its ideal position, producing a band of unwanted frequencies near the carrier.

These noise instabilities (amplitude, frequency and phase), occurring inside the oscillator loop, are directly linked to the noise generated by the active and the frequency-determining elements. In Figure I-2 (a), amplitude instability refers to amplitude fluctuations on a period of time leading to drift in the power output of the system, frequency instability results from fluctuations in the period of oscillation and the phase instability refers to the fluctuations in the zero crossing position.

Every RF and microwave oscillator exhibits frequency instability. This stability can be broken down into two components: long-term and short-term stability [8-10]. Long-term frequency stability is caused by aging processes in the oscillator elements and materials used in the elements or temperature variations, and is usually referred to as a drift. Short-term stability, usually known as phase noise or spectral purity, is related to random and/or periodic frequency fluctuation around the nominal frequency.

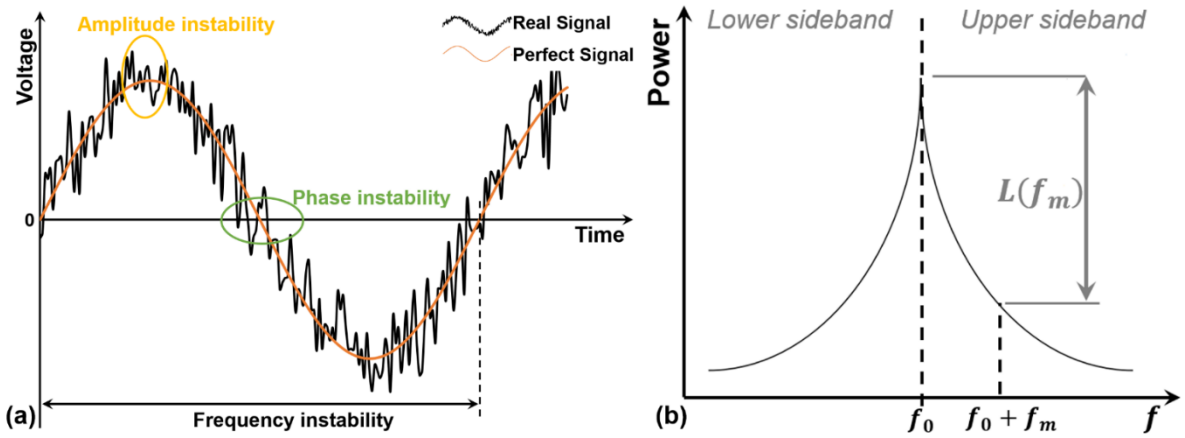

Figure I-2 (a) Generated sinusoidal signal of an oscillators (b) Power spectrum of a real signal generated by an oscillator, Single sideband density relates either to lower or upper sideband.

In the design of oscillators, it is important to take into account the sources mechanisms that degrade the oscillator's frequency stability. To account for the noise components that occur on the top of the sine-wave signal of the oscillator, the instantaneous output voltage of an oscillator can be expressed as:

$$v(t) = (V_0 + \Delta V_0(t))\sin(2\pi f_0 t + \Delta\phi(t)) \quad \text{(I.1)}$$

where V_0 and f_0 are the nominal peak amplitude and frequency respectively, and ΔV_0 and $\Delta\phi(t)$ are the deviation of amplitude from nominal and the deviation of phase from nominal respectively.

I.2.a.i Phase noise

The short-term instability or the phase noise components are the ones of interest in this thesis. There are two types of phase noise: deterministic frequency variations that are discrete spurious peaks appearing in the spectrum and can be related to power line frequencies, mechanical vibrations, acoustic sensitivity, etc. and the random fluctuations inside the oscillation loop caused by the thermal noise, shot noise and excess noise (such as flicker noise) of the resonator, of the amplifier and the other loop elements (as an example a varactor phase shifter). These mechanisms manifest over different offset frequency ranges.

The fundamental definition of phase noise is a power spectral density of phase fluctuations for a given offset frequency f_m from the carrier, described by:

$$S_\phi(f_m) = \frac{\Delta\phi^2(f_m)}{BW} \qquad \frac{rad^2}{Hz} \qquad \text{(I.2)}$$

where BW (Hz) is the measurement system bandwidth, $S_\phi(f_m)$ is double sideband (DSB) phase noise spectral density, which includes fluctuations from both upper and lower sidebands of the carrier.

Likewise, the single sideband (SSB) phase noise spectral density is also used to measure the phase noise (Figure I-2 (b)). It is the ratio of the power in one sideband due to phase modulation by noise (for 1 Hz bandwidth) to the total signal power (carrier plus sidebands) [10]:

$$L(f_m) = 10\log(S_\phi(f_m)) - 3dB \qquad \frac{dBc}{Hz} \qquad \text{(I.3)}$$

Since phase and frequency are directly linked (the angular frequency is the time derivation of the phase), the spectral densities of frequency $S_f(f_m)$ and phase $S_\phi(f_m)$ instabilities are also related:

$$S_f(f_m) = f_m^2 \; S_\phi(f_m) \qquad \frac{Hz^2}{Hz} \qquad \text{(I.4)}$$

However, $S_\phi(f_m)$ and $L(f_m)$ are commonly used to specify the short-term stability, since they can be measured with straightforward metrology setup.

In the past decades, studies have been carried out to model the noise behavior inside the oscillator in order to predict its phase noise [11-16].

A simple and well-known model has been proposed by D.B. Leeson [11] to describe the phase noise behavior in a linear feedback oscillator. It is based on linear time invariant oscillator properties, such as resonator quality factor, feedback gain and noise figure. Therefore, some corrections to the results are necessary to account for nonlinear effects which

must be present in the physical oscillator. Leeson has proposed that the phase noise fluctuations of the active device (amplifier) are converted into oscillator's frequency fluctuations through the oscillation loop. Under the assumption that the amplitude instabilities are insignificant, the spectral density of the oscillator's frequency fluctuations can be computed directly from the spectral density of the amplifier's phase fluctuations ($\overline{\Delta\phi^2}_{Amp}$ in rad²⁄Hz):

$$\overline{\Delta f^2} = \left(\frac{df}{d\phi}\right)^2 \overline{\Delta\phi^2}_{Amp} \qquad \frac{Hz^2}{Hz} \qquad \text{(I.5)}$$

where $^{df}/_{d\phi}$ stands for the stability coefficient that can be determined from the resonator loaded quality factor Q_{RF} and the oscillation frequency f_0. This relationship shows that a higher phase-to frequency slope ($^{d\phi}/_{df}$), or equivalently a higher Q_{RF}, ensure a more stable output frequency (f_0).

$$\frac{d\phi}{df} = \frac{2Q_{RF}}{f_0} \qquad \text{(I.6)}$$

Using equation (I.5) and (I.6), the oscillator's SSB phase noise can be expressed as follow:

$$L(f_m) = 10\log\left(\left(\frac{f_o}{2\sqrt{2}Q_{RF}f_m}\right)^2 + 1\right) + 10\log\left(\overline{\Delta\phi^2}_{Amp}\right) \qquad \frac{dBc}{Hz} \qquad \text{(I.7)}$$

The latter equation highlights the conversion of the amplifier flicker noise, with a -10 dB/dec slope, into oscillator phase noise with a -30 dB/dec slope.

In this formula, which was proposed as a model for short-term frequency fluctuations of an oscillator, it is considered that the resonant device is ideally stable in the short term and ascribe all the noise to the amplifier. The model included a simple expression for the amplifier noise, taking into account, on the one hand, its additive far-from-the-carrier white noise floor, which is originating from thermal noise and governed by the amplifier's noise figure, and on the other hand, its multiplicative close-to-the-carrier flicker noise. These two noise types are separated by a cutoff frequency $f_{c_{HF}}$. These assumptions are well explained in [17] and [18].

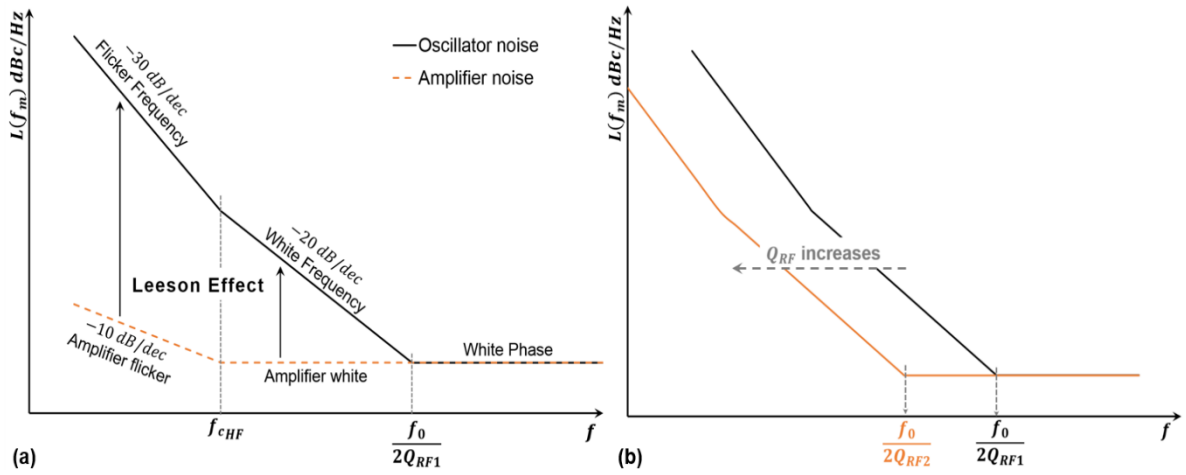

Figure I-3 (a) Typical SSB phase noise spectrum of an oscillator, based on Leeson's model. (b) The evolution of the oscillator close-to-the-carrier SSB phase noise as a function of the resonator's Q

Figure I-3 (a) shows the Leeson effect in a typical oscillator, in which the amplifier shows white and flicker phase noise. In fact, it points out that the flicker noise is mainly a conversion process noise and is related to the amplifier's low frequency noise and that the white phase noise originates either from a conversion process or from an additive noise process. The phase fluctuations are converted into frequency fluctuations inside the resonator's 3-dB bandwidth:

$$f_{3dB} = \frac{f_0}{2Q_{RF}} \tag{I.8}$$

Equation (I.8) highlight that the cutoff frequency of the loop f_{3dB} decreases with the increase of resonator's quality factor Q_{RF}, and therefore, the close-to-the-carrier phase noise will decrease as well (Figure I-3 (b)). On the other hand, the increase in the oscillation frequency f_0 will lead to a further increase in phase noise.

Up until now, the Leeson's noise model is a very used approach for the determination of the phase noise in feedback oscillators. Nevertheless, there are several limitations in this model and a direct application of the Leeson formula without care can lead to erroneous results. Some of these limitations are summarized as follows:

- It considers the resonant device ideally stable in the short term and ascribe all the noise to the amplifier.
- It does not give any approach to compute the amplifier phase noise (except far-from-the-carrier, the additive phase noise), particularly if it comes from a nonlinear conversion of baseband noise. It is thus impossible to optimize an oscillator phase noise using Leeson's approach alone.

- It is useful to predict the oscillator phase noise from the amplifier phase noise, if this noise can be measured independently. However, in the oscillator, the amplifier sees different RF loads during the test which may modify its phase noise contribution to the loop noise.

In our case, Leeson approach has been used to simulate the noise behavior of the optoelectronic oscillator, despite the complexity of the system, since the noise in these systems does not only originate only from the microwave amplifier but also from different other optical, microwave and low-frequency active and even passive devices used inside the oscillation loop, as it will be shown later. Also, in the description of the optoelectronic oscillator on Agilent Advanced Design System (ADS), it is possible to simulate the open loop system but not the closed-loop one (this will be detailed later). Leeson approach is thus a useful tool to "close the loop" and estimate the optoelectronic oscillator phase noise.

I.2.a.ii Phase noise measurements

Phase noise measurement techniques have evolved over time along with advances in analyzer technology. Three essential measurement methods, ranging in complexity, are spectrum analyzer measurements, passive techniques and active techniques [19].

- ***Spectrum analyzer measurements***

This direct method is the simplest way to measure the power spectral density of frequency sources in terms $L(f_m)$.

This apparent simplicity hides, however, some limitations, in particular the difficulty to measure the close-to-carrier phase noise of a free running oscillator because of the frequency drift during the measurement, and its low sensitivity far-from-the-carrier due to the poor signal-to-noise ratio. In addition, the noise sidebands or phase noise of the analyzer's local oscillator (LO), and the analyzer's noise floor impact the phase noise measurements results.

- ***The passive technique***

It is known as frequency discriminator method. This approach uses either a resonator or a delay line (electric or optic) to convert the frequency fluctuations into phase fluctuations. The phase fluctuations are then detected by a double balanced mixer and measured on a low frequency spectrum analyzer (generally, an FFT analyzer). The frequency discriminator including a delay line [20], which is wide band, is chosen for the flexibility in measuring a free-running oscillators, and particularly integrated VCOs which are difficult to lock on a classical phase noise measurement system.

Unfortunately, this method suffers from insufficient measurements sensitivity, especially close-to-the-carrier. Longer delay lines may improve sensitivity, but on the other hand, it may reduce the signal-to-noise ratio of the measurement setup and limit the maximum offset frequency. The insertion loss of the delay-line can also limit the practically achievable delay to some 100 ns at microwave frequencies, which is too short to characterize many oscillators. The measurement noise floor can be improved however by reducing the noise

contribution of the detection stage: the mixer and the baseband amplifier. This is realized by using two identical mixers (and following amplifiers) and a cross-correlation technique on the FFT analyzer [16,21]. With this technique, commercial DRO sources can be measured [21], but not ultra-high spectral purity sources (high quality synthesizers, sapphire sources, optoelectronic oscillators…).

An alternative solution is the use of an optical delay line in place of the microwave delay line, featuring lower losses for a large delay (ex: 20 μs for a 4 km fiber), large enough for sensitive phase noise measurements at microwave frequencies [22,23]. A higher performance can be achieved when a cross-correlation method is used, but with more complex setup and costly equipment [24].

- ***The active technique***

This technique is also referred to as phase detector method or the two-source technique. It requires a reference oscillator operating exactly at the same frequency as the oscillator under test and featuring a lower phase noise. It measures voltage fluctuations directly proportional to the combined phase fluctuations of the two input sources.

The PLL phase noise measurement method yields the best phase noise detection capability and the widest measurement coverage. It is also almost insensitive to amplitude modulation (AM) noise and is capable of tracking slow drifting sources. However, the phase noise of the reference source should be as low as possible, which can be costly. Modern commercial benches are today well fitted to characterize both synthesized and free running sources. As an example, Agilent E5052B signal source analyzer, which is available at LAAS-CNRS and is used to measure the phase noise optoelectronic oscillators presented in this thesis.

- ***Phase noise of a two ports microwave components***

Oscillators phase noise is a critical parameter to be characterized, but it has to be underlined that studying the phase fluctuation added by a two port device is also important, particularly if this device has to be included in a phase/frequency loop (PLL, oscillator) or if the approach chosen to model the oscillating loop is the one of Leeson (like in our case for optoelectronic oscillators). The residual phase noise measurement method [16, 25] is used to study the phase noise of two ports microwave components in open-loop configuration.

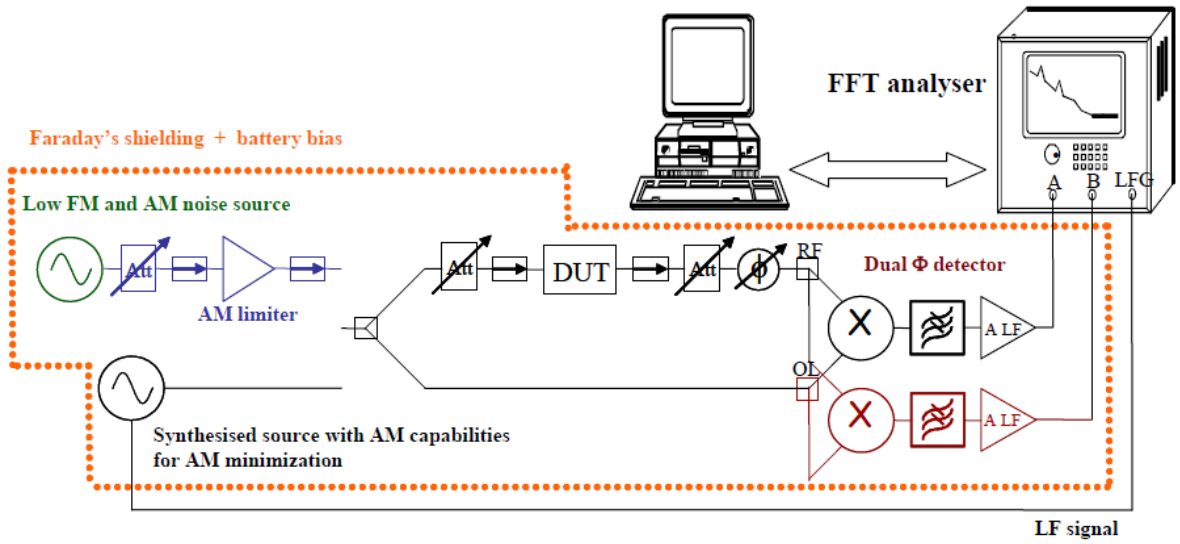

Figure I-4 Residual phase noise measurement set up (phase detection: 1 to 18 GHz; low frequency observation band from 1 Hz to 100 kHz; DUT: device under test) [25].

The measurement bench developed is shown in Figure I-4. This method is based on phase detection with a cross correlation technique in order to improve the measurement noise floor. It allows residual phase noise characterization in the microwave range from 1 to 18 GHz of transistors and other devices such as amplifiers, mixers, frequency dividers, multipliers and even of optoelectronic devices and functions (optical link, optical amplifier…).

The strong points of this method include the possibility to control different parameters (there is no need for a loop phase control), the ability to measure from linear to nonlinear mode and to analyze separately the contribution of each component of the oscillation loop thanks to the open-loop approach.

I.2.a.iii Microwave oscillators with best phase noise performances

Significant progress has been made in the last decades to improve the performance of the microwave oscillators, especially in their short-term stability, but more challenges and issues need to be addressed to meet the often exclusive requirements of low phase noise together with the other performance criteria, such as frequency tunability.

The resulting phase noise performance will generally depend on the application frequency (carrier frequency f_0) as well as on the offset frequency range of interest. For instance, phase noise at offsets from a few kHz to tens of MHz is typically significant in high speed data systems because phase noise on clock and data signals results an excessive bit error rate.

Figure I-5 is drawn mainly to show some examples of the best phase noise performance of microwave oscillators using different technologies and techniques. For instance, in the case of ceramic DRO, the phase noise performances are slightly different if

different amplifiers are used in the loop, such as SiGe HBT (silicon-germanium hetero-junction bipolar transistor) or Si BJT (silicon bipolar junction transistor) [5,16,26-28].

As mentioned before, a higher oscillation frequency (application frequency) degrades the phase noise, which is clearly visible in the case of quartz oscillators [29-31]. Furthermore, it is appropriate to note here that in the X band, only the sapphire WGM DRO feature an ultra-low phase noise level, especially when the oscillator frequency is stabilized using a frequency discriminator with carrier rejection technique [28].

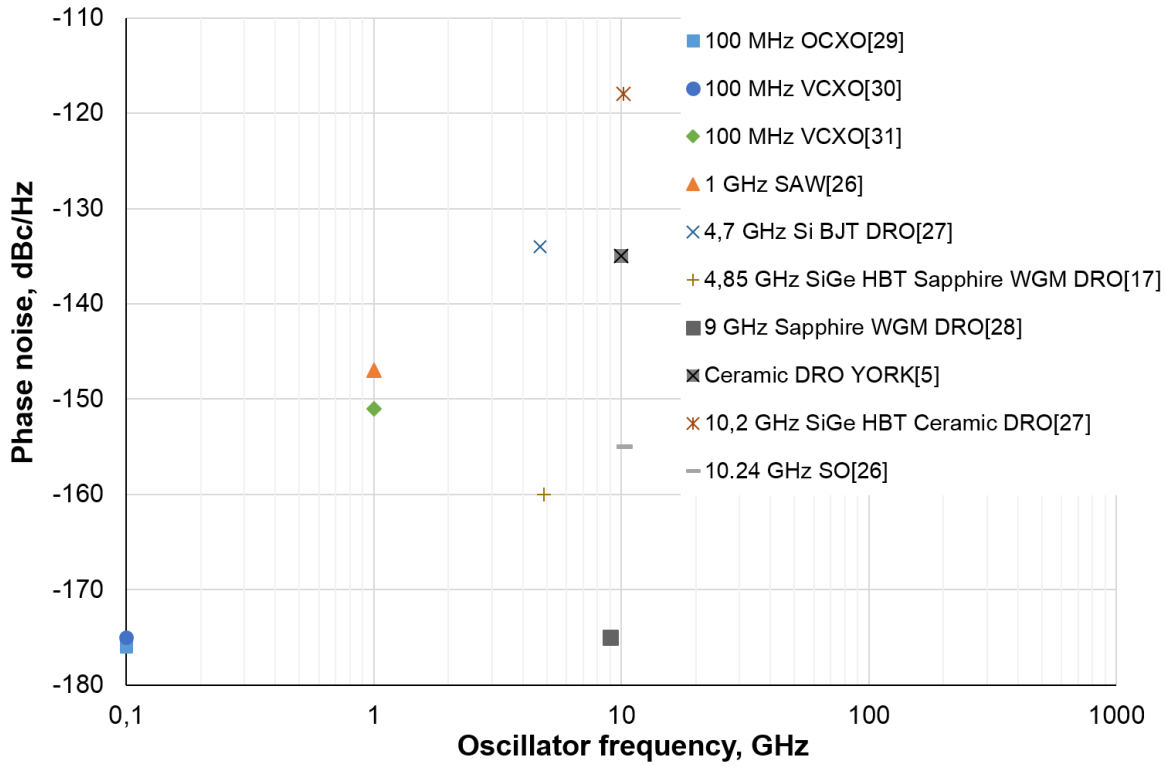

Figure I-5 Best phase noise results obtained at 10 kHz offset frequency, using microwave oscillators. OCXO: oven controlled quartz oscillators; VCXO: voltage controlled quartz oscillator; Si BJT: silicon bipolar junction transistor; SiGe HBT: silicon-germanium hetero-junction bipolar transistor; SO: sapphire oscillator.

Even though the RF/microwave oscillators exhibit interesting performance near few GHz, they become undesirably noisy and unstable when the applications frequency increases. A breakthrough technology can be positioned in a competitive map if it is able to deliver some specific performance that is either better or comparable to the best microwave electronic oscillator at frequencies above 10 GHz, and up to millimeter wave range. Such a goal can be achieved by embedding optical technology into traditional electrical systems. It is known as photonic RF systems. The widespread adoption of the photonic RF technology is mainly attributed to its advantages which include low loss, light weight, high frequency operation and immunity to electromagnetic interference.

I.3 Optoelectronic oscillators

The first reported microwave oscillator using optics was credited to NASA's Jet Propulsion Laboratory (JPL) in 1991. R. Logan *et al.* [32] have developed a fiber-optic stabilized electronic oscillator (FOSO). A better performance system was then presented [33] by employing a mode-locked laser diode in an "all photonic" delay-line stabilized oscillator.

In 1994, a novel photonic oscillator, characterized by a high spectral purity, was reported by X.S. Yao *et al.* [34]. This oscillator was based on converting the continuous light energy from a pump laser to radio frequency and microwave signals [35,36], and labelled with the acronym OEO for optoelectronic oscillator. This system is capable of producing spectrally pure RF oscillations with good frequency tunability and low phase noise.

Up to now, two essential types of OEO have been proposed: the first one is the optical delay line based OEO and the second one is the OEO based on a resonant device. The latter can be based on active or passive cavity.

I.3.a Delay line based OEO

The delay line based optoelectronic oscillator (DL-OEO) has been the first type of OEO reported [34,36]. It is realized with a laser source, an electro-optic modulator (EOM) and an optoelectronic feedback loop, which consists of an optical part and an electrical part. To activate the optoelectronic oscillation, the optoelectronic loop must be closed on the EOM (Figure I-6).

The light beam is modulated by an electro-optic modulator (EOM) in response to the feedback signal from the feedback loop and passed through a long fiber link to be finally detected by a photodetector. The optical fiber serves as a delay, providing the needed quality factor for low noise oscillation and the photodetector converts the optical signal into an electrical signal to interlink the optical and the electrical part. The latter one is realized by an electrical amplifier, a filter and a phase shifter. The microwave amplifier is required to compensate for loss around the loop and the filter is needed to select the desired frequency of interest, while suppressing the unwanted modes caused by the wave that propagate in the loop and add up in phase. However, it has been demonstrated that if the optical link gain was greater than the loop loss in the OEO, the RF amplifier became unnecessary [37,38]. This is possible if gain making devices are included in the optical link, such as optical amplifiers or even, in some cases, high power lasers and photodiodes.

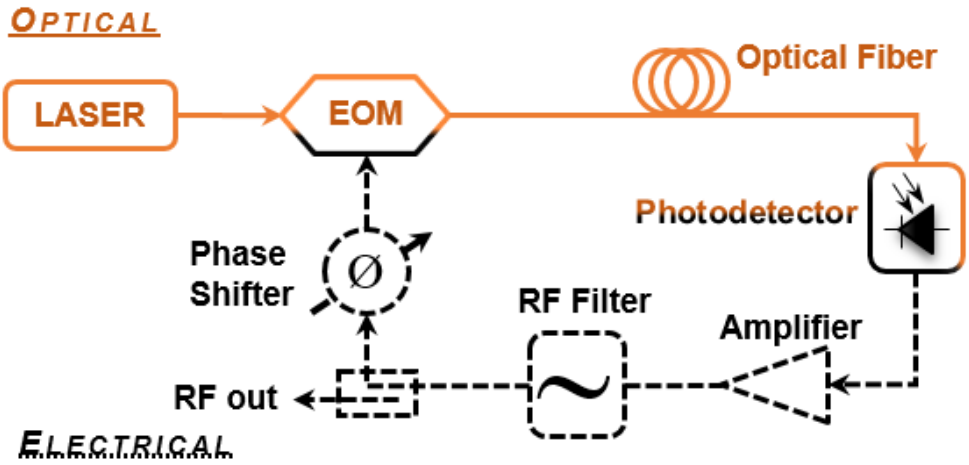

Figure I-6 Detailed construction of a delay line based OEO; EOM: electro-optic modulator.

It is worthwhile pointing out here that the OEO is characterized by the spacing between the modes, known as free spectral range FSR (in Hz), and that is given by the inverse loop trip time and can be define as:

$$FSR = c/nL \tag{I.9}$$

where c is the speed of light, n is the effective refractive index of the optical fiber and L is the optical fiber length.

As mentioned above, the steepness of the phase-to-frequency slope ($^{d\phi}/_{df}$) is an essential parameter as it reflects the stability of the OEO versus a perturbation in the loop phase (and thus is related to the phase noise) (equation (I.5) and (I.6)). In the case of an OEO based on optical delay line, this slope is proportional to the time delay (τ) of the signal propagating inside the delay line:

$$\frac{d\phi}{df} = -2\pi\tau \tag{I.10}$$

Therefore, it is evident from equation (I.10) that the phase noise of the OEO decreases with the delay time. So by lengthening the optical fiber, which features an extremely low transmission loss, the phase noise could be reduced greatly, and that is to say higher short-term stability. To this extent, the equivalent loaded quality factor can be expressed in function of the oscillator frequency (f_0) and the delay as follow:

$$Q_{RF} = \pi\tau f_0 \tag{I.11}$$

According to equation (I.11), the OEO's loaded quality factor (Q_{RF}) is directly proportional to the oscillation frequency, thus the higher the application frequency is, the

higher will be the quality factor. This behavior is opposite to that of the microwave resonator where the generation of high-frequencies signals suffers from low Q_{RF}.

While it is true that lengthening the delay line is so beneficial in terms of quality factor and phase noise, it is also true that with the increase of the delay time, the free spectral range (FSR) becomes smaller, and thus the number of modes increases, leading to a high spurious level. So, in order to eliminate the unwanted modes and to lower the spurious level, a very narrow-band high Q microwave filter is needed [39,40]. Figure I-7 (a) depicted the phase noise performance of a single loop OEO with an RF filter having Q of 4000. A relatively high spurious level of -66 dBc at 45 kHz offset appears. Whereas, when using a higher Q microwave filter of 38000, a reduction of about 30 dB in the spurious level for the first side mode has been demonstrated, beside a decrease in the spurious number (Figure I-7 (b)).

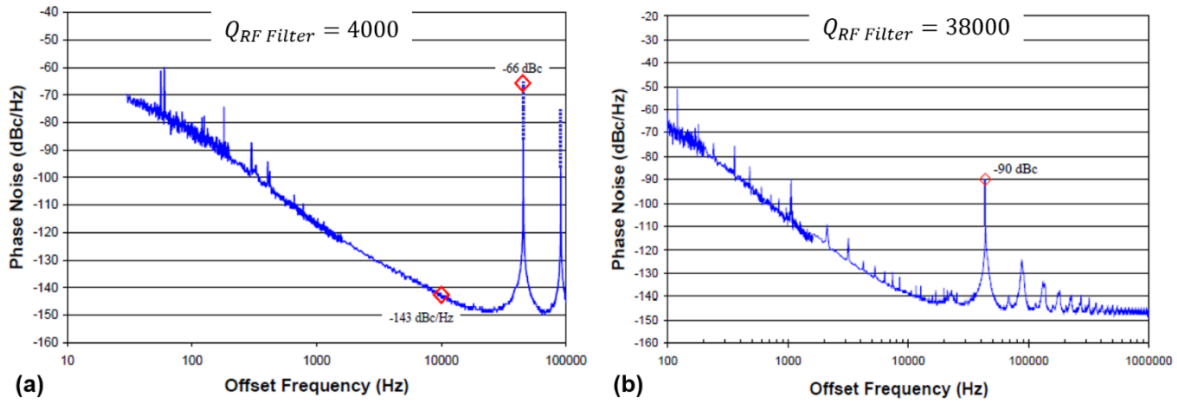

Figure I-7 From [40]: Phase noise of single loop OEO with RF filter having (a) $Q = 4000$ (b) $Q = 38000$

However, such filters are not always available at low cost and are difficult to realize at multi-GHz frequencies. For this reason, another method to reduce the spurious level has been proposed [41,42], which is based on two (or more) fiber loops with short and long lengths in parallel. With such a configuration (Figure I-8), the multi-loop OEO will be characterized by relatively high loaded quality factor, strong mode selectivity and low spurious level, since the short fiber fixes the FSR and therefore it serves to reduce the influence of the modes of the longer fiber, which sets the high loaded Q.

The temperature stability of these systems is related to the delay, and thus to the temperature stability of the optical fiber (effective length and effective index). This stability is in the range of 7 ppm/K, which is better than many microwave systems but still not as good as temperature compensated DROs or, of course, quartz stabilized oscillators. Therefore, an active temperature control of the fiber spool has to be set up to get sufficient medium-term or long-term frequency stability performance.

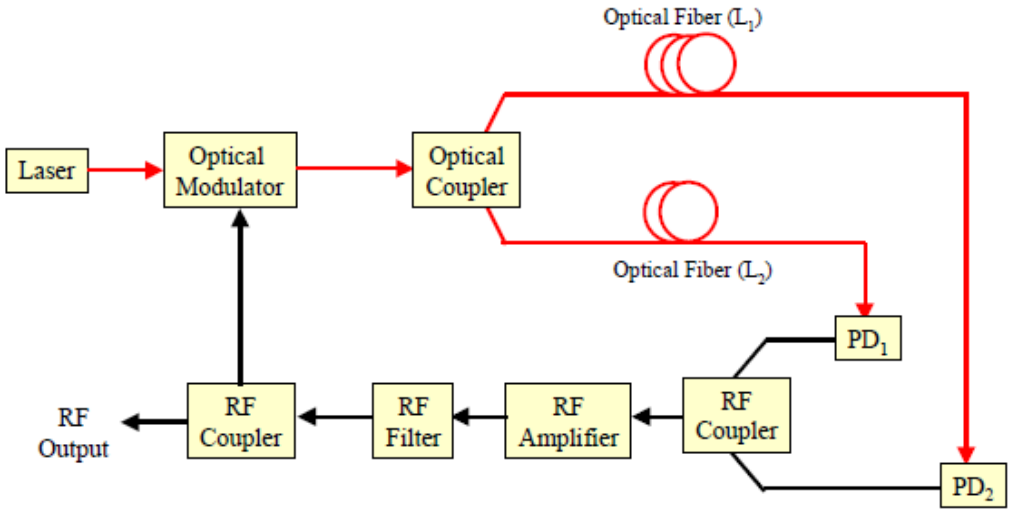

Figure I-8 From [40] Dual optical loop OEO configuration

Figure I-9 presents the phase noise of a single loop OEO using 4.4 km fiber and the phase noise of a dual loop OEO with fiber length of 8.4 and 2.2 km. The spurious level is improved by more than 30 dB when the dual loop OEO is used, in addition to the overall reduction of the phase noise.

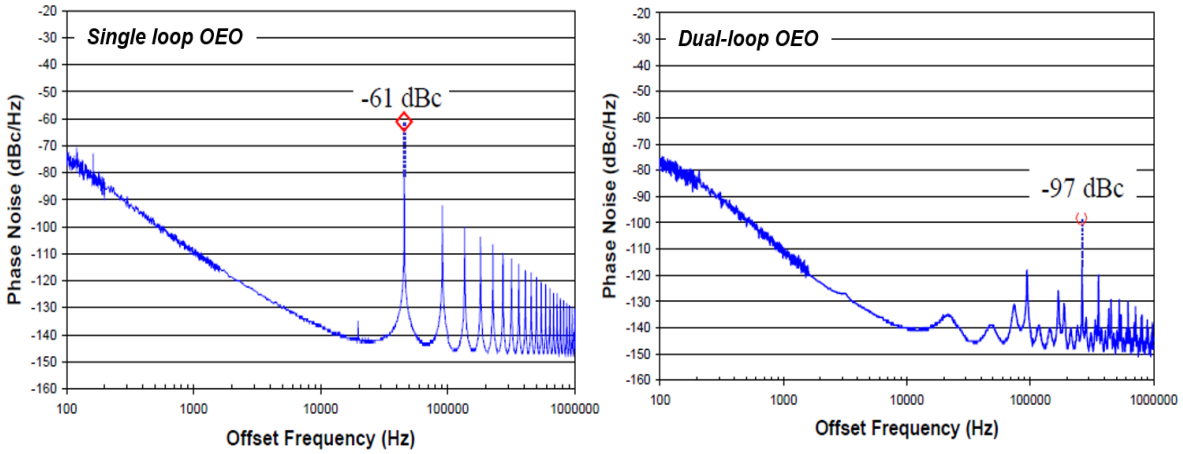

Figure I-9 From [40] Phase noise performance of single and dual optical loop OEO.

In order to maintain a high Q OEO system while eliminating the unwanted modes, a dual injection-locked optoelectronic oscillator has been introduced [43,44], which demonstrated an oscillator output with ultra-low phase noise and an ultra-low spurious level. Even though these solutions are at high level and quite effective, they need bulky and complex configurations to be used.

Apart from the undesired effects, some outcomes of the presence of many modes in the oscillator were noted to be advantageous. In fact, by using a microwave tunable filter in the loop, the OEO, which is known now as tunable OEO, will be able to generate signals at

the selected frequency, and continuously tunable within the FSR, while featuring the same phase noise performance regardless the frequency selected [45].

I.3.b Coupled OEO

These early OEO configurations were followed by a novel architecture in which a microwave oscillation and an optical oscillation are generated and directly coupled with each other [46]. That is the reason why this configuration is known as a coupled optoelectronic oscillator (COEO). The COEO uses an active optical cavity. It generates simultaneously spectrally pure microwave signals as in a microwave oscillators, and short optical pulses as in a mode locked laser.

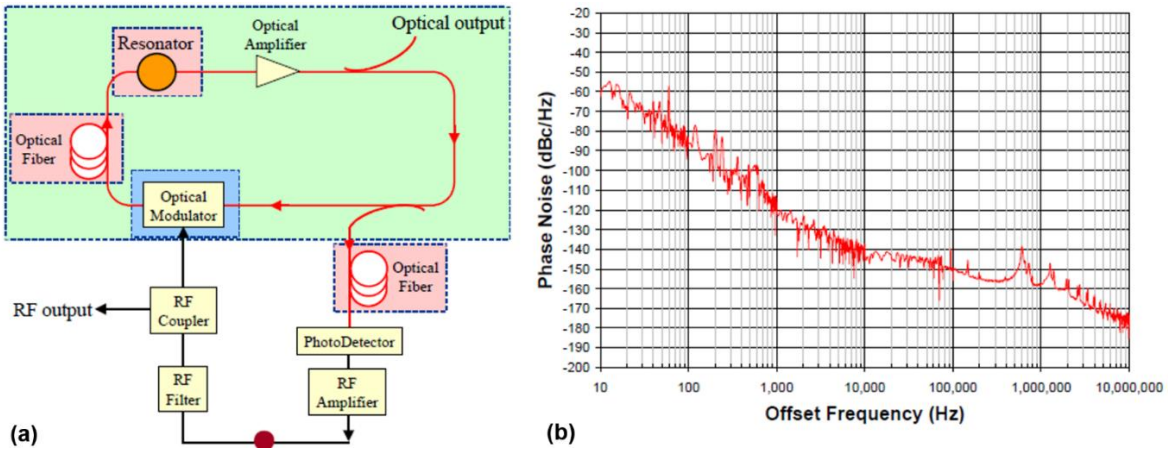

Figure I-10 From [48] (a) COEO configuration with optical loop around a high Q elements, where the gain loop is modulated with an optical amplitude modulator. (b) Phase noise at 10 GHz of a COEO with a short fiber in the optical loop (330m).

In the case of the COEO, the source of light (laser) is included in the system and is a ring laser which is constructed with an optical amplifier (semiconductor optical amplifier (SOA) or Erbium-doped fiber amplifier (EDFA)), directly modulated [46] or by means of a fast amplitude modulator [47] (see Figure I-10 (a)), and which has its output feedback to itself to generate the optical oscillator. This ring laser is a multimode mode-locked laser that is used as a carrier for the microwave signal, which also takes benefit of the enhanced Q factor due to the resonator effect (multipath loop).

Regarding the phase noise, an ultralow phase noise level has been reported by the Jet Propulsion Laboratory (JPL) in 2005 with this approach [48]. Figure I-10 (b) depicts the phase noise at 10 GHz of a COEO that consists of only 330m longer fiber in the optical loop. The phase noise level is lower than -140 dBc/Hz at 10 kHz offset and decreases to -178 dBc/Hz at 10 MHz offset. A similar low noise level can be obtained with an OEO basic configuration (see Figure I-9), that has 4.5 km optical fiber and the same RF amplifiers phase noise level [40].

Another feature of the COEO, is that only a small number of low level spurious modes are present at high offset frequencies (e.g. 650 kHz) compared to a larger number of them with higher power levels in a long fiber OEO. The COEO is actually a resonator based OEO, but the resonator is active and behaving in laser mode.

In addition to the long optical fiber delay as an optical energy storage element, optical resonators, such as fiber Fabry-Perot resonator and fiber ring resonator can be used to construct the different architectures of the OEO. The use of the optical resonator can dramatically reduce the size of the OEO especially in the case of the micro-disk resonator since it is the key element to realize an integrated version of an oscillator.

I.3.c Optical resonator based OEO

As mentioned earlier, the OEO based on delay optical fiber suffers from a high number of parasitic modes, a large size, and because of this large size, it is hard to stabilize in temperature. These limitations may restrict the practical use of this oscillator.

An elegant solution has been proposed to overcome these drawbacks, and it consists of replacing the optical delay line by a high optical quality (Q_{Opt}) factor resonator [49,50], to provide a sufficiently long storage time (large optical delay) and thus to produce an oscillation featuring narrow linewidth and low phase noise. These optical resonators can be implemented in different configurations and techniques, e.g. fiber Fabry-Perot resonator, optical microsphere and micro-disks resonators, fiber ring resonator and others types of resonators. They are covered and discussed in chapter II. The high-Q optical resonators are of great help in reducing the size of the OEOs and in producing an integrated OEO device with other components and devices in one compact package.

I.3.c.i Mode matching

In order to sustain an oscillation with a loop gain (in the closed loop) greater than the losses, certain mode matching conditions for this type of optoelectronic oscillator are required between the resonator modes, the laser frequency and the RF oscillation frequency. Figure I-11 illustrates the different modes present in the OEO loop. These conditions are necessary to satisfy a proper mode matching:

1. The laser frequency υ_{laser} matches one of the transmission peaks of the optical resonator, in order to get high optical power on the photodetector input. Figure I-11 (a) shows the position of the laser carrier υ_{laser} with its modulation sidebands to be locked with one of the resonator modes (in Figure I-11 (b)) under this matching condition. Note also that the laser should be of high spectral purity, which was not mandatory in the delay line based OEO.
2. The optoelectronic oscillation frequency is proportional to the free spectral range of the resonator (Figure I-11 (c)), i.e.,

$$f_{RF} = k.FSR \tag{I.12}$$

where k is a positive integer.

Notably, the free spectral range FSR of the resonator is directly linked to the cavity length (L) and to its refractive index (n), as in the case of the optical delay line, see equation (I.9).

When the above mode matching conditions are satisfied, the mode spacing of the OEO becomes the FSR of the resonator. Thus, the cavity length of the resonator can be made small to enlarge the mode spacing of the oscillation and to allow an easy selection of one single mode for the oscillator by the microwave filter (in the electrical loop). Hence, unlike delay line based OEO case, the bandwidth of the RF filter is not required to be narrow, which is not usually available. A bandwidth in the order of 10 MHz or greater is generally sufficient and achievable for many large size resonators (fiber rings, Fabry-Perot). With small size resonators, such as mini-disks resonators, no microwave filter at all is required (the FSR of these resonators is in the GHz range).

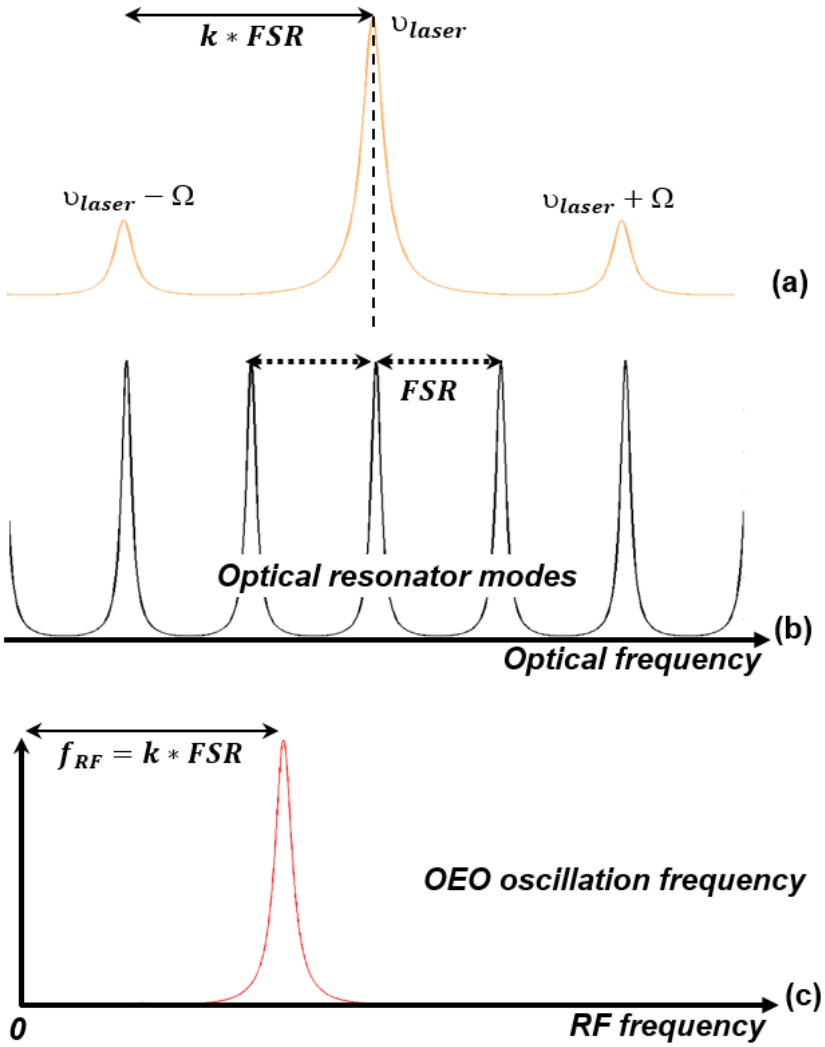

Figure I-11 Illustration of the different modes present in an OEO and the above mode matching conditions; Ω: modulation frequency.

I.3.c.ii System stabilization

Not only the mode matching must be ensured, but it should be maintained over time. In fact, when it comes to practical implementation, the desired performance of an optoelectronic oscillator is threatened by the aging of its components and by the changes of the environmental conditions, such as temperature fluctuations, stress, or other disturbances. Over time, these disturbances may result in a frequency shift of both the laser frequency and the transmission peak of the resonator, and if these shifts exceed certain range, the mode matching condition (1) cannot be longer satisfied, which causes a malfunction of the OEO.

So for the purpose of maintaining the matching condition (1), a control system, known also as stabilization technique, must be used to reduce the frequency difference between the laser frequency υ_{laser} and the transmission peak of the resonator. This can be achieved by either actively locking the laser frequency to the respective transmission peak, or alternatively, actively locking the resonator to the laser. The choice of these two frequency locking techniques depends on the intended application.

To date, several frequency locking methods have been developed, such as the laser frequency stabilization by polarization spectroscopy of a reflecting reference cavity [51] and the Pound-Drever-Hall stabilization technique (PDH) [52]. These methods will be detailed in Chapter IV. But broadly speaking, in the two locking techniques, a monitoring system is used to monitor the difference between the laser frequency and the transmission peak to generate an error signal. Then, based on this error signal, a frequency correction mechanism is used to reduce the frequency difference, by applying a control signal either to the laser or to the cavity of the resonator.

In some cases, it is also possible to set up a direct optical feedback lock (dubbed as self-injection lock) between the laser and the resonator [53-55]. Part of the signal induced in the resonator is fed-back to the laser, and locks its frequency to the one of the resonator. This locking process is stable if the FSR of the resonator is large (small resonators) and if the optical path between the laser and the resonator is short enough. The feedback signal can be a part of the transmission signal through the resonator, which is externally fed-back to the laser, or the natural low level feedback signal due to the Rayleigh scattering effect inside the resonator.

I.3.c.iii Microwave and optical quality factors

The optical resonators are characterized by their optical quality (Q_{opt}) factor. However, when analyzing the stability or the phase noise performance of an OEO, the considered quality factor (see equation (I.6), (I.8) and (I.11)) is the microwave quality (Q_{RF}) factor. Hence comes the necessity to compute an equivalent Q_{RF} factor from the Q_{opt} factor.

The equivalent microwave quality factor is linked to the optical quality factor by the following equation [56]:

$$Q_{RF} = Q_{opt} \frac{f_0}{f_{opt}} \quad \text{(I.13)}$$

where f_0 and f_{opt} are the microwave frequency and the optical frequency, respectively.

This is easy to understand, since what is transferred in these systems between the optical frequencies and the microwave frequencies is the resonator bandwidth, which remains unchanged.

Based on equation (I.13), a very high Q_{opt} factor resonator has to be chosen, since the equivalent Q_{RF} factor is divided by the ratio between the microwave and optical frequencies. For instance, if the application frequency is at 20 GHz and uses a 1.5 μm laser, the frequency ratio is around 10^4, thus Q_{RF} is reduced by 10^4 compared to Q_{opt}. Therefore, a Q_{opt} of 10^8 results in a Q_{RF} of 10^4 at 20 GHz, and of only 5000 at 10 GHz. Therefore Q_{opt} factors in excess of 10^8, or even 10^9, are required in the foreseen applications of these resonators.

I.3.d Noises in the OEO: Best phase noise performance

In such a complex system, the performance of an optoelectronic oscillator is affected by the interplay between optical, microwave and low-frequency active and passive components in the loop. Thus, many studies have been carried out to improve the phase noise performance of the OEO. The phase noise performance is affected mainly by:

- Laser amplitude noise (AM) and frequency noise (FM) conversions to RF phase noise, either through the fiber chromatic dispersion, the interferometric phenomenon (optical parasitic reflections in the system), the resonator or the photodiode nonlinearity.
- The nonlinear optical effects generated inside the optical resonator, like the Brillouin scattering, Rayleigh scattering, Raman scattering and four wave mixing.
- The microwave amplifier noise.
- The low-frequency noise of the electronic control components, such as the ones of the laser stabilization system, for instance.

These noises have been studied and detailed in Chapter III.

Optoelectronic oscillators with best phase noise performance

Table I.1 summarizes the best (up until now) phase noise performance of an optoelectronic oscillator based on the three configuration listed above, i.e. optical delay line (DL-OEO), coupled optoelectronic oscillator (COEO), optical resonator OEO, such as fiber ring resonator (FRR) and whispering-gallery mode resonator (WGMR). These results are presented for OEO at 10 GHz (oscillation frequency) and at 10 kHz offset frequency. Their optical quality factor vary between 10^6 and 10^9.

Based on this table, the DL-OEO and the COEO exhibit the best phase noise performance so far with a phase noise lower than -150 dBc/Hz at 10 kHz offset from a 10 GHz carrier. Even though these results are still not as good as that the ones achieved with the microwave oscillator based on sapphire WGM DR [28] (see Figure I-5) in the low microwave range (up to 10 GHz), the optoelectronic oscillators can be more compact and are more stable in temperature than sapphire DROs, and they features very high potential at higher frequencies where the performance of sapphire loaded cavities is largely degraded.

OEO type	$\boldsymbol{FSR}$	***Phase noise***
DL-OEO (SMF fiber) [57]	20 kHz	-160 dBc/Hz
DL-OEO (Zero dispersion fiber) [58]	50 kHz	-140 dBc/Hz
Dual-loop DL-OEO (SMF) [40]	25 kHz	-140 dBc/Hz
YIG-Tuned OEO [45]	45 kHz	-128 dBc/Hz
COEO (SMF) [48]	650 kHz	-140 dBc/Hz
COEO (Dispersion-shifted fiber + SMF) [59]	210 kHz	-149 dBc/Hz
Tunable WGMR OEO (LiTaO3) [60]	46 GHz	-100 dBc/Hz
WGMR OEO (CaF_2 disk) [61]	12.45 GHz	-95 dBc/Hz
Classical hyperparametric WGMR OEO [62]	9.9 GHz	-120 dBc/Hz
Raman detuning hyperparametric WGMR OEO [62]	35 GHz	-115 dBc/Hz
WGMR OEO (SiO_2 Silica disk) [63]	10.7 GHz	-90 dBc/Hz
Immunized FRR-OEO (P-M fiber) [63]	2 MHz	-128 dBc/Hz

Table I.1 Best phase noise performance of several type of optoelectronic oscillators at 10 GHz, at 10 kHz offset frequency.

I.4 Conclusion

The oscillators are enlarging their application area but they still need improvement to address the growing markets and requirements for a special and very high performance functions. This chapter presents an overview of the different oscillator topologies and types, starting with the microwave oscillators that are used to generate spectrally pure signals (high short-term stability). For instance, the microwave oscillator based on sapphire WGM DR provides an excellent phase noise level of about -174 dBc/Hz at 10 kHz offset frequency from

a 10 GHz carrier. Nevertheless, the microwave oscillators suffer from some degree of bulkiness and complexity regarding the technology used, and even more importantly, their microwave quality factor decreases when a higher frequency applications is required.

To overcome these drawbacks, an oscillator that is based on both microwave and optical technology has been developed. Taking into account the advantages of the optical element, i.e. extremely low loss and small size, and under intense research, these optoelectronic oscillators are showing promising results in comparison with their pure microwave competitors, since these OEO are capable of generating spectrally pure RF oscillations with excellent short-term and medium-term stability, and with a performance level which improves when the frequency application increases.

With all these qualities, it is important to highlight the fact that the fiber ring resonator (FRR) based OEO configuration is not yet completely mature. Several degradation mechanism or noises limit its operation conditions and especially its phase noise performance. These limitations are the main study cases for these systems, and significant progress has been made in the last decade on the noise modeling of the devices and elements that are used in the oscillator loop, to be able to simulate the oscillator noise performance.

The following manuscript, in the next chapters, discusses these degradations mechanisms and the potential improvements along with noise simulations, in order to provide an OEO configuration based on fiber ring resonator (FRR) which features a very low phase noise, together with a very high Q_{opt} factor and a very high loaded microwave Q_{RF} factor as well.

I.5 References

1. Rohde, U. L., Poddar, A. K., Schoepf, J., Rebel, R. & Patel, P. Low noise low cost ultra-wideband N-push VCO. *IEEE MTT-S International Microwave Symposium Digest, 2005*, 1171-1174 (2005).
2. Khanna, A. P. S. & Hauptman, J. 18 to 40 GHz 13 dBm GaAs FET YIG tuned oscillator, *IEEE MTT-S International Microwave Symposium Digest*, *1991,* 209-2012 (1991).
3. Kajfez, D. & Guillon, P. *Dielectric Resonators*. Norwood, MA: Artec House, Inc. (1986).
4. Khanna, A. P. S. Microwave oscillators: The state of the technology. *Microwave J.* **49**, 22-28 (2006).
5. Howe, D. A. & Hati, A. Low-noise X-band oscillator and amplifier technologies: comparison and status. *Proc. IEEE Freq. Control Symp.*, 2005, Vancouver, BC, 481-487 (2005).
6. Sallin, M., Zhou, L., Broomfield, C. & Everard, J. K. A. Broad tuning ultralow noise DROs at 10 GHz utilizing ceramic based resonators. Proc. *Joint 2003 IEEE Freq. Control Symposium and 17th European Frequency and Time Forum*, 411-416 (2003).
7. Wenzel oscillators: http://www.wenzel.com/
8. Barnes, J. A., Chi, A. R., Cutler, L. S., Healey, D. J., Leeson, D. B., McGunigal, T. E., Mullen, J. A., Smith, W. L., Sydnor, R. L., Vessot, R. F. C & Winkler, G. M. R. Characterization of frequency stability. *IEEE Trans. Instrum. Meas.* **20**, 105-120 (1971).
9. Howe, D. Frequency stability. *Encyclopedia of RF and Microwave Engineering, Wiley Publ. U.S.A.,* 1706-1720 (2005).
10. Ferrer-Pikal, E. S., Vig, J. R., Camparo, J. C., Culter, L. S., Maleki, L., Riley, W. J., Stein, S. R., Thomas, C., Walls, F. L. & White, J. D. Draft revision of IEEE STD 1139-1988 standard definitions of physical quantities for fundamental, frequency and time metrology-random instabilities. *Freq. Control Symp., 1997, Proceedings of the 1997 IEEE International*, Orlando, FL, 338-358 (1997).
11. Leeson, D. B. A simple model of feedback oscillator noises spectrum. *Proc. IEEE* **54**, 329-330 (1966).
12. Rizzoli, V., Mastri, F. & Masotti, D. General noise analysis of nonlinear microwave circuits by the piecewise Harmoni-Balance Technique. *IEEE Trans. Microw. Theory Techn.* **42**, 807-819 (1994).
13. Hajimiri, A. & Lee, T. H. A general theory of phase noise in electrical oscillators*. IEEE J. Solid State Circuits* **33**, 179-194 (1998).
14. Ngoya, E., Rousset, J. & Argollo, D. Rigorous RF and microwave oscillator phase noise calculation by envelope transient technique. *2000 IEEE MTT Symp. Digest* **1**, 91-94 (2000).

15. Llopis, O. & Cibiel, G. Phase noise metrology and modelling of microwave transistor – applications to the design of state of the art dielectric resonator oscillators. *SPIE Fluctuations and Noise Conferences*, Santa Fe, USA, 179-191 (2003).
16. Cibiel, G., Escotte, L. & Llopis, O. A study of the correlation between high-frequency noise and phase noise in low-noise silicon-based transistors. *IEEE Trans. Microw. Theory Techn.* **52**, 183-190 (2004).
17. Cibiel, G. Contribution à l'analyse d'amplificateurs microondes à très faible bruit de phase: application à la réalisation d'une source à très haute pureté spectrale en bande C. PhD Thesis, Toulouse III, Paul Sabatier University, France (2003).
18. Rubiola, E. & Brendel, R. A generalization of the Leeson effect. *arXiv:1004.5539, physics.ins-det* (2010).
19. Llopis, O. *Mesures en hyperfréquences. Chapitre. La mesure du bruit de phase en hyperfréquences*. Hermès Sciences Publications, Lavoisier (2004).
20. Lance, A., Wendell, D. S. & Labaar, F. Phase noise and AM noise measurements in the frequency domain. *Infrared and Millimeter Waves* **11**, 239-289 (1984).
21. Régis, M. Contribution à la conception des oscillateurs microondes à haute pureté spectrale à base de silicium et silicium-germanium. PhD. Thesis, Toulouse III, Paul Sabatier University, France (1998).
22. Onillon, B., Constant, S. & Llopis, O. Optical links for ultra-low phase noise microwave oscillators measurement. *Proc. IEEE Freq. Control Symp.*, 2005, Vancouver, BC, 545-550 (2005).
23. Brahimi, H. Etude en bruit de systèmes optiques hyperfréquences modélisation, caractérisation et application à la métrologie en bruit de phase et à la génération de fréquence. PhD. Thesis, Toulouse University, Paul Sabatier University, France (2003).
24. Rubiola, E., Salik, E., Huang, S., Yu, N. & Maleki, L. The photonic delay technique for phase noise measurement of microwave oscillators. *J. Opt. Soc. Am. B* **22**, 987-997 (2005).
25. Cibiel, G., Regis, M., Tournier, E. & Llopis, O. AM noise impact on low level phase noise measurements. *IEEE Trans. Ultrason., Ferroelect. Freq. Control* **49**, 784-788 (2002).
26. Rohde, U., Poddar, A. & Calbaza, D. Searching for Low-Phase synthesizer. Microwave & RF (2014).
27. Régis, M., Llopis, O., Van Haaren, B., Plana, R., Grhule, A., Rayssac, J. & Graffeuil, J. Ultra-low phase noise C and X band bipolar transistor dielectric resonator oscillators. *Proc. IEEE Int. Freq. Contr. Symp.,* 507-511 (1998).
28. Ivanov, E. N. & Tobar, M. E. Low phase noise sapphire crystal microwave oscillators: current status. *IEEE Trans. Ultrason. Ferroelect. Freq. Control* **56**, 263-269 (2009).
29. Wenzel Premium 100 MHz SC Ultra low noise crystal oscillator datasheets, no. 501-04623.

30. McClelland, T., Stone, C. & Bloch, M. 100 MHz crystal oscillator with extremely low phase noise. *Frequency and Time Forum, 1999 and the IEEE International Frequency Control Symposium, 1999, Proceedings of the 1999 Joint Meeting of the European* **1**, 331-334 (1999).
31. Boroditsky, R. & Gomez, J. Ultra-low phase noise 1 GHz OCXO. *Frequency Control Symposium, 2007 Joint with the 21st European Frequency and Time Forum. IEEE International*, 250-253 (2007).
32. Logan, R. T., Maleki, L. & Shadaram, M. Stabilization of oscillator phase using a fiber-optic delay-line. *Proc. 45th Annu. Symp. Frequency Contr.*, 508-512 (1991).
33. Logan, R. T. & Maleki, L. Ultra-stable microwave and millimeter wave photonic oscillators. *46h IEEE Frequency Contr. Symp.*, 420-424 (1992).
34. Yao, X. S. & Maleki, L. High frequency optical subcarrier generator. *Electron. Lett.* **30**, 1525-1526 (1994).
35. Yao, X. S. & Maleki, L. A novel photonic oscillator. *Telecommun. Data Acquisition Prog.* **42-122***,* 32-43 (1995).
36. Yao, X. S. & Maleki, L. Optoelectronic microwave oscillator. *J. Opt. Soc. Am. B* 1**3**, 1725-1735 (1996).
37. Yao, X. S. & Maleki, L. Optoelectronic oscillator for photonic systems. *IEEE J. Quantum Electron.* **32**, 1141-1149 (1996).
38. Nelson, C. W., Hati, A., Howe, D. A. & Zhou, W. Microwave optoelectronic oscillator with optical gain. *2007 IEEE International Frequency Control Symposium Joint with the 21st European Frequency and Time Forum*, Geneva, 1014-1019 (2007).
39. Eliyahu, D., Sariri, K., Kamran, M. & Tokhmakhian, M. Improving short and long term frequency stability of the opto-electronic oscillator*. IEEE Int. Freq. Cont. and PDA Exhibition*, 580-583 (2002).
40. Eliyahu, D. & Maleki, L. Low phase and spurious level in multi-loop opto-electronic oscillators. *IEEE Int. Frequency Control Symposium and PDA Exhibition Jointly with the 17th European Frequency and Time Forum*, 405-410 (2003).
41. Yao, X. S. & Maleki, L. Multi-loop optoelectronic oscillator. *IEEE J. of Quant. Electron* **36**, 79-84 (2000).
42. Eliyahu, D., Sariri, K., Taylor, J. & Maleki, L. Optoelectronic oscillator with improved phase noise and frequency stability. *Proc. SPIE, Photonic West* **4998B** (2003).
43. Zhou, W. & Blasche, G. Injection-locked dual optoelectronic oscillator with ultra-low phase noise and ultra-low spurious level. *IEEE Trans. Microw. Theory Techn.* **53**, 929-933 (2005).
44. Okusaga, O., Adles, E.J., Levy, E.C., Zhou, W., Carter, G.M. Menyuk, C.R. & Horowitz, M. Spurious mode reduction in dual injection-locked optoelectronic oscillators. *Opt. Express* **19**, 5839-5854 (2011).

45. Eliyahu, D. & Maleki, L. Tunable, ultra-low phase noise YIG based optoelectronic oscillator. *Proceedings of MTT-S* **3**, Philadelphia, PA, USA, 2185-2187 (2003).
46. Yao, X. & Maleki, Lute. Dual microwave and optical oscillator. *Opt. Lett.* **22**, 1867-1869 (1997).
47. Yao, X., Davis, L. & Maleki, L. Coupled optoelectronic oscillators for generating both RF signal and optical pulses. *J. Lightwave Technol.* **18**, 73-78 (2000).
48. Eliyahu, D. & Maleki, L. Modulation response (S21) of the coupled opto-electronic oscillator. *Proc. IEEE Int. Freq. Cont.*, 850-856 (2005).
49. Vahala, K. J. Optical microcavities. *Nature* **424**, 839-846 (2003).
50. Heebner, J., Grover, R. & Ibrahim, T. *Optical microresonators: theory, fabrication, and application* (Spring, 2008).
51. Hansch, T. W. & Couillaud, B. Laser frequency stabilization by polarization spectroscopy of a reflecting reference cavity. *Opt. Commun*. **35**, 441-444 (1980).
52. Drever, R. W. P., Hall, J. L., Kowalski, F. V., Hough, J., Ford, G. M., Munley, A. J. & Ward, H. Laser phase and frequency stabilization using an optical resonator. *Appl. Phys. B* **31**, 97-105 (1983).
53. Dahamni, B., Hollberg, L. & Drullinger, R. Frequency stabilization of semiconductor lasers by resonant optical feedback. *Opt. Lett.* **12**, 876-878 (1987).
54. Hollberg, L. & Ohtsu, M. Modulatable narrow-linewidth semiconductor lasers. *Appl. Phys. Lett.* **53**, 944-946 (1988).
55. Liang, W., Ilchenko, V. S., Savchenkov, A. A., Matsko, A. B., Seidel, D. & Maleki, L. Whispering gallery mode resonator based ultra-narrow linewidth external cavity semiconductor laser. *Opt. Lett.* **35**, 2822-2824 (2010).
56. Merrer, P. H., Brahimi, H. & Llopis, L. Optical techniques for microwave frequency stabilization: resonant versus delay line approaches and related modelling problems. *2008 IEEE Topical MWP*, Gold Coast, Australia, 146-149 (2008).
57. Eliyahu, D., Seidel, D. & Maleki, L. RF amplitude and phase-noise reduction of an optical link and an opto-electronic oscillator. *IEEE Trans. Microw. Theory Techn.* **56**, 449-456 (2008).
58. Volyanskiy, K., Chembo, Y. K., Larger, L. & Rubiola, E. Contribution of laser frequency and power fluctuations to the microwave phase noise of optoelectronic oscillators. *J. Lightwave Technol.* **28**, 2730-2735 (2010).
59. Salik, E., Yu, N., & Maleki, L. An ultralow phase noise coupled optoelectronic oscillator. *IEEE Photon. Technol. Lett.* **19**, 444-446 (2007).
60. Savchenkov, A. A., Ilchenko, J., Liang, W., Eliyahu, D., Matsko, A. B., Seidel, D. & Maleki, L. Voltage-controlled photonic oscillator. *Opt. Lett.* **35**, 1572-1574 (2010).

61. Merrer, P. H., Saleh, K., Llopis, O., Berneschi, S., Cosi, F. & Nunzi Conti, G. Characterization technique of optical whispering-gallery mode resonators in the microwave frequency domain for optoelectronic oscillators. *Appl. Opt.* **51**, 4742-4748 (2012).
62. Maleki, L., Ilchenko, V. S., Savchenkov, A. A., Liang, W., Seidel, D. & Matsko, A. B. High performance, miniature hyper-parametric microwave photonic oscillator. *2010 IEEE Frequency Control Symposium (FCS),* 558-563 (2010).
63. Volyanskiy, K., Salzenstein, P., Tavernier, H., Pogurmirskiy, M., Chembo, Y. K. & Larger, L. Compact optoelectronic microwave oscillators using ultra-high Q whispering gallery mode disk-resonators and phase modulation. *Opt. Express* **18**, 22358-22363 (2010).
64. Saleh, K., Llopis, O. & Cibiel, G. Optical scattering induced noise in fiber ring resonators and optoelectronic oscillators. *J. Lightwave Technol.* **31**, 1433-1446 (2013).

Chapter II: Optical Resonator

II.1 Introduction

High quality factor optical resonators [1,2] (also known as resonant optical cavities) with different configurations, have been extensively investigated in the last decades, because of their importance not just in the microwave photonics oscillator [3], but also in many different applications such as narrow linewidth laser stabilization [4], optical frequency combs generation [5], optical filters [6,7], sensors [8,9], and so forth.

An optical resonator can be realized in different configurations, size and form. Among the most well-known high Q factor resonators are Fabry-Perot, whispering gallery mode and the fiber ring resonators. These resonators are presented in the first section of this chapter.

Despite the fact that the fiber ring resonators did not reach maturity in the field of the optoelectronic oscillators, they could feature a very high optical quality factor, and when used in an optoelectronic oscillator system, a good phase noise performance can be achieved. Given their importance in several applications, it is mandatory to have a global knowledge of an optical resonators properties, such as their coupling regime, quality factor, internal losses, et cetera…

These parameters can be obtained through different characterization techniques, along with parameter extraction techniques based on analytical modeling of these resonators. In the second and third part of this chapter, a detailed analytical study is provided and the characterization techniques are discussed, especially the RF spectrum approach which was developed at LAAS-CNRS. It is based on the transfer of the optical resonance down to the radio frequency spectrum and thus allows their measurements with electrical techniques. This optical resonator metrology has been validated in various experimental studies, with several fiber ring resonators, as it is shown here.

II.2 Optical resonator technologies

Many different resonator technologies can be involved in the applications listed above, with some of which featuring ultra-high Q factors, such as fiber Fabry-Perot resonator [10], which is formed by two mirrors at the two ends of the resonator, a microresonator operating with whispering gallery modes [11], and a passive or active resonator formed of a fiber ring with one or two fiber couplers [12]. Each of these resonators and other optical resonator technologies have their respective advantages and disadvantages.

II.2.a Fabry-Perot resonator

A Fabry-Perot (FP) resonator is basically realized with two highly reflecting mirrors maintained parallel. However, this configuration suffers from several problem such as diffraction and angular misalignment, which reduce the finesse and the quality factor. Of the various geometrics examined, spherical Fabry-Perot resonators (Figure II-1 (a)), in which the spherical mirrors are employed to ease the mirror alignment, have the lowest diffraction loss and are easier to set up [13,14]. These resonators are used in a variety of applications, including laser spectrum analysis.

In addition, FP resonators may also be realized using optical fiber. In this case, similarly to the free space case, it consists of two highly reflecting coating (e.g. mirror) on the two ends of a segment of optical fiber [15]. An alternative way to make a fiber Fabry-Perot resonator (Figure II-1 (b)) is to replace the two reflective coatings by forming a fiber Bragg grating at or near both ends to replace the reflective coatings [16].

In the past years, ultra-stable and ultra-high quality factor Fabry-Perot cavities were the heart of many research activities. Fabry-Perot cavities, which are made entirely from ultra-low-expansion glass (ULE), have demonstrated to be insensitive to both temperature fluctuations and mechanical vibrations. These ultra-stable resonators feature a finesse up to 250000, and an ultra-high quality factor, close to 10^{10} [10, 17]. An all-silicon resonator has been also demonstrated to be insensitive to temperature fluctuations and may reduce the vibration noise. In this case, an extremely high finesse and ultra-stable cavity has been obtained [18].

As represented in Figure II-1 (a), the incident light entering the FP resonator will undergo multiple reflections within the mirrors so that the light can interfere with itself several times. The light will experience a constructive interference as it reflects back and forth inside the resonator if and only if twice the spacing between the mirrors is an integer number of the wavelength of the laser. Otherwise, a destructive interference will take place. As the incoming light makes multiple round-trip within this cavity before exiting, the effective storage time dramatically increases. The effective storage time τ_{eff} of a fiber Fabry-Perot resonator can be expressed as:

$$\tau_{eff} = \tau_d \frac{(1+R)}{(1-R)} \quad \text{(II.1)}$$

where τ_d is the fiber transmission delay and R is the reflective coefficient.

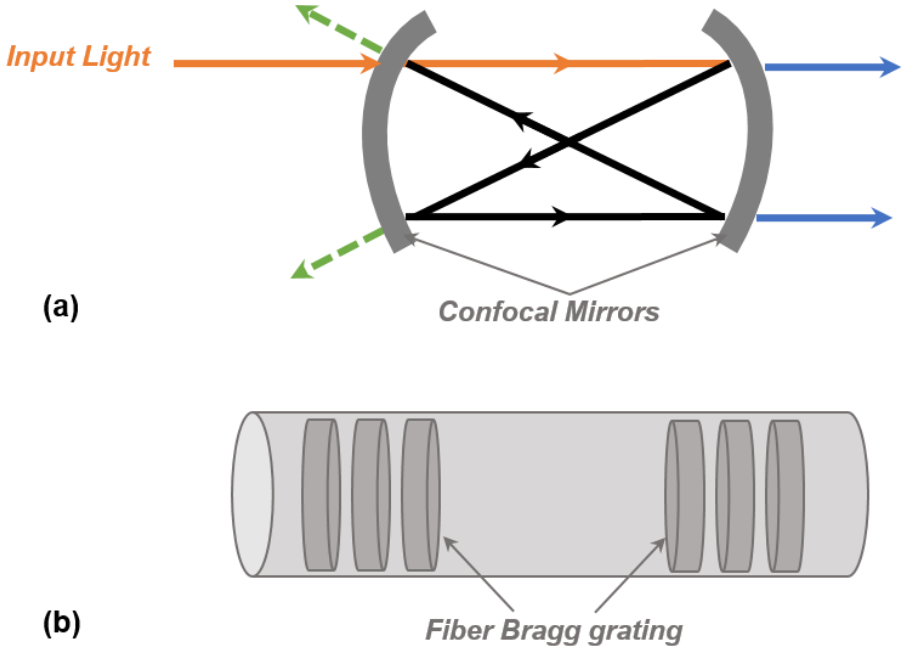

Figure II-1 (a) Basic configuration of a wave propagating in a confocal Fabry-Perot resonator; (b) Fabry-Perot resonator based on a fiber Bragg grating.

When the reflective coefficient is equal to 0.99, the storage time is increased by 199 (i.e. τ_{eff}= 199 τ_d), and that is to say that for a given required energy storage time τ_{eff}, the fiber length needed is reduced by 199 times. For instance, a fiber Fabry-Perot resonator with a 20 m long fiber can be used to have an effective delay time equivalent to a delay by a 3 km long fiber.

II.2.b Whispering-gallery mode resonator

Another attractive class of optical resonators exploits the confinement of light beams in dielectric structures having circular symmetry that support optical Whispering Gallery Modes (WGM). In an optical WGM resonator, the light is trapped in a circling orbit supported by total internal reflections from boundaries of the resonator.

They feature outstanding properties, like extremely small mode volume, very high power density, and exceptional Q factor values, if they are designed with smooth dielectric-air interface and using low loss optical materials. Q factors ranging from 10^8 to 10^{11} have been obtained with these type of resonators [19-21].

WGM resonators exist in a variety of geometrical structures that have been extensively studied and investigated from the simplest ones going to more exotic structures. Among these geometries, the most common ones are the cylindrical [22], microspheres [23], microdisks [24], and microtoroidal [25] resonators. Furthermore, they can be fabricated from several materials, such as silicon [26], fused silica [27], calcium fluoride (CaF_2) [28], magnesium fluoride (MgF_2) [29] and other optical glasses and crystals. Each has its unique features and limitations. So, in order to properly choose the right geometry together with the appropriate material, three major parameters must be considered: the loaded Q-factor, the easiness of fabrication and the integrability [19].

For system compactness, it can be interesting to study resonators made in electro-optics materials, such as WGM resonators made of lithium niobate ($LiNbO_3$). These resonators can combine the filtering and phase stabilizing function of a resonator together with a low V_π RF modulator [30,31]. The Q factor in these resonators is however a bit lower than the one observed in other crystalline materials, such as CaF_2 or MgF_2.

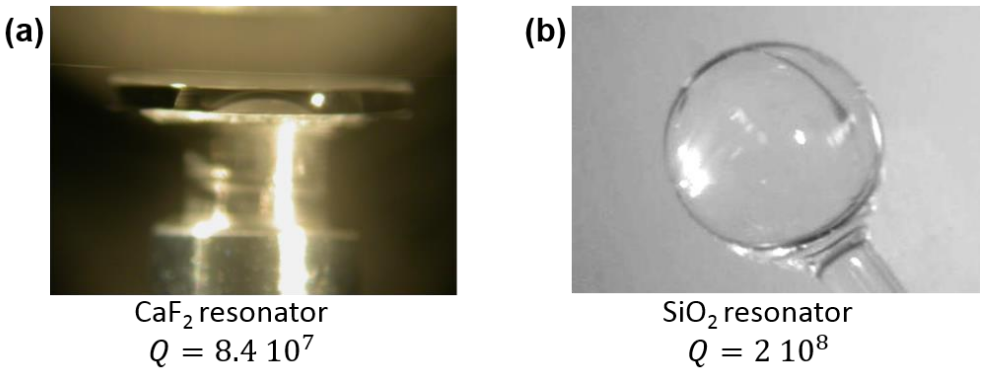

Figure II-2 (a) 5.5 mm whispering gallery mode CaF_2 disk resonator [32]; (b) whispering gallery mode SiO_2 3.3 mm minisphere resonator [33].

Figure II-2 provides two examples of whispering gallery mode resonators that have been characterized in LAAS-CNRS laboratory. The first one (Figure II-2 (a)), is a disk WGM resonator based on calcium fluoride (CaF_2) with a diameter of 5.5 mm. It has been fabricated in CNR-IFAC (Firenze, Italy) and features a Q_{opt} factor of 8.4 10^7 [32]. The second one (Figure II-2 (b)) is a minisphere WGM resonator based on silica (SiO_2) with a 3.3 mm in diameter; it has been fabricated in ENSSAT-FOTON (Lannion, France), and demonstrated a value of 2 10^8 for Q_{opt} factor [32,33].

However, the main disadvantage of these type of resonators lies first in the coupling techniques, and secondly in the excitation and selection of a precise resonant mode. Coupling is made using the evanescent field of the resonator by putting it close to a stretched fiber or a prism. This requires a sub-micrometer range tuning of the distance between the resonator and the coupling element. The stretched fiber technique is an efficient laboratory technique, but it is still difficult to imagine this technique performing in a real environment (particularly in

embedded systems). The prism technique has already been used in compact designs, but only one society up to now is able to provide such assembly which requires nano-scale mechanical techniques. On the side of the resonant modes, multiple optical frequency resonances combs co-exist in these resonators for both transverse electric (TE) and transverse magnetic (TM) modes. It is thus difficult to be able to select one mode, and an all-fiber polarization controller should be used before the WGM resonator.

II.2.c Fiber ring resonator

Another type of resonator featuring such a high Q factor is the fiber ring resonator (FRR) [34-36]. These devices can be constructed in a variety of sizes but still their sizes are bigger than the spheres or disks. However, their planar geometry makes them potentially usable in many systems, including embedded systems.

Fiber ring resonator can be easily constructed from standard optical components. Generally, this resonator is realized with one or two low loss fibered optical directional couplers that are linked with an optical fiber (Figure II-3). With a FRR, the resonator coupling difficulties are solved using these low loss fiber couplers. The quality factor of these resonators is dependent on the additional losses in the couplers, in the fiber fusion splices and on the longitudinal fiber losses. However, they can reach a relatively high quality factor ($Q_{opt} > 10^9$).

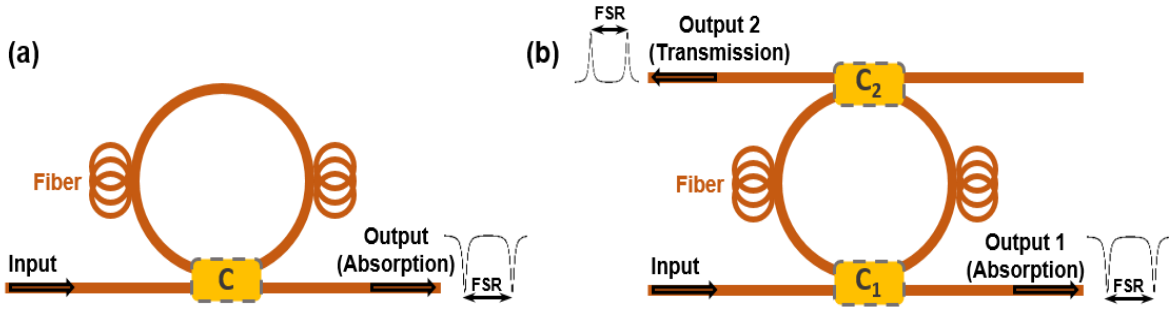

Figure II-3 (a) Direct coupling fiber ring resonator; (b) double coupler Add/Drop ring resonator; C: optical coupler.

The Add/Drop configuration of a FRR is the one used in the optoelectronic oscillator system. Using this configuration, the resonance occurs if the total integrated phase shift of the incident light wave around the resonator ring is an integer multiple of 2π (rad). So in this case, the incident light wave constructively interferes with its replica coming from the third port of C_1 after a round trip inside the resonator (see Figure II-4). Thus, the circulating light build-up to a high transmission peak at the resonator's second output (Output 2 in Figure II-3 (b)) since the two light waves are in phase. At the resonator's first output (Output 1), the interference is destructive if the transmitted waves are out-of-phase and this corresponds to a transmission minimum [37].

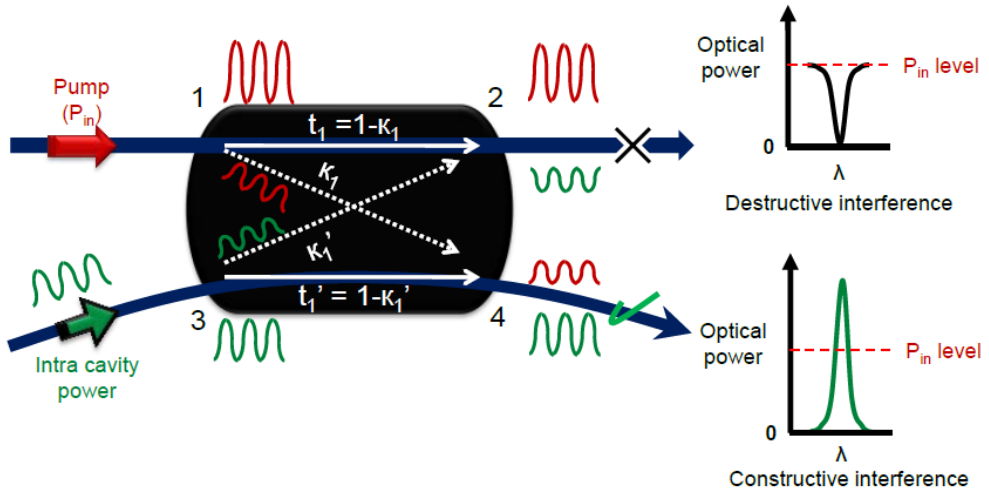

Figure II-4 [37] Illustration of the constructive and destructive interferences at the input coupler C_1, when the laser frequency is resonant inside the resonator.

The free spectral range FSR of these fiber ring resonator can be computed like the one of the optical delay line. It is linked to the total fiber length (L) in the ring, and to its refractive index (n) ($FSR = c/nL$, equation I.9). However, for the same equivalent Q factor, the FSR of the fiber ring resonator is much larger than the one of the delay line. Indeed, the resonator is equivalent to a delay line that has been folded and in which the signal is recirculating many times. Therefore, the spurious peaks that are observed on the delay line OEOs are shifted towards much higher frequency offsets in the fiber resonator based OEO. As an example, a 20 m ring resonator, featuring a Q factor of 3 10^9, will result in an FSR of 10 MHz, meanwhile the same performance in Q can be obtained with a 1 km delay which will feature a FSR of 200 kHz, and thus spurious peaks every 200 kHz from the carrier.

The full-width at half-maximum ($FWHM$) $\Delta f_{1/2}$ of a resonator is expressed as a ratio of the FSR to the finesse (F) of the resonator:

$$\Delta f_{1/2} = {FSR}/{F} \tag{II.2}$$

From equation (II.2), it is clear that the resonance $FWHM$ is inversely proportional to the finesse (F), and since the finesse decreases with increasing losses in the resonator, the spectral width increases with increasing loss. Thus, when the finesse is large ($F \gg 1$), the resonator spectral response is sharply peaked at the resonance frequencies (f_{Res}), and so the resonator is more sensitive to small fluctuations in the incident laser frequency.

The resonator's Q factor can be deduced from the resonance $FWHM$ ($\Delta f_{1/2}$) thanks to the following formula:

$$Q = \nu_0 / \Delta f_{1/2} \tag{II.3}$$

where $\nu_0 = w_0/2\pi$ is the optical frequency.

As discussed in chapter I, the microwave quality factor is proportional to the optical quality factor of the resonator (equation I.13), so in order to get a high Q_{RF}, a very high Q_{opt} resonator is needed, and that is to say a relatively long fiber ring (L) has to be chosen. On the other hand, a high Q_{opt} resonator may cause an increase of the power inside the cavity, which in return reduces the thresholds of many nonlinear optical effects. All these effects and instability will affect the phase noise performance of the optoelectronic oscillator, as we will see in the following chapters,

II.3 Analytical model of an optical ring resonator

As first established by A. Yariv [38,39], a simple and ideal description of an optical resonator in linear regime is depicted as monomode straight and ringing waveguides connected together through an ideal coupler (Figure II-5 (a)). This resonator can be characterized by three essential parameters: the coupler direct transmission coefficient ($\rho \in [0,1]$), the roundtrip attenuation or amplitude amplification coefficient (α, real positive number) and ring roundtrip phase or known also as the phase shift (φ). The temporal dependence is given as e^{jwt}.

By varying α and/or ρ coefficient, the coupling regime is changed from the under-coupling to the selective amplification regimes (Figure II-5 (b)). If α < 1, the ring resonator has internal losses. This is likely to occur in the under-, over- and critical regimes; if α = 1, the resonator's output is equal to its input, which is known as transparency regime; if α > 1, the ring behaves as an amplifier and the regime is known as selective amplification. However, α can't be greater than a threshold value corresponding to the system's oscillation: $\alpha_{th} = 1/\rho$.

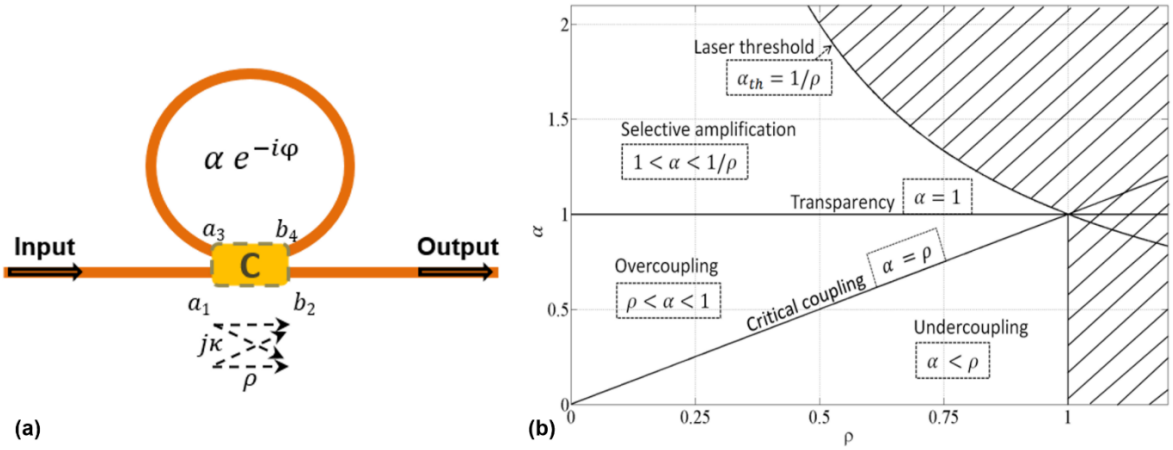

Figure II-5 (a) The generic geometry for waveguide ring resonator; C: optical coupler. (b) Representation of the different coupling regimes as a function of α and ρ.

Using the same formalism as Yariv, which is a frequency approach, and under the conditions that a single unidirectional mode of the resonator is excited and that the coupling is lossless, then the coupling can be described by a matrix relation and by means of two real constants k and ρ, and a unitary matrix:

$$\begin{bmatrix} b_2 \\ b_4 \end{bmatrix} = \begin{bmatrix} \rho & jk \\ jk & \rho \end{bmatrix} \begin{bmatrix} a_1 \\ a_3 \end{bmatrix} \tag{II.4}$$

$$|\rho^2| + |k^2| = 1 \tag{II.5}$$

where the complex mode amplitude b_i and a_i are normalized such that their squared magnitude corresponds to the modal power ($a_1 = 1$). In addition, these equations are completed by the transmission condition around the ring where:

$$a_3 = \alpha e^{-j\varphi} b_4 \tag{II.6}$$

and the propagation phase shift φ is expressed as follow:

$$\varphi = \frac{n_g L}{c} w \tag{II.7}$$

where n is the effective refractive index and L is the length of the ring resonator.

II.3.a Resonator's transfer function

Based on equations (II.4) and (II.6), the resonator's transfer function can be expressed as:

$$A(\varphi) = \frac{b_2}{a_1} = \frac{\rho - \alpha\, e^{-j\varphi}}{1 - \alpha\rho\, e^{-j\varphi}} = |A(\varphi)|\, e^{j\phi} \tag{II.8}$$

and the intensity absorption ($|A(\varphi)|^2$) and the structural phase ($\phi(\varphi)$) of the resonator are readily expressed from equation (II.8) as,

$$|A(\varphi)|^2 = \frac{\alpha^2 + \rho^2 - 2\alpha\rho\cos(\varphi)}{(\alpha\rho)^2 + 1 - 2\alpha\rho\cos(\varphi)} \tag{II.9}$$

$$\phi(\varphi) = arctan\left(\frac{\alpha\sin(\varphi)}{\rho - \alpha\cos(\varphi)}\right) - arctan\left(\frac{\alpha\rho\sin(\varphi)}{1 - \alpha\rho\cos(\varphi)}\right) + K \tag{II.10}$$

where K denotes a real positive constant.

A particular attention has to be paid to the phase slope F_D given by:

$$F_D = \left.\frac{d\phi(\varphi)}{d\varphi}\right|_{\varphi=0} = \frac{\alpha(1-\rho^2)}{(1-\alpha\rho)(\rho-\alpha)} \tag{II.11}$$

and to its sign at resonance $\phi(\varphi = m2\pi)$, where m is some integer. In fact, the sign of F_D, positive or negative, refers to "fast light" regime ($\tau_g < 0$) , and "slow light" regime ($\tau_g > 0$) [40-42], respectively, since the group delay time (τ_g) is calculated as a function of the phase shift $\varphi(w)$ as [43]:

$$\tau_g = -\left.\frac{d\phi(w)}{dw}\right|_{\varphi=0} \tag{II.12}$$

Fast and slow light are explained as interference effects between ballistic light through the coupler ($E_b = \rho.a_1$) and circulated light within the ring fiber ($E_c = k.a_3$) [44]. Furthermore, the dispersion, which can be characterized by the group delay time, depends strongly on the coupling coefficient (ρ) and the round-trip loss (α). This means that the dispersion could be controlled and changed through ρ and α, and that is important in applications where the coupling coefficient is dynamically controlled by electro-optical effects or nonlinear optical effects [41].

Furthermore, the resonator $FWHM$ ($\Delta f_{1/2}$) is linked to the transmission intensity at half-maximum ($\left|A_{1/2}\right|^2$), which is given from equation (II.9) by

$$\left|A_{1/2}\right|^2 = \frac{|A_{max}|^2 + |A_{min}|^2}{2} = \frac{\alpha^2 + \rho^2 - 4(\alpha\rho)^2 + (\alpha^2\rho)^2 + (\alpha\rho^2)^2}{(1-(\alpha\rho)^2)^2} \quad \text{(II.13)}$$

where $|A_{max}|^2$ is the maximum transmission intensity at a far-off resonance frequency (i.e. $|A_{max}|^2 = |A(\varphi)|^2|_{\varphi=\pi} = \frac{(\alpha+\rho)^2}{(1+\alpha\rho)^2}$) and $|A_{min}|^2$ is the minimum transmission intensity at the resonance frequency (i.e. $|A_{min}|^2 = |A(\varphi)|^2|_{\varphi=0} = \frac{(\alpha-\rho)^2}{(1-\alpha\rho)^2}$). And the transmission intensity at half-maximum can also be expressed as:

$$\left|A_{1/2}\right|^2 = |A(\varphi)|^2|_{\varphi=\varphi_{1/2}} = \frac{\alpha^2 + \rho^2 - 2\alpha\rho\cos(\varphi_{1/2})}{(\alpha\rho)^2 + 1 - 2\alpha\rho\cos(\varphi_{1/2})} \quad \text{(II.14)}$$

The phase shift at half-maximum ($\varphi_{1/2}$) can be directly determined by using the equality between equations (II.13) and (II.14):

$$\varphi_{1/2} = arccos\left(\frac{2\alpha\rho}{1+(\alpha\rho)^2}\right) \quad \text{(II.15)}$$

Therefore, $FWHM$ ($\Delta f_{1/2}$) can be expressed, from equation (II.7) and (II.15), as follow:

$$\Delta f_{1/2} = \frac{c}{\pi n_g L} arccos\left(\frac{2\alpha\rho}{1+(\alpha\rho)^2}\right) \quad \text{(II.16)}$$

This relation implies that the resonator $FWHM$ ($\Delta f_{1/2}$) is affected severally by the coupling coefficient and by the losses in the resonator. In addition, it shows a monotonous decrease of $\Delta f_{1/2}$ as $\alpha\rho$ tends to 1 (laser oscillation regime threshold), and that is to say that the phase shift at half-maximum $\varphi_{1/2}$ will decrease between $[\pi/2, 0[$ when the product $\alpha\rho$ increases between $[0,1[$.

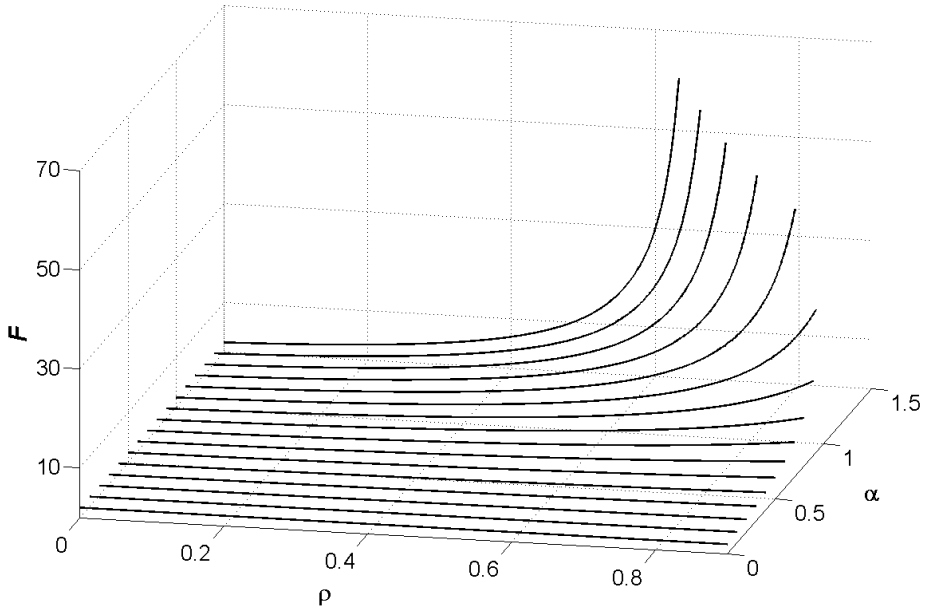

Figure II-6 Finesse F of a fiber ring resonator, in function of ρ and α parameters. $L = 10.27m$.

Taking into account the importance of the finesse parameter, since it is used to evaluate the sharpness and the resonator quality factor at resonance, it is worth to point out that the finesse increases as the coupling regime varies from under-coupling to selective amplification regime, and even more remarkably, it increases strongly as the resonator approaches the laser oscillation threshold, as it is shown in Figure II-6.

At under-coupling regime, shown in Figure II-7, the transmission minimum at the resonance frequency decreases progressively towards zero (zero at the critical coupling), the transmission maximum increases as α increases, and in addition the slope of the overall phase transition become steeper. In fact, when $\alpha < \rho$, the circulated light component is smaller than the ballistic light component, so the additional circulated light (as α increased) will slightly change the phase of the overall transmitted light. On this condition, the slope of the phase transition is positive around the resonance and shows an anomalous dispersion (where $\tau_g < 0$), which is related to the "fast light" regime. When the loss parameter and the transmission parameter become equal ($\alpha = \rho$), the transmission minimum becomes zero, and that is when critical coupling regime occurs. In under-coupling regime and at critical coupling $K = 0$ (in equation (II.10), and therefore $\phi \in [-\pi/2, \pi/2]$. It is noteworthy that F_D is not defined for the critical coupling since $\phi(\varphi)$ is discontinuous for $\varphi = m2\pi$.

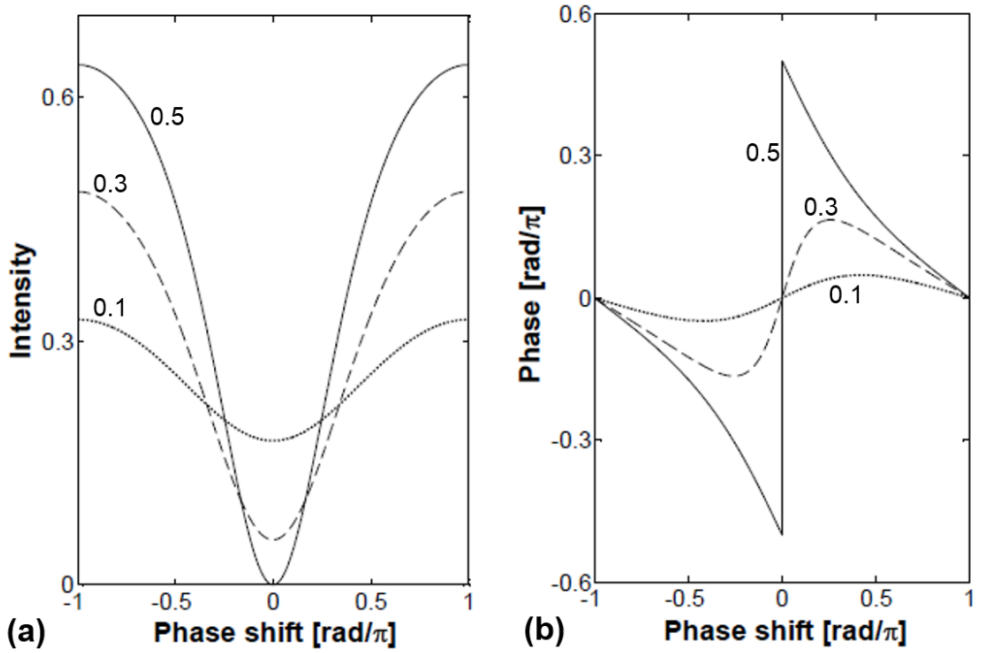

Figure II-7 (a) The transmission intensity and (b) the transmitted phase as a function of the phase shift on the under-coupling condition for an fixed $\rho = 0.5$ *and for different* $\alpha = 0.1, 0.3$ *and* 0.5*.* $L = 10.27m$*.*

When α is further increased, as $\rho < \alpha < 1$, the coupling enters the over-coupling regime (see Figure II-8 (a) and (b)). In this regime, the circulated light is the major component in the total transmitted light and this could explain the increases of the transmission minimum when α tends toward 1, and the negative slope observed, in addition the transmission maximum rises towards 1 as α increases. In contrast to the under-coupling condition, the group delay becomes positive and the normal dispersion occurs. This is related to the “slow light” regime.

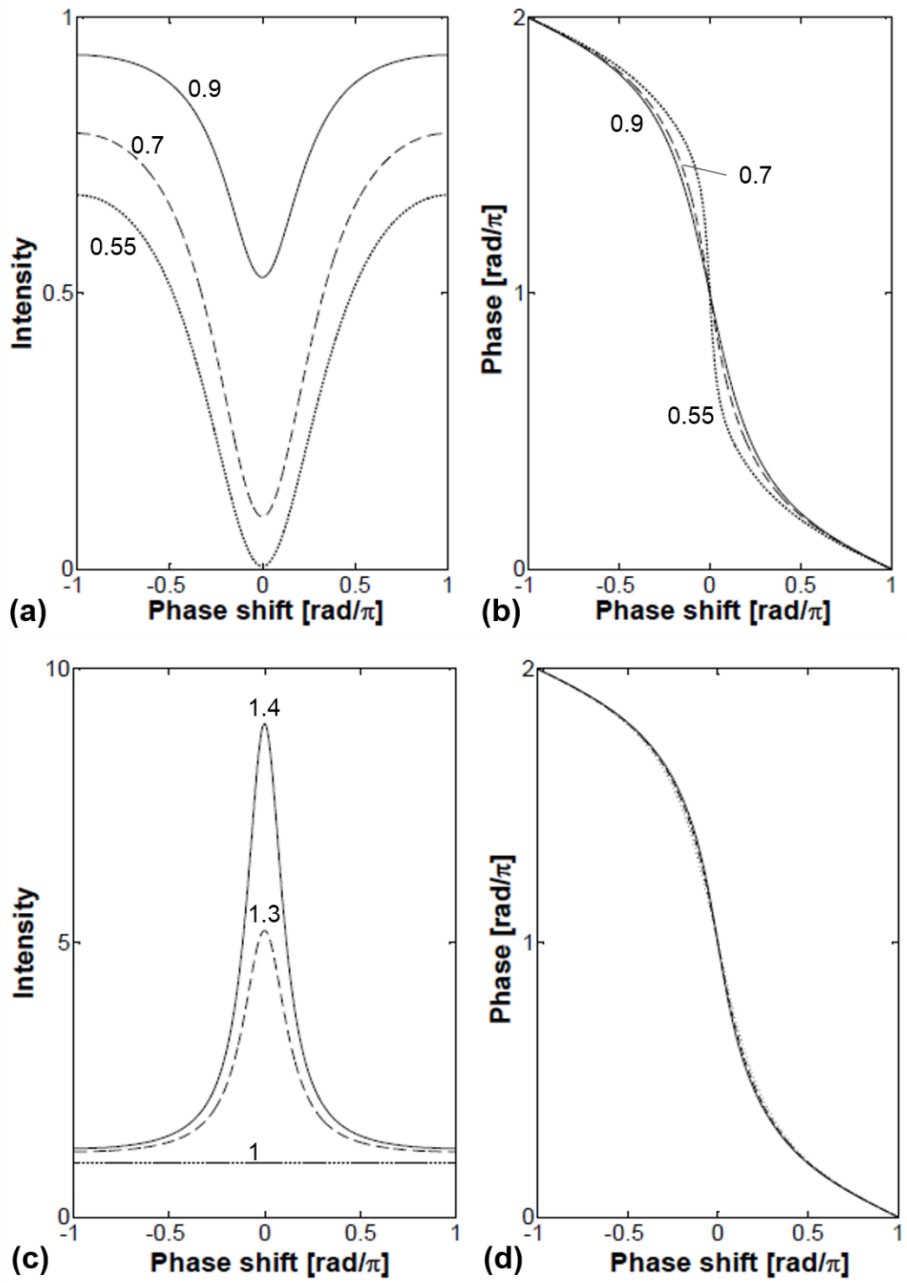

Figure II-8 (a) The transmission intensity and (b) the transmitted phase as a function of the phase shift on the over-coupling condition for an fixed $\rho = 0.5$ and for different $\alpha = 0.55, 0.7\ and\ 0.9$. (c) The transmission intensity and (d) the transmitted phase on the transparent condition for $\alpha = 1$ and on the selective amplification regime for $\alpha = 1.2\ and\ 1.4$. $L = 10.27m$.

Once the roundtrip attenuation (α) reaches 1, the coupler is purely transparent; that is, no coupling occurs and the output power is equal to the input power (i.e. transparency regime). For $\alpha > 1$, the cavity acts like a selective amplifier, and the transmission intensity (Figure II-8 (c)) shows a gain peak at the resonance frequency. This gain increases with the increase of α and the slope of the phase transition becomes steeper. Clearly, as was the case in the

over-coupling regime, the phase profile shows a normal dispersion, that is to say a negative phase slope (i.e. positive group delay). In selective amplification, transparency or over-coupling regime, $K = 0$ when $\varphi \in [-\pi, -acos(\rho/\alpha)] \cup \left[acos\left(\frac{\rho}{\alpha}\right), \pi\right]$, $K = -\pi$ when $\varphi \in \left[-acos\left(\frac{\rho}{\alpha}\right), 0\right]$ and $K = \pi$ when $\varphi \in \left[0, acos\left(\frac{\rho}{\alpha}\right)\right]$ and therefore $\phi \in [0,2\pi]$ (Figure II-8 (b) and (d)). Finally, at the condition $\alpha\rho = 1$, the transmission diverges, placing the system in the laser oscillation regime.

Note that since one can get the same intensity profile at under- and over-coupling regimes (see equation (II.9), Figure II-7 (a) and Figure II-8 (a)), the phase profile will help to discriminate each regime, and that is why it is important to get the phase and the intensity profiles for a reliable characterization of the resonator.

These analytical descriptions show that a qualitative observation of both intensity and phase profile allows the determination of the coupling regime of the resonator, and thus of the relationship between the two parameters α and ρ describing the linear resonator. Last but not least, A. Yariv's formalism makes it possible to obtain the exact solution for the phase and intensity profiles without doing any assumption. It has to be noted that a high finesse cavity assumption was considered to estimate the Q factors of the resonator, as it is shown in the next section.

II.3.b Optical quality factors

The resonator's Q factor can be deduced from the resonator $FWHM$ measurement thanks to equation (II.3). The condition of $0 < \alpha\rho < 1$ and the exact expression of $\Delta f_{1/2}$, which is given by equation (II.16), yield to the following expression for the resonator's Q factor :

$$Q = w_0 \tau_L \left(2\ arccos\left[\frac{2\alpha\rho}{1 + (\alpha\rho)^2}\right]\right)^{-1} \quad \text{(II.17)}$$

where the constant $\tau_L = n_g L/c$ stands for the ring cavity roundtrip time. Excepted for transparency where $\Delta f_{1/2}$ is not defined ($A(\varphi) = 1$) because the resonator behaves as a purely dephasing component, equation (II.17) shows that the Q factor is getting higher as $\alpha\rho$ increases (Figure II-9).

In the specific case of high finesse resonators, it is usual to express the resonator's Q factor in terms of the intrinsic quality factor Q_0, which is characterized by the inside ring losses and corresponding to $\rho = 1$ in equation (II.17), and the external quality factor Q_e, which is linked to the couplers characteristics and obtained from the assumption of zero losses inside the ring, i.e. $\alpha = 1$ in equation (II.17), as

$$Q^{-1} = Q_0^{-1} + Q_e^{-1} \quad \text{(II.18)}$$

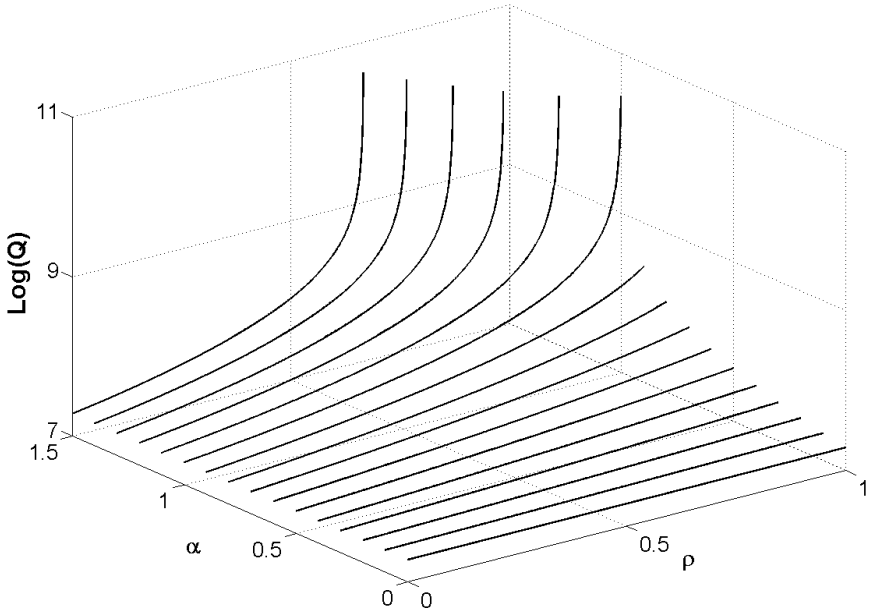

Figure II-9 (a) Optical quality factor (Q) in function of α and ρ parameters.

This Q factor expression, using Q_0 and Q_e with separated variables, makes the link between Yariv approach and H. Haus [45] phenomenological model.

For high finesse resonator, $\Delta f_{1/2}$ is small, and approximating $cos(\varphi)$ by its second order Taylor expansion $1-\varphi^2/2$ leads to the following expression for the resonator's Q factor, deduced from equation (II.17):

$$Q = \frac{w_0\,\tau_L\sqrt{1+\alpha^2\rho^2}}{2\sqrt{2}\,(1-\alpha\rho)} \tag{II.19}$$

Now, to express Q^{-1} as a sum in which the dependence on α and ρ is separated, the second order mixed derivative of Q^{-1} with respect to α and ρ must be zero. This rigorously happens if and only if $\alpha\rho = 1$, but the decomposition into two separated functions can be assumed for $\alpha\rho \cong 1$, which agrees with the high finesse assumption. Elementary differential calculus shows that the expressions of Q_0 and Q_e are then

$$Q_0 = -\frac{w_0\,\tau_L}{2\ln(\alpha)} \tag{II.20}$$

$$Q_e = -\frac{w_0\,\tau_L}{2\ln(\rho)} \tag{II.21}$$

II.3.c Intra-cavity power enhancement factor

It is desirable to control the intra-cavity power inside the resonator by quantifying its intra-cavity power enhancement factor ($IPEF$) as a function of α and ρ (equation (II.22)), since due to the intra-cavity power build up at resonance, many nonlinear optical effects are

generated inside the resonator, for example the stimulated Brillouin scattering, which may be harmful [12] or beneficial [46] depending on the application.

In the case of a passive cavity (i.e. $\alpha < 1$), $IPEF$ reaches its maximum in the critical coupling regime ($\rho = \alpha$). However, in the case of an active cavity (i.e. $\alpha > 1$), $IPEF$ increases remarkably as the resonator approaches the laser oscillation threshold ($\rho = 1/\alpha_{th}$) (Figure II-10).

$$IPEF = \frac{|b_4|^2}{|a_1|^2}\bigg|_{\varphi=0} = \frac{1-\rho^2}{(1-\alpha\rho)^2}\bigg|_{\varphi=0} \tag{II.22}$$

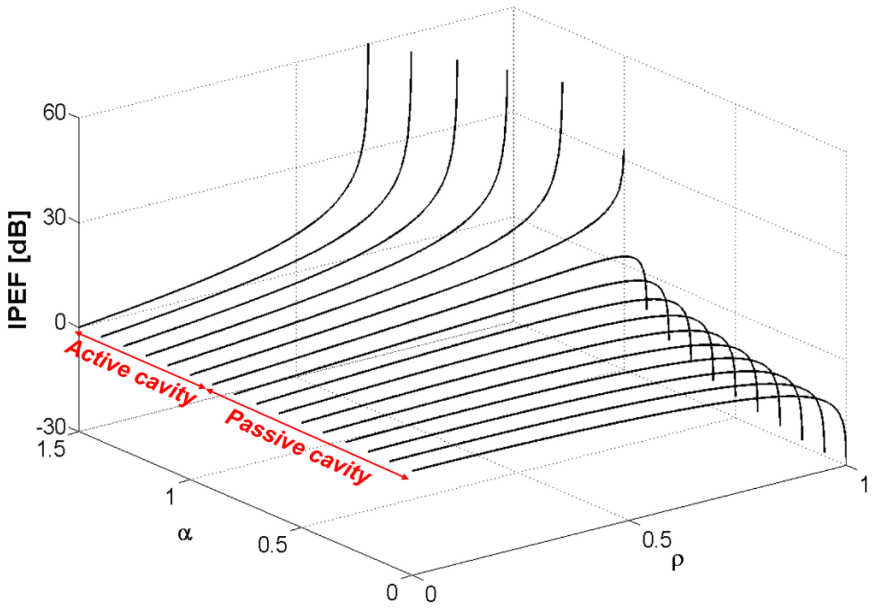

Figure II-10 Intra-cavity enhancement factor ($IPEF$) in function of α and ρ parameters.

II.4 Characterization techniques

The optical resonator should be experimentally characterized in order to determine the coupling regime and to measure its real parameters, especially its free spectral range (FSR), full-width at half-maximum ($\Delta f_{1/2}$), loaded optical quality factor (Q), transmission or rejection losses and its phase versus frequency slope. Therefore, the extraction of other parameters can be carried out by solving the different equations described in the above section. These parameters include the intrinsic quality factor (Q_0), external quality factor (Q_e), intra-cavity losses (α), transmission coefficient (ρ), and last but not least its intra-cavity power enhancement factor ($IPEF$).

In a high Q factor resonator, it is difficult to induce a sufficient amount of light from conventional lasers. For example, a Q factor of 10^9 near $\lambda = 1550$ nm results in a 3-dB

bandwidth of 200 kHz, which is lower than the spectral width of a semiconductor laser. Using a high spectral purity laser (such as a fiber laser) can be part of the solution. However, when the laser light is injected in the resonator, it heats the resonator (even at low power, because of the photons lifetime), the resonator frequency is thus shifted, and consequently, the signal is lost.

To address these problems, several techniques have been investigated to accurately measure the resonator properties. These techniques are either based on optical domain approaches or on radio frequency domain approaches. The first one is the wavelength scan method, which uses the slow tuning of a high spectral purity laser to scan the resonant modes. The second one is the cavity ring down method, which is a time domain approach. And the third one is a microwave domain characterization approach, which features an extremely high spectral resolution. These methods are detailed below, focusing specially on the microwave domain characterization technique.

II.4.a Wavelength scan method

The scan method consists in scanning the laser frequency to explore the frequency comb. The laser must feature a narrow enough linewidth to go through the resonance, which is not always obvious with high Q factors. A resonator with a Q factor of 2 10^9 at 1550 nm features a 3 dB bandwidth in the range of 100 kHz, and cannot be scanned with, as an example, a semiconductor laser.

In this case, an amplified erbium-doped fiber laser can be used. At LAAS, a Koheras Adjustik laser is used to this purpose. It is tunable on a frequency range of 120 GHz thanks to the variation of its temperature. Moreover, a more accurate piezoelectric control can be used (on a 2 GHz range). This laser presents also a very narrow linewidth, of about 1 kHz, that allows a precise observation of one optical resonant mode and of its width. For moderately high Q factors, this method provides a good measurement of the free spectral range (FSR), and a good estimation of the optical quality factor. Figure II-11 (a) shows the results obtained on a 1 m long fiber ring resonator with a $FWHM$ ($\Delta f_{1/2}$) of 2.72 MHz and a Q_{opt} of 7.1 10^7 [33].

However, the precision of such measurement is not only limited by the laser linewidth, but also by the frequency shift due to the self-heating, that is very difficult to control when measuring ultra-high Q and/or small volume devices, even when using very slow frequency scan and reduced laser power. This frequency shift even occurs in high Q fiber ring resonator (Q_{opt} > 10^9) [33]. Consequently, the result is a strong dissymmetry between a scan performed with an increasing frequency and another one with a decreasing frequency. Under these conditions, the Q factor is overestimated on one side, and underestimated on the other side [33]. Figure II-11 (b) and (c) depicts an example of the optical scan method problem. When the laser's wavelength is decreasing during the scan, the resonator is very narrow since the thermal effect is opposed to the laser shift (Figure II-11 (b)). In the opposite case, i.e. when the laser's wavelength is increasing, the resonance becomes wide because the resonance

frequency is following the laser frequency (Figure II-11 (c)). Same results on WGM resonators are presented in [47]. Therefore, to characterize ultra-high Q resonators, dedicated techniques have been set up.

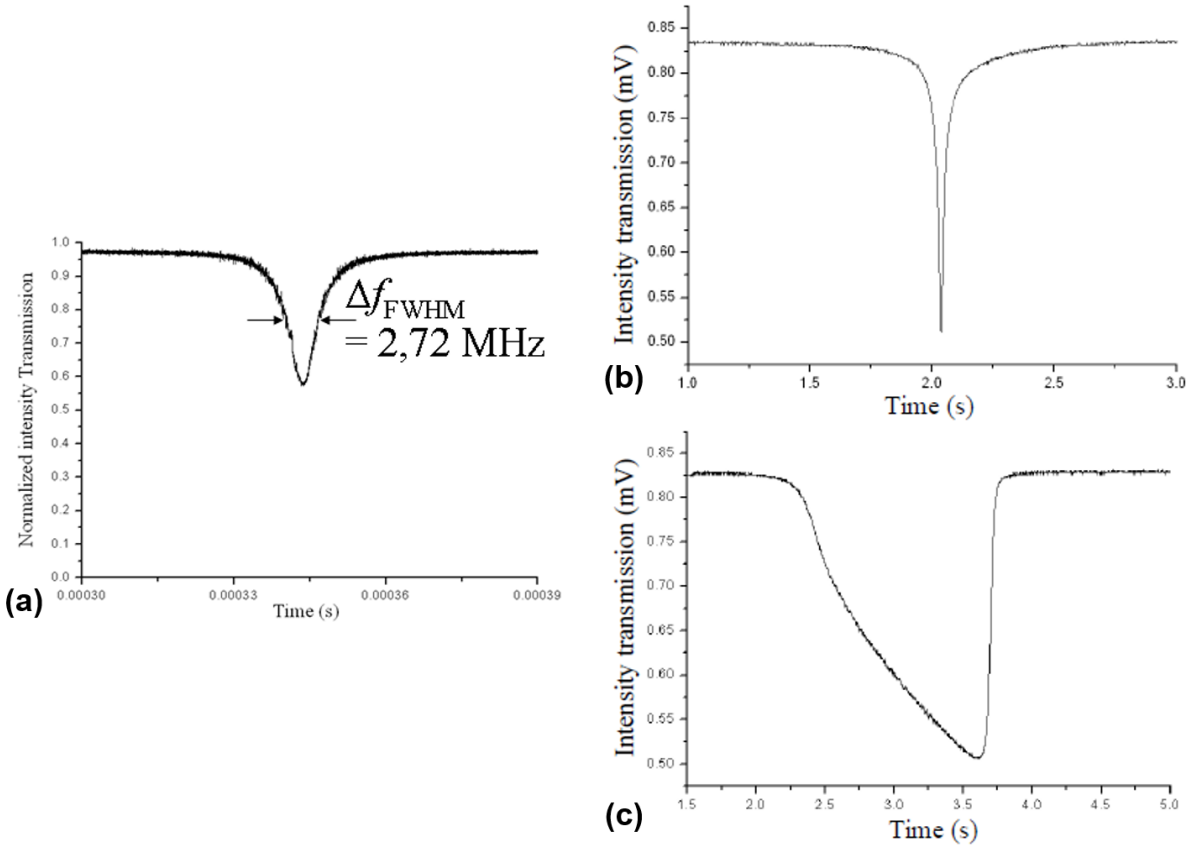

Figure II-11 [33] (a)Wavelength scan measurement of a 1m long fiber ring resonator, the measured $FWHM$ of 2.72MHz corresponds to a $Q = 7.1\ 10^7$(b) Thermal effects on a high Q fiber ring resonator during a wavelength scan: increase or (c) decrease of the laser frequency.

II.4.b Cavity ring down method

The cavity ring down method [29,48,49] avoids the difficulty of the comparison between the laser linewidth and the resonant mode, because the measurement occurs directly in the time domain. The principle is the same as for the scan method, but in this case the laser frequency is quickly tuned with a controlled frequency sweep speed.

It is based on the measurement of the photon lifetime inside the resonant cavity by studying its relaxation regime. This technique is mostly applied to measure resonators with very high intrinsic finesse without the use of a stabilized laser. It provides not only the state of the resonator coupling regime but also the different contribution of the resonator's parameters to its global loaded optical Q factor as well, that is to say, the intrinsic or unloaded factor Q_0 and the external factor Q_e. Nevertheless, this method, based on Haus formalism, can only be accurate with resonator's quality factor higher than 10^7 and must include a least square fitting method to recover the amplitude and phase transition.

An example of the measurement result that can be obtained with a fiber ring resonator is shown in Figure II-12. This measurement has been performed at ENSSAT Lannion (France) with a 20 m long fiber ring resonator featuring an intrinsic quality factor (Q_0) of $5.1\ 10^9$ and an external quality factor (Q_e) of $9.1\ 10^9$, which means that the resonator is in an under-coupling regime ($Q_e > Q_0$). Based on equation (II.8), the loaded Q_{opt} is calculated and is equal to $3.3\ 10^9$.

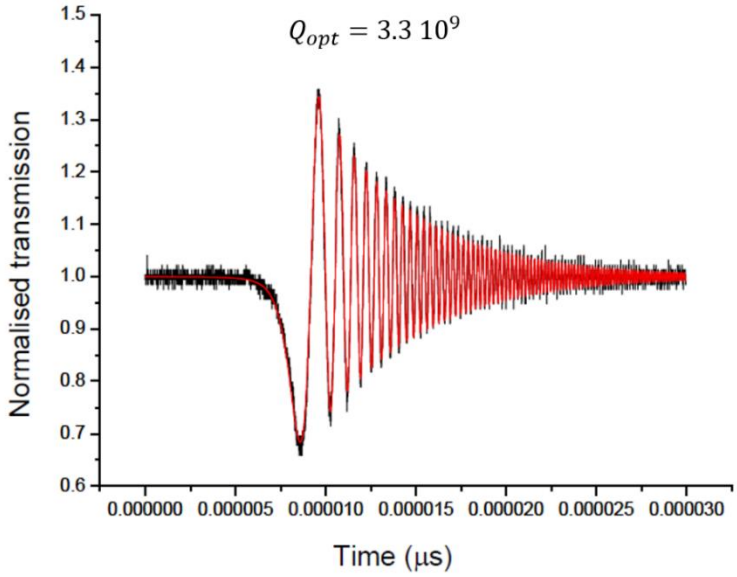

Figure II-12 Cavity ring down measurement of a 20m long fiber ring resonator (Foton-ENSSAT, Lannion)

II.4.c Radio frequency spectral characterization technique

The RF spectral characterization approach [32] gives directly the resonator transfer function. It is indeed based on a technique which transfers the optical resonances down to the radio frequency domain, and thus allows their measurement with electrical techniques, and more precisely using a microwave Vector Network analyzer (VNA). Both the amplitude and phase of the optical resonance can be measured with a very high frequency precision, as good as 1 Hz, which is much higher than any other technique available in the optical domain. This technique has been used to characterize several types of resonators, featuring Q_{opt} factors ranging from 10^6 to 10^{10}.

Another advantage of this technique, especially in the optoelectronic oscillator case, is that its setup is very similar to the OEO system, but in open-loop configuration. Therefore, the resonator is characterized in a configuration which is as close as possible to the final system in which it will be used.

II.4.c.i Measurement setup

The microwave characterization bench is depicted in Figure II-13. This characterization starts once the laser is stabilized onto one of the resonator's resonant frequencies by using a low-frequency Pound-Drever-Hall (PDH) feedback loop [36,50-52], which is based on using the phase information of a laser signal passing through the resonator (this technique will be detailed in chapter IV).

Other techniques may be used to lock the laser and resonator frequencies, such as thermal lock [47] or direct optical lock [53,54], or a combination of both techniques [55]. However, these techniques are not well suited to the proposed characterization approach, firstly because the thermal lock involves a small shift between the resonator and the laser frequencies (in such a case, a single sideband modulator is needed to recover the resonator transfer function), and secondly because both techniques are not as stable as the PDH loop in case of a small room temperature drift. Also, the optical locking is only possible if a non-isolated laser is closely connected to the resonator, which is a hard to control configuration.

As soon as the laser is locked into one resonance, a sweeping low power RF signal (~10 GHz) coming out of VNA's port 1 (i.e. RF output) drives the Mach-Zehnder modulator (MZM), biased at $V_{\pi/2}$ in order to get a linear modulation. The resulting modulation optical sidebands travel along an all-fiber polarization controller so as to select TE (transverse electric) or TM (transverse magnetic) modes, and then go through the optical resonator side modes. The response is finally recovered on a fast photodiode (PD), with a sufficiently large bandwidth and analyzed on port 2 of the VNA (i.e. RF input port). Finally, the optical resonator's transfer function (amplitude and phase) is displayed on the VNA in the electrical domain.

If the laser is precisely stabilized at the resonance center, the RF response is the optical response translated to the RF domain thanks to the frequency mixing effect of the photodiode. Because it is not the mode on which the laser is locked which is measured, this technique is limited to the characterization of sufficiently large resonators, for which the FSR falls in a frequency range reachable by an optoelectronic modulator and a fast photodiode. Practically, it can be used up to a resonator FSR of about 50 GHz, which corresponds to circular resonators of about 1 mm in diameter (or a bit larger, depending on the optical index).

If the VNA has been correctly calibrated (see below), the RF losses at the resonant frequency are twice the optical losses in dB at the resonance center, due to the photodiode's quadratic detection. However, the overall slope of the transfer function is unchanged while it is brought back to the RF domain.

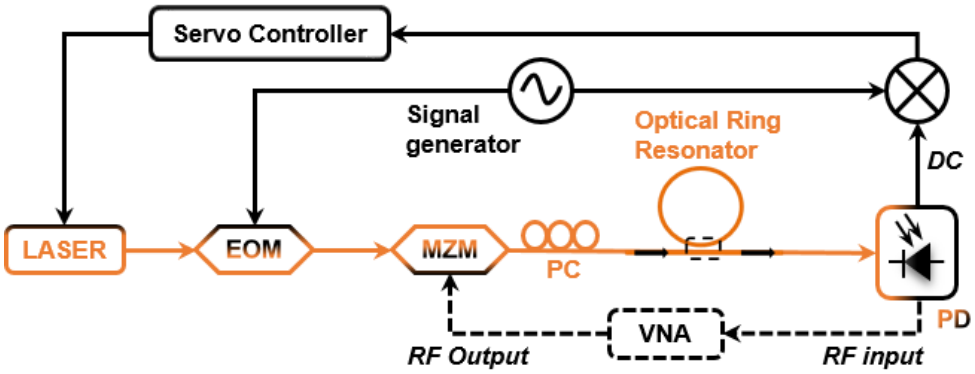

Figure II-13 Experimental setup of the microwave characterization technique using a vector network analyzer (VNA). EOM: electro-optic modulator; MZM: Mach-Zehnder modulator; PC: polarization controller; PD: photodiode.

Using this technique, any problem in the characterization bench is immediately detected via the resonance shape (amplitude of the transfer function). One major problem was identified in the locking process, where a possible shift between the laser's frequency and the resonator's resonant frequency may occur. Another possible problem could be the two states of polarization behavior of the optical carrier, leading to two optical modes propagation inside the resonator.

Furthermore, even though the VNA is a highly linear receiver featuring sufficient spectral purity, a number of imperfections may limit the measurement accuracy. Firstly, the laser must be precisely locked at the center of one resonance of the resonator. In case of a slightly laser detuning with the resonance, the beating response of the two lateral sidebands won't reproduce the complex transfer function of the resonator. On the VNA, two maximum are observed in this case on the resonance curve, together with a change in the phase slope at the center of the resonance.

This problem can be avoided thanks to the offset function of the PDH loop. Another solution would be to use a single sideband modulator in place of a conventional Mach-Zehnder modulator. This could be particularly useful in case of a dispersive resonator, for which the two lateral resonances under investigation may occur at different offset frequencies from the central one. However, this configuration is scarce on a frequency bandwidth reachable with electronic devices, i.e. below 50 GHz offset from the central resonance peak.

Secondly, one must calibrate the VNA in order to measure the transfer function without taking into account the effect of the access RF cables and optical fibers. This is performed by proceeding to a calibration when the resonator is bypassed by a short fiber. Then to cancel the remaining resonator's pigtail fiber length (l), a virtual time delay τ is added to the calibration correction such that $\tau = n_g l/c$. An inaccurate delay could affect the measurements, precisely the slope of the phase transition of the transfer function. However, in case of high Q resonators characterization, the possible error on the phase slope is

extremely small. As an example, a 1 cm error on a pigtail length will only lead to a relative error of 3 10^{-3} on the measured equivalent delay (and Q factor) of a $Q = 10^7$ resonator.

II.4.c.ii Measurement example

Figure II-14 (a) shows an example of such a measurement performed when the laser source (Koheras Adjustik E15 laser) is locked onto an active fiber ring resonator (described in II.5).

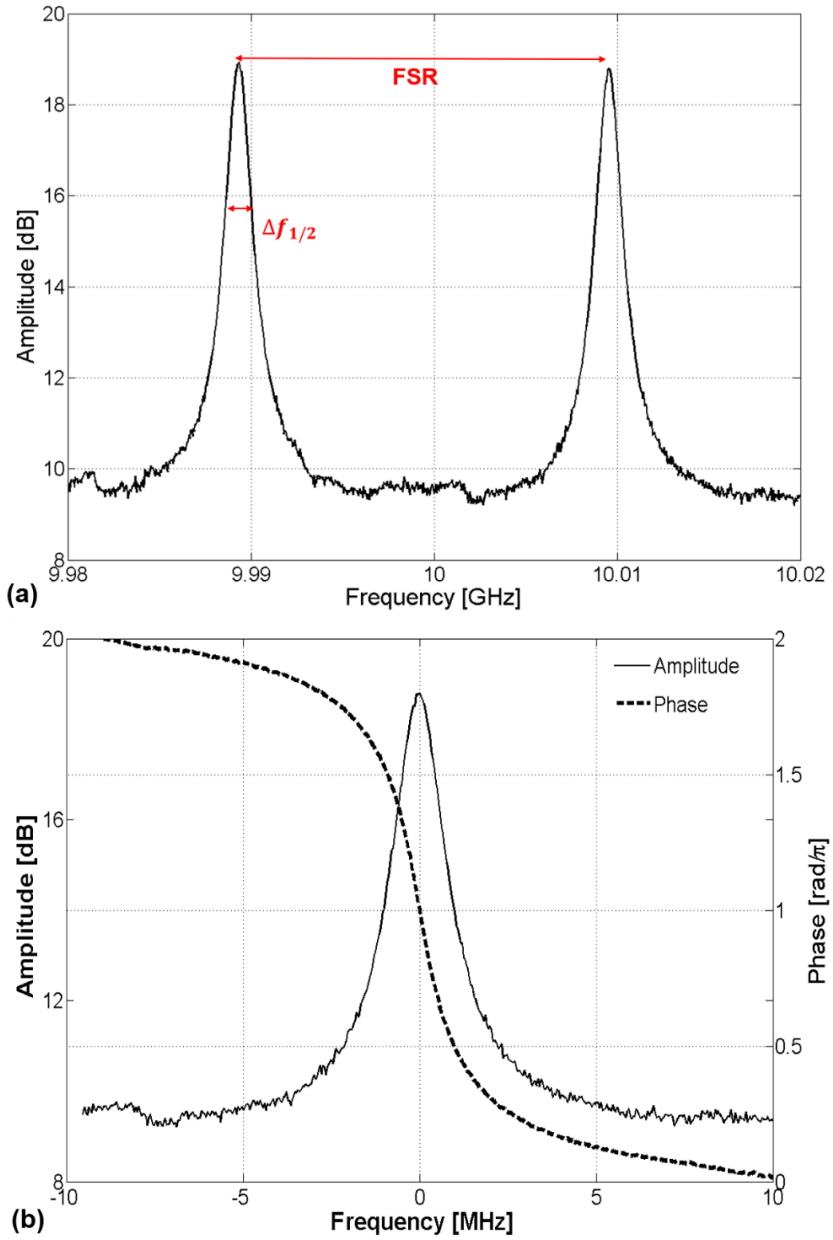

Figure II-14 (a) Transfer function of an active fiber ring resonator measured using the RF-spectrum characterization bench. (b) A focus on one resonance in the transfer function.

This response transcribes accurately the resonator frequency comb, and focusing on the amplitude response of some resonant modes (from 9.96 to 10.02 GHz in this case), gives access to the measurement of the resonator parameters like the free spectral range (FSR), $FWHM$ ($\Delta f_{1/2}$), Q_{opt} and the finesse F. Here, the measured Q_{opt} factor is 1.66 10^8, for ν_0 and $\Delta f_{1/2}$ equal to 193 THz and 1.16 MHz respectively.

The profile and slope of the phase transition (Figure II-14 (b)) at the resonance are as important as the amplitude response since they provide additional information and conditions to accurately identify the state of the resonator's coupling regime. Along with amplitude response, they can be fitted by the analytical expressions of the transfer function (equations (II.9) and (II.10)), so as to extract the main resonator's coefficients: ρ (or coupling coefficient κ), α and other different parameters.

II.5 Active fiber ring resonator and parameters extraction

An experiment has been carried out to demonstrate the validity of the RF-spectrum characterization technique and the analytical studies, using an active optical fiber ring resonator. Figure II-15 depicts the active optical resonator which was designed using a fibered 2x2 optical bidirectional coupler linked to a 2.1m-long erbium-doped (DrakaElite eHPW-9) fiber amplifier (variable gain). The coupler's transmission coefficient (ρ) is 50% (i.e. $\rho \cong 0.707$). An isolator is added to prevent backward reflections and to ensure unidirectional light wave propagation.

By varying the laser pump power (or current), it is possible to change the roundtrip cavity losses (α) of the resonator and therefore to control the coupling regime from under-coupling to over-coupling, and up to the selective amplification.

The laser used in this experiment is a fiber laser (Koheras Adjustik) with a very narrow linewidth (1 kHz) emitting at λ = 1550 nm. The laser lock on a resonance is achieved first by varying the laser temperature and then using a piezoelectric control input. Once locked, the amplitude and the phase of the resonator's output have been measured while varying the intra-cavity losses α (by changing the laser pump power, P_{Pump}), in order to assess the different coupling regimes.

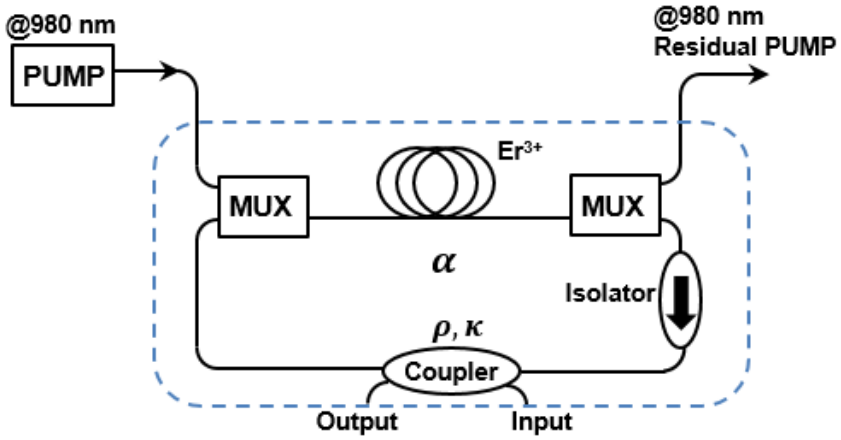

Figure II-15 Active fiber ring resonator configuration. MUX: multiplexing.

Figure II-14 (b) depicts the transfer function (amplitude and phase) for a pump power of 21.5 dBm. From its amplitude curve, which shows a gain peak, and its negative phase slope at the resonance, it is obvious that the resonator is in selective amplification regime.

Parameters extraction

The experimental data (amplitude and phase) are fitted with equations (II.9) and (II.10) using the least mean square algorithm, which is based on only two parameters, i.e. the intra-cavity losses (or gain) α and the transmission coefficient ρ. Figure II-16 shows the fitted and measured data for both the amplitude and phase of the output transfer function under two different laser pump powers (7.5 and 21.5 dBm). The α and ρ parameters are thus extracted from the numerical fitting method, and are presented in Table II.1.

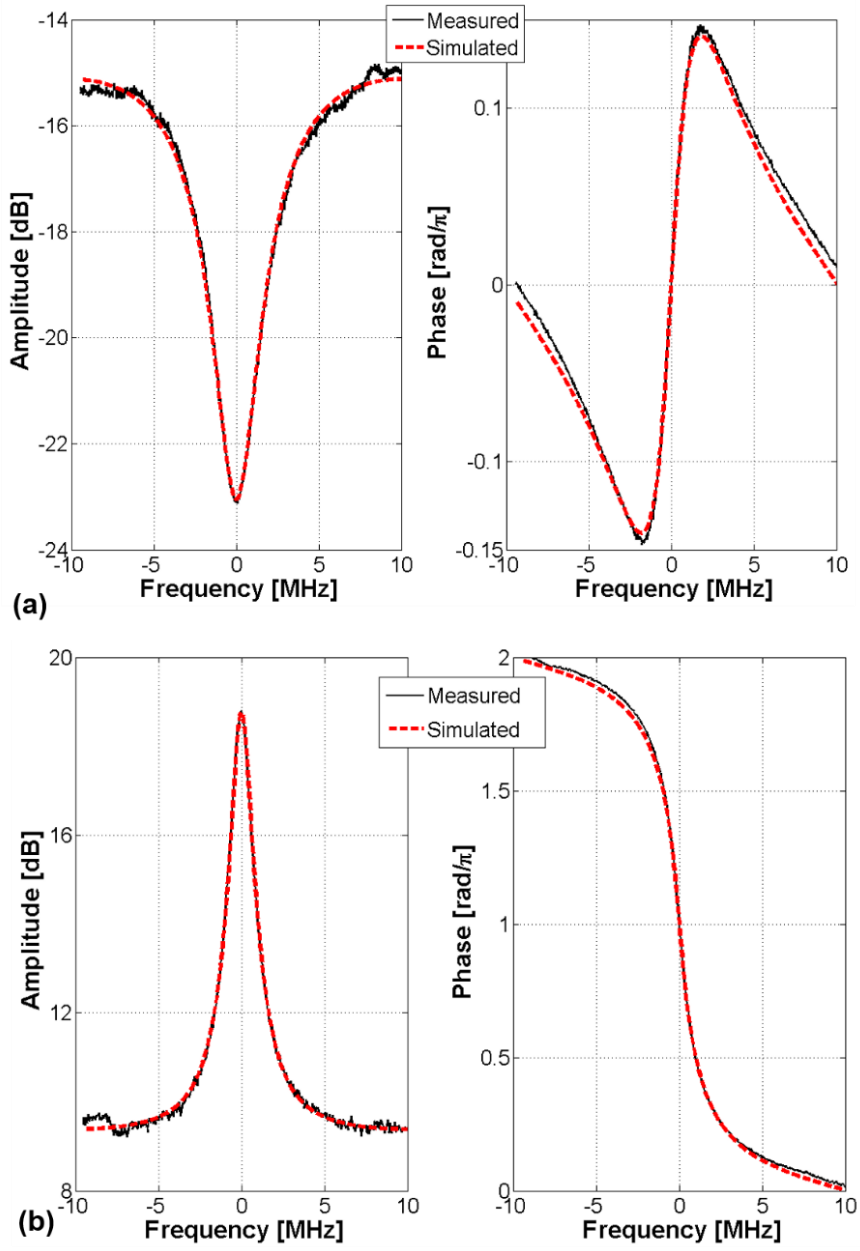

Figure II-16 Experimental data and curve fitting of the amplitude and phase of the output signal (a) $P_{pump} = 7.5\ dBm$, (b) $P_{pump} = 21.5\ dBm$.

For low laser pump power (7.5 dBm, i.e. low gain amplifier, Figure II-16 (a)), the resonator is in under-coupling regime, which means that the intra-cavity losses must be lower than the coupler transmission coefficient, i.e. $\alpha < \rho$. For high P_{Pump} (21.5 dBm, Figure II-16 (b)), precisely for $1 < \alpha < 1/\rho$, the selective amplification is obtained. Once α and ρ are obtained, Q_0 and Q_e factors can be calculated from equation (II.20) and (II.21), respectively, and Q values are then computed from equations (II.17) and (II.18). The obtained values of the fitting parameters meet well the conditions for each coupling regime.

When the resonator is in its selective amplification regime, α is a gain ($1 < \alpha < 1/\rho$) and the intrinsic quality factor Q_0 is negative. The computed Q values are compared to the measured data, 3.3 10^7 and 1.66 10^8 for 7.5 and 21.5 dBm of laser pump power, respectively, in order to obtain the error percentage. A good agreement is found between measured and computed values of Q from the extracted α and ρ data.

		P_{Pump}= 7.5 dBm	P_{Pump}= 21.5 dBm
α		0.503	1.2
ρ		0.72	0.69
Q_0		4.37 10^7	-1.65 10^8
Q_e		9.75 10^7	8.44 10^7
Q_{opt}	**Equation (II.17)**	≈ 3.43 10^7 (2% error)	≈ 1.6 10^8 (3.6% error)
	Equation (II.18)	≈ 3.17 10^7 (3% error)	≈ 1.72 10^8 (3.5% error)

Table II.1 Fitting parameters values for $P_{pump} = 7.5\ dBm$ and $P_{pump} = 21.5\ dBm$, the fitted Q_{opt} values are computed using equation (II.17) and (II.18) and then compared with the measured value for both cases.

It is notable that even though the cavity ring down approach allows to get the same parameters, the fitting procedure in the spectrum-RF approach allows a simple and more accurate extraction of the resonators' state and parameters. In fact, the modulus and phase transfer function are immediately observed with spectrum-RF method which is not the case with cavity ring down approach. This allows a visual and straightforward deduction of the coupling regime and of the relationship between α and ρ coefficients. This relationship is immediately fed to the least mean square algorithm as initial condition.

II.6 100m long passive fiber ring resonator

During the thesis of K. Saleh [37], a 100m long immunized fiber ring resonator (IFRR) has been implemented in order to suppress the stimulated Brillouin scattering (SBS). This IFRR is made of two fibered 2x2 optical directional couplers (with an 8% of coupling coefficient), linked with a single mode polarization-maintaining (P-M) fiber. In addition, an optical isolator has been inserted in the optical link, and an optical inline polarizer has been added at the resonator input. The polarizer will eliminate the possibility of two polarization states behavior of the optical carrier at the FRR input, since the P-M fibers in the resonator assembly can only maintain the carrier's states of polarization and do not ensure one and only polarization state behavior.

The optical isolator is an essential component which makes it possible to eliminate the SBS. In fact, when an isolator is inserted in a fiber of total length (L), with its own stimulated

Brillouin scattering threshold (SBST), the isolator virtually cuts the fiber into two new lengths (L_1 and L_2) regarding the Brillouin gain. Consequently, the SBS interaction between the fiber's two sections is absent and the fiber SBST is increased because it is replaced by two other SBSTs related to the new fiber sections, L_1 and L_2. Thus, the SBS Stokes wave will be completely cut off and the stimulated Rayleigh scattering (STRS) will also be reduced [37, 56]. Despite all these benefits, the optical isolator is not an ideal component, and particularly it adds losses in the loop. Thus, the use of this device reduces the FRR Q_{opt}.

After implementation, the IFRR has been demonstrated to have the following characteristics: Q_{opt} = 2.1 10^9, 92 kHz $FWHM$, 2.04 MHz FSR, 4 dB optical transmission loss (which is equivalent to 7.7 dB RF transmission loss) and 22.7 dB power rejection. Unfortunately, a degradation of this resonator has been observed in a new RF characterization that is presented in Figure II-17.

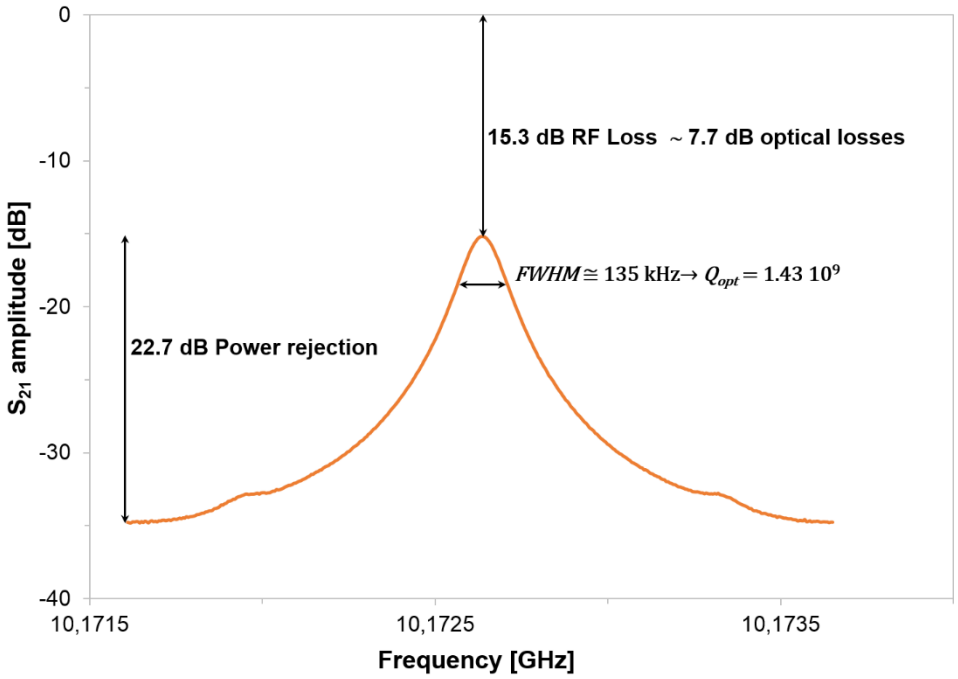

Figure II-17 RF transmission characteristics of the 100m long immunized fiber ring resonator.

The resonator $FWHM$ has clearly increased from 92 to 135 kHz, which means that the loaded optical quality factor has decreased as well to 1.43 10^9. This reduction is properly linked to the increase of the optical losses inside the cavity per round trip (from 4 dB to 7.7 dB) that may be associated with the degradation of the insertion losses of the components, such as the optical couplers and the optical isolator. Consequently a degradation of the phase noise performance of the system should be expected. Therefore, a detailed investigation has to be performed to gain precise insights on the causes of the degradation of the optical components insertion losses.

II.6.a FRR 100m P-M without isolator

A study has been carried out on the possibility to get a resonator with a Q close to or higher than 10^{10} without using an optical isolator. The breakthrough here was to find the optimal optical couplers that have the lowest additional losses. To do so, an FRR model, which was developed on the microwave simulation software ADS-Agilent during the thesis of K. Saleh [37], has been used.

Figure II-18 shows the ADS simulation results for the quality factor and the optical transmission losses obtained for 100m FRR, versus the coupler losses and for three different coupling factors: 1, 3 and 5%. Taking into account the resonator's quality factor and transmission losses, the higher Q_{opt} is found for 1% coupling coefficient. On the other hand, the lower transmission losses is found for 5% coupling coefficient.

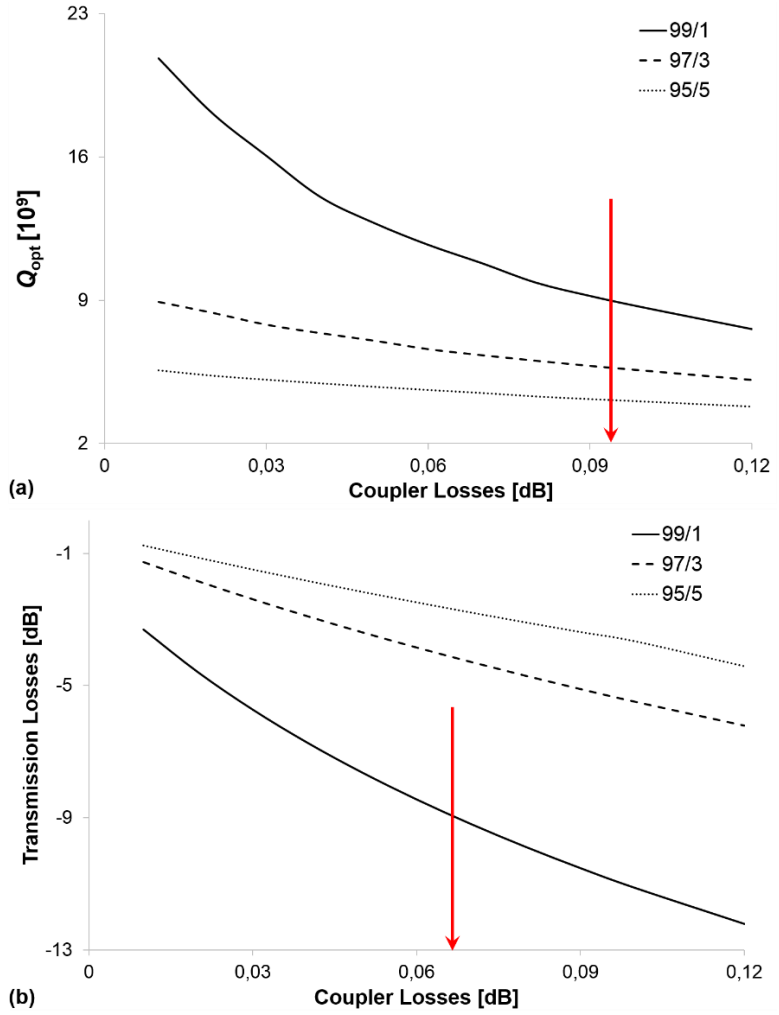

Figure II-18 100m long FRR (a) optical quality factor Q_{opt} (b) optical transmission losses, versus the coupler losses and for 3 coupling factor: 1, 3 and 5%.

In order to get the higher optical quality factor while maintaining an acceptable optical transmission losses level, two optical P-M couplers, which have a 1% of coupling coefficient and very low coupler additional losses (< 0.1 dB), were chosen, together with a 100m low attenuation P-M panda Fujikura fiber (Figure II-19).

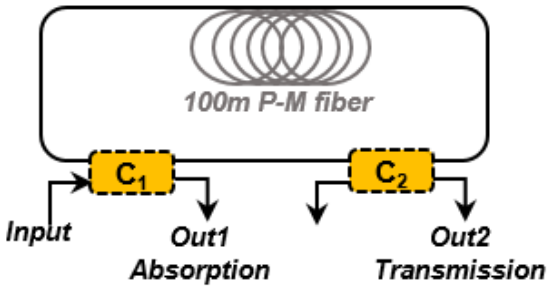

Figure II-19 100m fiber ring resonator architecture.

II.6.b FRR characterization

The radio frequency spectral characterization technique has been used to characterize this 100m long P-M FRR and to extract its loaded optical quality factor, its $FWHM$, as well as its transmission loss. Figure II-20 illustrates the RF transmission function of the FRR (Out2). Based on the measured data, this resonator has an optical quality factor of 8.9 10^9, 21.9 kHz of $FWHM$ and an RF transmission loss of 17.6 dB, which corresponds to an optical transmission loss of 8.8 dB (since the RF transmission loss is doubled in the microwave domain because of the photodiode quadratic detection).

The couplers losses can be estimated using both the simulated (Figure II-18) and the measured data (Figure II-20). For a Q_{opt} of 8.9 10^9, the coupler losses are around 0.094 dB. On the other hand, for an optical transmission loss of 8.8 dB, the coupler losses are around 0.067 dB (see the red arrow in Figure II-18). The difference between the two extracted values can be explained by the fact that in the simulated model of the resonator, the two couplers are identical, which is not generally the case in practice since the coupler losses and the coupling coefficient as well depend on several factors in the fabrication process of the couplers.

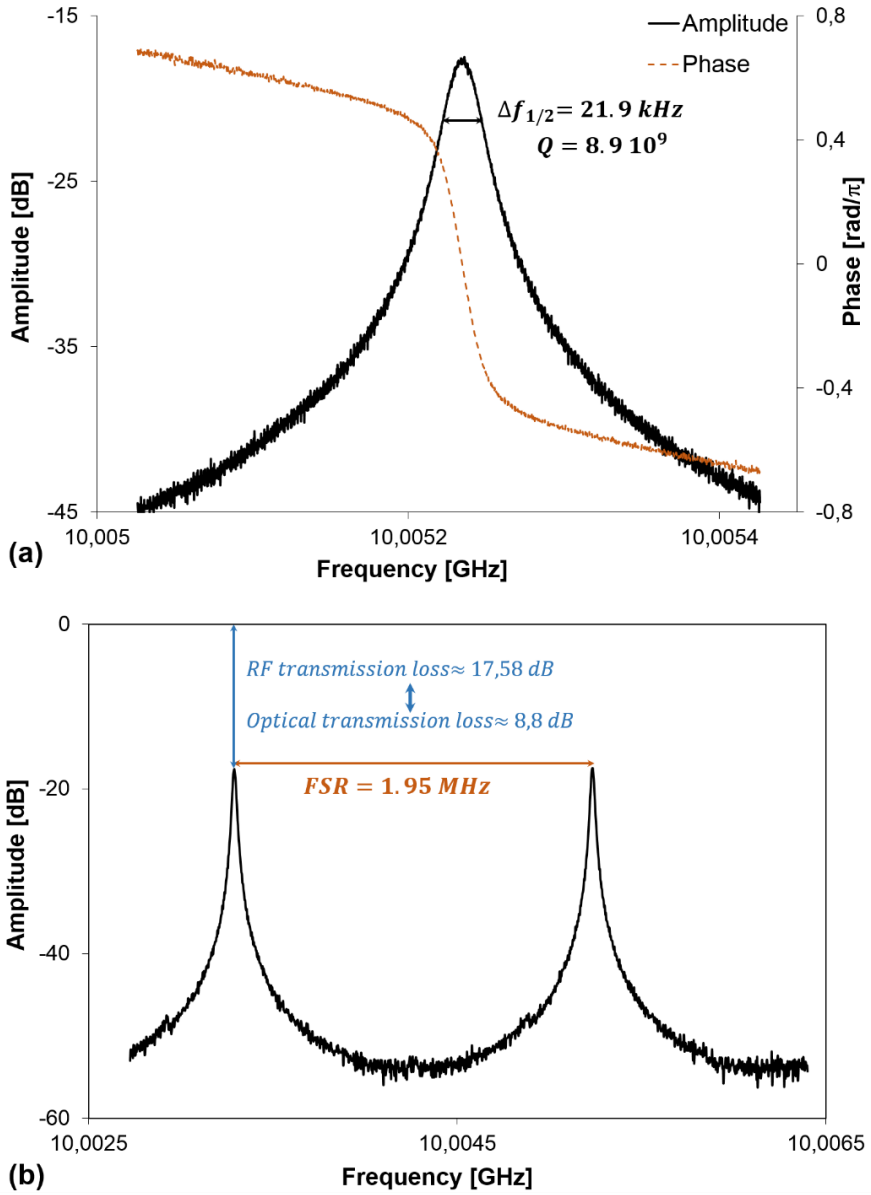

Figure II-20 (a) RF transmission function of a 100m long fiber ring resonator. (b) A focus on one resonance in the transfer function.

II.7 Conclusion

This chapter focuses mainly on the optical resonators that are used in myriad of applications, and especially the ones used in the optoelectronic oscillators, such as whispering gallery mode resonator and fiber ring resonator.

In addition to its simplicity in fabrication and characterization, a fiber ring resonator, with well-chosen material (low losses fibers and couplers, for instance), can reach relatively high quality factors, in excess of 10^9 or even 10^{10}. With a detailed analytical modeling of a resonator, it has been demonstrated that the coupling regime can be determined directly from

the shape of the amplitude and phase slope of its transmission transfer function. Furthermore, almost all the main properties of the resonator, such as quality factors: loaded, internal and external, can be computed directly from two principal parameters: the coupler direct transmission coefficient ρ and the intra-cavity losses α, which are also used to identify the coupling regime.

Once fabricated, an optical resonator must and can be characterized using different metrology methods, which were presented here. A special focus is given to the radio frequency spectrum approach, since it has been shown through experimental studies that this approach gives access to the main parameters characterizing an optical resonator. This technique requires a calibration step, and also a fine tuning of the locking system to ensure a precise alignment between the laser frequency and the resonance on which it is locked. It is only limited by the bandwidth of the optoelectronic components, which prevents its use with large FSR resonators (FSR > 50 GHz).

II.8 References

1. Vahala, K. J. Optical microcavities. *Nature* **424**, 839-846 (2003).
2. Heebner, J., Grover, R. & Ibrahim, T. *Optical microresonators: theory, fabrication, and application* (Springer, 2008).
3. Savchenkov, A. A., Ilchenko, V. S., Byrd, J., Liang, W., Eliyahu, D., Matsko, A. B., Seidel, D. & Maleki, L. Whispering-gallery mode based optoelectronic oscillators. *Frequency Control Symposium (FCS), 2010 IEEE International,* Newport Beach, CA, 554-557, doi: 10.1109/FREQ.2010.5556268 (2010).
4. Liang, W., Ilchenko, V. S., Eliyahu, D., Savchenkov, A. A., Matsko, A.B., Seidel, D. & Maleki, L. Ultralow noise miniature external cavity semiconductor laser. *Nat. Commun.* **6**, 1-6 (2015).
5. Kippenberg, T. J., Holzwarth, R. & Diddams, S. A. Microresonator-based optical frequency combs. *Science* **332**, 555-559 (2011).
6. Mandal, S., Dasgupta, K., Basak, T. K. & Ghosh, S. K. A generalized approach for modeling and analysis of ring-resonator performance as optical filter. *Optics Communications* **264**, 97-104 (2006).
7. Merrer, P.H., Llopis, L., Nicole, P. & Constant, S. Modeling and practical demonstration of multiple optical fiber ring resonators in the microwave domain. *Microw. Opt. Technol. Lett.* **54**, 1552-1556 (2012).
8. Maxwell, A., Huang, S.W., Ling, T., Kim, J.S, Ashkenazi, S. & Guo, L.J. Polymer microring resonators for high-frequency ultrasound detection and imaging. *IEEE. J. Sel. Topics Quantum Electron.* **14**, 191-197 (2008).
9. Blair, S. & Chen, Y. Resonant-enhanced evanescent-wave fluorescence biosensing with cylindrical optical cavities. *Appl. Opt.* **40**, 570-582 (2001).
10. Ludlow, A. D., Huang, X., Notcutt, M., Zanon-Willette, T., Foreman, S. M., Boyd, M. M., Blatt, S. & Ye, J. Compact, thermal-noise-limited optical cavity for diode laser stabilization at $1x10^{-15}$. *Opt. Lett.* **32**, 641-643 (2007).
11. Righini, G. C. Whispering gallery mode microresonators: fundamentals and applications. *Riv. Nuovo. Cimento* **34**, 437-488 (2011).
12. Saleh, K., Llopis, O. & Cibiel, G. Optical scattering induced noise in fiber ring resonators and optoelectronic oscillators. *J. Lightwave Technol.* **31**, 1433-1446 (2013).
13. Hercher, M. The spherical mirror Fabry-Perot interferometer. *Appl. Opt.* **7**, 951-966 (1968).
14. Young, M. *Optics and Lasers: Including Fibers and Optical Waveguides*. (Springer Berlin Heidelberg, 1992). Chapter 6, 129-142.
15. Lee, C. E. & Hocker, H. F. Interferometric optical fiber sensors using internal mirrors. *Electron. Lett.* **24**, 193-194 (1988).
16. Yu, F. T. S., Tin, S. *Fiber Optic Sensors* (Dekker, 2002). Chapter 2, 41-74.
17. Webster, S. A., Oxborrow, M., Pugla, S., Millo, J. & Gill, P. Thermal-noise-limited optical cavity. *Phys. Rev. A* **77**, 033847 (2008).

18. Kessler, T., Hagemann, C., Grebing, C., Legero, T., Sterr, U. & Riehle, F. A sub-40 mHz linewidth laser based on a silicon single-crystal optical cavity. *Nat. Photon.* **6**, 687-692 (2012).
19. Righini, G. C., Dumeige, Y., Féron, P., Ferrari, M., Nunzi Conti, G., Ristic, D. & Soria, S. Whispering gallery mode microresonators: Fundamentals and applications. *Riv. Nuovo Cimento Soc. Ital. Fis.* **34**, 435-488 (2011).
20. Savchenkov, A. A., Ilchenko, V., Matsko, A. & Maleki, L. Kilohertz optical resonances in dielectric crystal cavities. *Phys. Rev. A* **70**, 051804 (2004).
21. Lin, G., Diallo, S., Henriet, R., Jacquot, M. & Chembo, Y. K. Barium fluoride whispering gallery mode disk resonator with one billion quality factor. *Opt. Lett.* **39**, 6009-6012 (2014).
22. Birks, T. A., Knight, J. C. & Dimmick, T. E. High-resolution measurement of the fiber diameter variations using whispering gallery modes and no optical alignment. *IEEE Photon. Technol. Lett.* **12**, 182-183 (2000).
23. Ward, J. & Benson, O. WGM microresonators: sensing, lasing and fundamental optics with microspheres. *Laser & Photon. Rev.* **5**, 553-570 (2011).
24. Borselli, M., Srinivasan, K., Barclay, P. E. & Painter, O. Rayleigh scattering, mode coupling, and optical loss in silicon microdisks. *Appl. Phys. Lett.* **85**, 3693-3695 (2004).
25. Hossein-Zadeh, M. & Vahala, K. J. Free ultra-high-Q microtoroid: a tool for designing photonic devices. *Opt. Express* **15**, 166-175 (2007).
26. Borselli, M., Johnson, T. J. & Painter, O. Beyond the Rayleigh scattering limit in high-Q silicon microdisks: theory and experiment. *Opt. Express* **13**, 1515-1530 (2005).
27. Armani, D. K., Kippenberg, T. J., Spillane, S. M. & Vahala, K. J. Ultra-high-Q toroid microcavity on a chip. *Nature* **421**, 925-9928 (2003).
28. Savchenkov, A. A., Matsko, A. B., Ilchenko, S. & Maleki, L. Optical resonators with ten million finesse. *Opt. Express* **15**, 6768-6773 (2007).
29. Dumeige, Y., Trebaol, S., Ghişa, L., Nguyên, T. L. N., Tavernier, H. & Féron, P. Determination of coupling regime of high-Q resonators and optical gain of highly selective amplifiers. *J. Opt. Soc. Am. B* **25**, 2073-2080 (2008).
30. Matsko, A. B., Maleki, L., Savchenkov, A. A. & Ilchenko, V. S. Whispering gallery mode based optoelectronic microwave oscillator. *J. Mod. Opt.* **50**, 2523-2542 (2003).
31. Savchenkov, A. A., Ilchenko, V. S., Byrd, J., Liang, W., Eliyahu, D., Matsko, A. B., Seidel, D. & Maleki, L. Whispering gallery mode based opto-electronic oscillators. *2010 IEEE International Frequency Control Symposium*, 554-557 (2010).
32. Merrer, P. H., Saleh, K., Llopis, O., Berneschi, S., Cosi, F., Nunzi Conti, G., Characterization technique of optical whispering gallery mode resonators in the microwave frequency domain for optoelectronic oscillators, *Appl. Opt.* **51**, 4742-4748 (2012).
33. Merrer, P. H., Llopis, O., Bonnefont, S., Ghisa, L., Dumeige, Y., Féron, P., & Cibiel, G. Microwave filtering using high Q optical resonator. *Microwave Conference, 2008. EuMC 2008. 38th European, Amsterdam, 2008*, 381-384, doi: 10.1109/EUMC.2008.4751468 (2008).

34. Zhang, F. & Lit, J. W. Y. Direct-coupling single-mode fiber ring resonator. *J. Opt. Soc. Am. A* **5**, 1347-1355 (1988).
35. Heebner, J. E., Wong, V., Schweinsberg, A., Boyd, R. W. & Jackson, D. J. Optical transmission characteristics of fiber ring resonators. *IEEE. J. Quantum Electron.* **40**, 726-730 (2004).
36. Merrer, P. H., Llopis, O. & Cibiel, G. Laser stabilization on a fiber ring resonator and application to RF filtering. *IEEE Photon. Technol. Lett.* **20**, 1388-1401 (2008).
37. Saleh, K. High spectral purity microwave sources based on optical resonators. Thesis delivered by Paul Sabatier University, Toulouse III, Toulouse-France (2012).
38. Yariv, A. Universal relations for coupling of optical power between micro-resonators and dielectric waveguides. *Electronics Letters* **36**, 321-322 (2000).
39. Yariv, A. Critical coupling and its control in optical waveguide-ring resonator systems. *IEEE Photon. Technol. Lett.* **14**, 483-485 (2002).
40. Heebner, J. E., Boyd, R. W. & Park, Q. Slow light, induced dispersion, enhanced nonlinearity, and optical solitons in a resonator-array waveguide. *Phys. Rev. E* **65**, 036619 (2002).
41. Totsuka, K. & Tomita, M. Slow and fast light in a microsphere-optical fiber system. *J. Opt. Soc. Am. B.* **23**, 2194-2199 (2006).
42. Tomita, M., Uesugi, H., Sultana, P. & Oishi, T. Causal information velocity in fast and slow pulse propagation in an optical ring resonator. *Phys. Rev. A* **84**, 043843 (2011).
43. Rasoloniaina, A., Huet, V., Nguyên, T.K.N., Le Cren, E., Mortier, M., Michely, L., Dumeige, Y. & Féron, P. Controling the coupling properties of active ultrahigh-Q WGM microcavities from undercoupling to selective amplification. *Sci. Rep.* **4**, 4023, doi: 10.1038/srep04023 (2014).
44. Totsuka, K. & Tomita, M. Dynamics of fast and slow pulse propagation through a microsphere-optical-fiber system. *Phys. Rev*. E **75**, 016610 (2007).
45. Haus, H.A. *Waves and fields in optoelectronics* (Prentice-hall, 1984).
46. Geng, J., Staines, S., Wang, Z., Zong, J., Blake, M. & Jiang, S. Highly stable low-noise Brillouin fiber laser with ultranarrow spectral linewidth. *IEEE. Photon. Technol. Lett.* **18**, 1813-1815 (2006).
47. Carmon, T., Yang, L. & Vahala, K. J. Dynamical thermal behavior and thermal self-stability of microcavities. *Opt. Express* **12**, 4742-4750 (2004).
48. Hahn, J. W., Yoo, Y. S., Kim, J. W. & Lee, H. W. Cavity ringdown spectroscopy with a continuous-wave laser: calculation of coupling efficiency and a new spectrometer design. *Appl. Opt.* **38**, 1859-1886 (1999).
49. He, Y. & Orr, B. J. Ringdown and cavity-enhanced absorption spectroscopy using a continuous-wave tunable diode laser and a rapidly swept optical cavity. *Chem. Phys. Lett.* **319**, 131-137 (2000).
50. Black, E. D. An introduction to Pound-Drever-Hall laser frequency stabilization. *Am. J. Phys.* **69**, 79-87 (2001).

51. Pound, R. V. Electronic frequency stabilization of microwave oscillators. *Rev. Sci. Instrum.* **17**, 490-505 (1949).
52. Drever, R. W. P., Hall, J. L., Kowalski, F. V., Hough, J., Ford, G. M., Munley, A. J. & Ward, H. Laser phase and frequency stabilization using an optical-resonator. *Appl. Phys. B.* **31**, 97-105 (1983).
53. Wieman, C. E. & Hollberg, L. Using diode lasers for atomics plysics. *Rev. Sci. Instrum.* **62** (1991).
54. Maleki, L., Matsko, A. B., Savchenkoc, A., Ilchenko, V., Liang, W., Seidel, D. & Byrd, J. Optical locking based on optical resonators with high quality factors. *US Patents* US6879752 B1 (2005).
55. McRae, T. G., Lee, K. H., McGovern, M., Gwyther, D. & Bowen, W. P. Thermo-optic locking of a semiconductor laser to a microcavity resonance. *Opt. Express* **17**, 21977-21985 (2009).
56. Takushina, Y. & Okoshi, T. Suppression of stimulated Brillouin scattering using optical isolators. *Electron. Lett.* **28**, 1155-1157 (1992).

Chapter III: OEO based on FRR – Modeling

III.1 Introduction

Minimizing phase noise is an increasingly critical requirement for applications, especially the ones that seek a stable time reference. So it is crucial to delineate all the factors which impact the systems short-term stability. In a complex system such as an optoelectronic oscillator, these factors are related to the noise of the various components in the loop, such as the microwave amplifier phase noise, the laser relative intensity noise, the laser frequency noise, the photodiode shot noise, the thermal noise and the nonlinear optical mechanisms that can occur in optical fibers. Even in the optimal case, where low-noise components are used, the conversion processes between these noise sources may induce a relatively high level of phase noise if they are not optimized. These conversion processes depend on the devices nonlinearities, on the fiber frequency dispersion and on the overall OEO topology.

Properly identifying the noise sources is only the first step towards being able to control and reduce them, if not eliminate them entirely. On the other hand, precise behavioral modeling of the OEO's components and their noise contributors is essential not just to be able to simulate and predict the oscillator phase noise but also to determine the optimal conditions to obtain the most desirable performance.

Among all these noises, the laser relative intensity noise could affect severely the oscillator phase noise, especially at low offset frequencies ($1/f$ noise). In fact, it could be up-converted to microwave phase noise through the nonlinearity of some of the OEO's components, and particularly the photodiode. In this chapter, particular relevance is given to the photodiode nonlinear behavior and its impact on the conversion process of the laser amplitude noise to microwave phase noise. To quantify and investigate this last phenomenon, a new physical nonlinear equivalent circuit model of a photodiode has been applied in a microwave circuit simulator, Agilent Advanced Design System (ADS). This new model is able to describe the conversion of the laser relative intensity noise into microwave phase noise. Consequently, a good computation and prediction of the phase noise performance of an OEO could be obtained. All these points are fully explored and detailed in this chapter.

III.2 Noise sources in an optoelectronic oscillator

As mentioned in Chapter I, in a microwave oscillator, the phase noise is mainly originated from the amplifier phase noise, through different processes, such as the conversion of the amplifier low-frequency noise and the addition of the amplifier high-frequency noise. However, it is not the case in an optoelectronic oscillator, since many of the elements used inside the oscillation loop, from optical and microwave components to low-frequencies components, are active devices or nonlinear devices, and thus may contribute to the oscillator phase noise.

If the microwave amplifier used in the OEO has a low residual phase noise, the far-from-carrier phase noise level will be limited by the optical noise-to-carrier ratio (NCR), which is related to the laser relative intensity noise (RIN) and to the photodiode thermal and shot noise. Furthermore, the close-to-the-carrier phase noise will be linked to the loaded quality factor and to the various nonlinear processes, which are able to up-convert the devices low-frequency (LF) noise components to higher frequencies (i.e. the RF oscillation frequency). The devices featuring LF noise in the optical link are mainly the laser and the optical fiber.

The laser is affected by amplitude and frequency fluctuations, which both feature a $1/f$ like shape at low frequency. The laser frequency noise (FM noise) can be demodulated due to the fiber dispersion or to the interferometric phenomenon related to parasitic reflections in the optical link. In addition, the laser amplitude noise (AM noise) can be converted into RF amplitude and phase noise by any component for which the transit-time depends on the optical power, and this is the case of the photodiode. The optical fiber may also generate a low-frequency RF phase fluctuations, particularly in the case of long spools (few kilometers) driven by high level optical power, or equivalently in the case of ultra-high Q fiber ring resonators. This is due either to nonlinear optical mechanisms that occur in optical fibers in these conditions, such as stimulated Brillouin scattering or, also, to the interaction of the optical wave with some silica non-homogeneities, which occur even at low optical power (Rayleigh scattering). In fact, the level of the optical power used should be carefully selected, owing to the fact that operating at low optical power levels degrades the NCR of the optical link, while a high optical power will lead to nonlinear effects.

In an OEO based on fiber ring resonator, for instance, if all the nonlinear optical effects are reduced or completely suppressed and the nonlinear conversions of the optical noises to RF noises are well controlled, the phase noise spectrum can only be limited by the microwave/RF amplifiers phase noise. In other words, the presence of all these nonlinear and scattering processes contributes severely to the frequency stability of the whole system.

III.2.a Nonlinear optical effects in optical fiber resonator

Several varieties of nonlinear optical effects may arise inside an optical fiber [1-3] leading to loss, pulse spreading or crosstalk. Very long and extremely low-loss fibers, small core diameters, higher optical powers, and narrow-band lasers would severely enhance the

nonlinear effects. The main nonlinear mechanisms in a standard fiber are divided into scattering and parametric processes.

In the scattering process, such as Brillouin, Rayleigh and Raman scatterings, optical fibers play an active role, that is to say that the process depends on molecular vibrations or density fluctuations of the fiber. These scattering processes can be present in spontaneous or stimulated mode. In the spontaneous mode, the optical material properties are unaffected by the presence of the incident light. While in stimulated mode, the optical material properties are modified [4].

In the parametric process, on the other hand, such as four-wave mixing, the state of the fiber material does not change. In fact, it involves the modulation of a medium parameter, such as the refractive index, and requires phase-matching between the propagating waves before it can build up along the optical fiber, which in this case plays a passive role except for mediating interaction among several optical waves.

All these mechanisms depend strongly on the optical power received by the optical fiber. Their presence limits the quality factor of a fibered resonator, and is prone to introduce additional noises to the optical signal travelling through the optical fiber, which can be converted into RF noise after being detected by the photodiode.

III.2.a.i Brillouin scattering

Brillouin scattering is an inelastic scattering process [5], and results from the interaction between optical waves and acoustic waves in the optical fiber. Because of the optical power, thermally excited acoustic waves (i.e. phonons) produce a periodic modulation of the refractive index, causing a backwards diffraction of the light propagating in the fiber and giving rise to frequency-shifted Stokes and anti-Stokes components. This process is called spontaneous Brillouin scattering [6,7], and can occur even at low optical powers.

At higher optical power, the presence of two counter-propagating waves with a frequency difference, i.e. the upper frequency lightwave and the lower frequency lightwave (called pump and probe, respectively), will give rise to the travelling acoustic wave via electrostriction and contribute to the phonon population. Consequently, the scattering cross-section will increase and a part of the energy will be transferred from the pump wave to the probe wave. The amplification of the probe only depends on the pump intensity power. This process is known as stimulated Brillouin scattering (SBS) [8-10], (see Figure III-1). Noted that this carrier depletion causes the NCR degradation of the optical link.

In the Stokes event, the photon loses energy to create a phonon. This is caused by the Doppler effect of the interaction between the light wave and the acoustic wave travelling in the same direction, and it reflects a negative frequency Brillouin shift. On the other hand, in an Anti-Stokes event and due to the interaction between the light wave and the acoustic wave travelling in an opposite direction, the photon gain energy by absorbing a phonon, and this therefore explains the positive frequency Brillouin shift. Furthermore, The Stokes power will

increase linearly as the optical power increases. However, as the backward Stokes intensity increases, it would serve as effective launching power to a second order Stokes wave. This second order Stokes wave will move in the same direction as the original optical wave, though its frequency shift is twice the first order one (ν_B) [11,12].

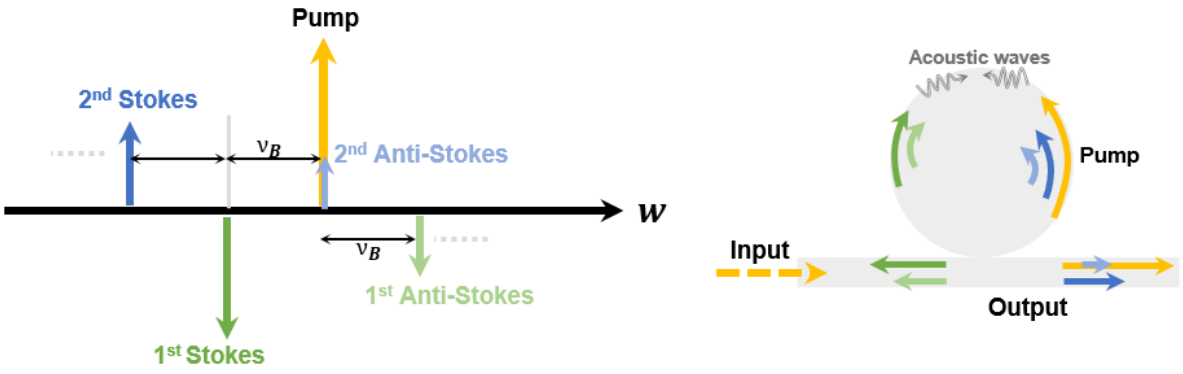

Figure III-1 Illustration of the mechanisms of the stimulated Brillouin scattering (1st and 2nd order) in a ring optical resonator. Downward (upward) arrows denote signals generated in the opposite (same) direction with the pump. The SBS process generates Stokes and anti-Stokes with a Brillouin shift (ν_B) from the resonator. The even-order Stokes (2nd, 4th...) co-propagate with the pump whereas the odd-order Stokes (1st, 3rd...) counter-propagates.

- ***Brillouin frequency shift and gain bandwidth***

The Brillouin frequency shift (ν_B) depends on the acoustic velocity within the fiber (c_{ac}), the refractive index (n), the wavelength of the optical carrier (λ_0), and the angle between the optical carrier and the scattered wave (θ, scattering angle) [13], and is given by

$$\nu_B = \mp \frac{2n}{\lambda_0} c_{ac} \sin\left(\frac{\theta}{2}\right) \tag{III.1}$$

Another important characteristic of the SBS is its gain spectrum (BGS) and especially the gain bandwidth ($\Delta\nu_B$), which is related to the damping time of acoustic waves related to the photon lifetime. Furthermore, this gain bandwidth depends on the Brillouin shift and varies slightly faster than ν_B^2.

In silica-based fibers, for instance, the Brillouin gain spectrum and Brillouin shift can differ significantly between fibers having different structures (i.e. different guided nature of optical modes) and different doping materials and levels in the fiber core [3,7,14,15]. For single-mode fiber (SMF28), the BGS has been reported to be equal to approximately 25 MHz, and the Brillouin shift is equal to 10.8 GHz [16]. For pure silica GeO_2 doped fiber (i.e. GeO_2 concentration is about 0.3% per mole), the BGS bandwidth and the Brillouin shift are 35 MHz and 11.25 GHz, respectively. However, broader width and smaller shift values occur for fiber cores with higher GeO_2 concentration. In addition, a Brillouin $\Delta\nu_B$ and ν_B in a GeO_2 doped highly nonlinear fiber (Ge-HNLF) are 50 MHz and 9.4 GHz, respectively, and by employing an

Al_2O_3 doped core (Al-HNLF) instead of GeO_2, these values increase to 230 MHz and 11.9 GHz, respectively [15,17].

- ***Laser RIN degradation caused by SBS***

It has been reported in [18], that the SBS may have an impact on the laser relative intensity noise. The measurements, represented in Figure III-2 (a), show clearly a degradation in the laser RIN between the input and the output of the fiber ring resonator, where the first stimulated Brillouin scattering is presented. In addition, it is shown also that the Brillouin first Stokes RIN is higher than the laser RIN at low frequency. This may be caused by the SBS's own Rayleigh-scattered wave, which induces noise to the SBS wave and degrades its RIN [19]. Nonetheless, a Brillouin RIN lower than the laser pump's RIN has been reported [20-22], and this is particularly important for some applications, especially in the case of the Brillouin fiber ring lasers [23].

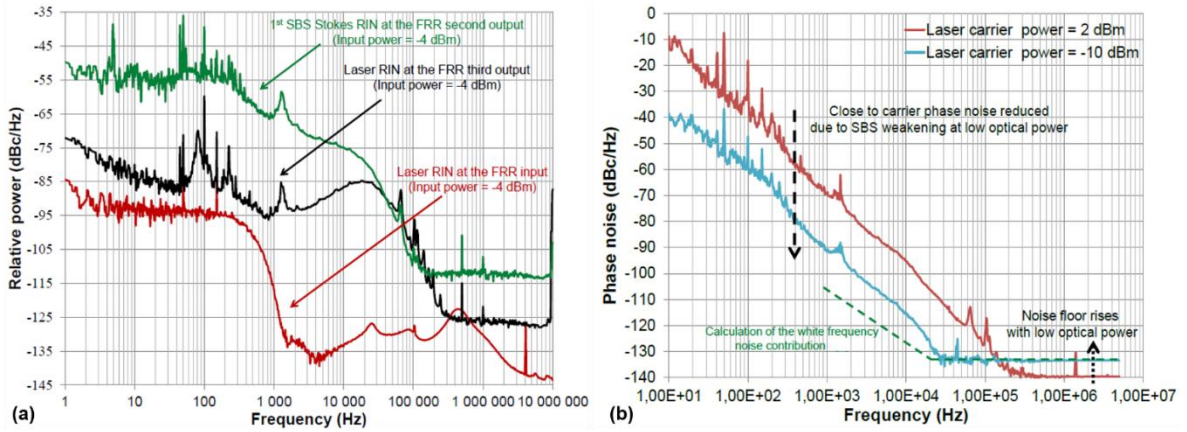

Figure III-2 [18] (a) Laser RIN degradation because of the SBS generation and the first Brillouin Stokes wave RIN measurement; (b) Phase noise of a 20m long FRR based on 10 GHz OEO for two different optical powers.

- ***OEO phase noise degradation caused by SBS***

Figure III-2 (b) depicts the phase noise of a 20m long fiber ring resonator based on 10 GHz OEO, for two different optical power levels: 2 and -10 dBm. As is evident, a significant enhancement of the close-to-carrier OEO phase noise for lower input optical power, especially when the optical power is under the first SBS threshold (SBST). These results demonstrate that the optical power at the resonator input must be maintained below the first SBST to avoid the SBS and its effects on the $1/f$ phase noise [24].

III.2.a.ii Rayleigh scattering

The Rayleigh scattering is a form of elastic scattering process and it is also related to the parametric process since the quantum state of the fiber's material remains unchanged. The spontaneous Rayleigh scattering is caused by thermal fluctuations in the medium, which

create refractive index fluctuations via the thermo-optic effect. As the dimensions of these density fluctuations are on the order of the wavelength of the incident light, the light can be scattered in many directions, and consequently amplitude and phase noises will be generated [19,25,26].

The density fluctuations can themselves be induced by the incident light via electrostriction, leading to the stimulated Rayleigh scattering (STRS) [27]. This Rayleigh backscattering does not induce a significant frequency shift in the scattered light, owing to the non-propagating density fluctuations. These frequency shifts are of few kHz in P-M fibers and increase at high input power levels [25]. Rayleigh scattering is the primary cause of losses in fibers operating in the wavelength range between 800 to 1300 nm (reaching few dB/km in single-mode silica fiber), but these losses decrease in the entire 1300-1600 nm region (e.g. 0.2 dB/km near 1550 nm) [28].

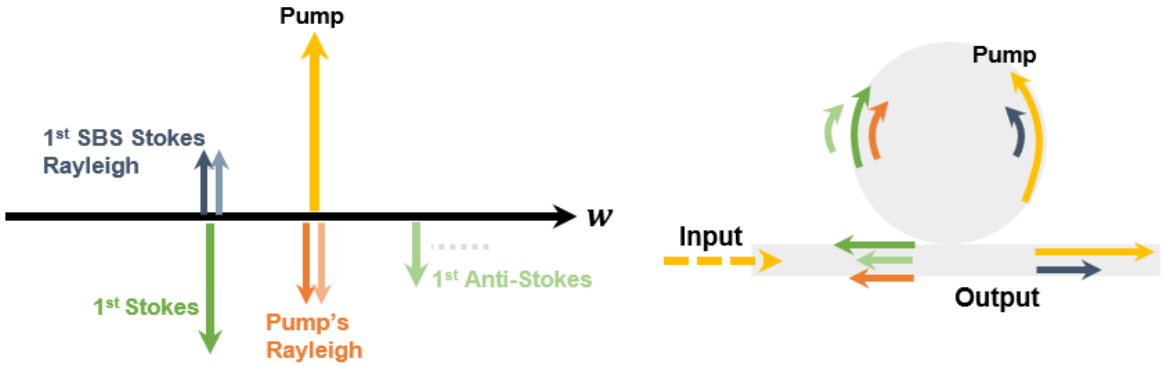

Figure III-3 Illustration of the mechanisms of the Rayleigh scattering in a ring optical resonator. Downward (upward) arrows denote signals generated in the opposite (same) direction with the pump.

- ***STRS and the laser RIN degradation***

The Rayleigh scattering has the potential to degrade the short-term stability performance of optoelectronic systems. Yet, it is not the most harmful scattering, since the SBS gain coefficient is two orders of magnitude higher than the one of STRS in long fiber lengths [29], except for P-M fiber where there is only one order of magnitude difference due to the polarization maintaining property [25].

In the OEO based on FRR case, it has been shown [18] that a rise in the laser RIN can result from the mixing process of the laser carrier and the Rayleigh scattering Stokes waves at the photodiode's input. This behavior, which is depicted in Figure III-4, is almost uniform below -6 dBm input optical power. This noise is generated inside the resonator bandwidth, but owing to the resonator's high Q_{opt}, this noise is filtered outside of the resonance bandwidth, and thus won't affect the OEO phase noise. However, when the input power exceeds -6 dBm, the RIN spectrum shape changes dramatically due to the SBS generation inside the resonator.

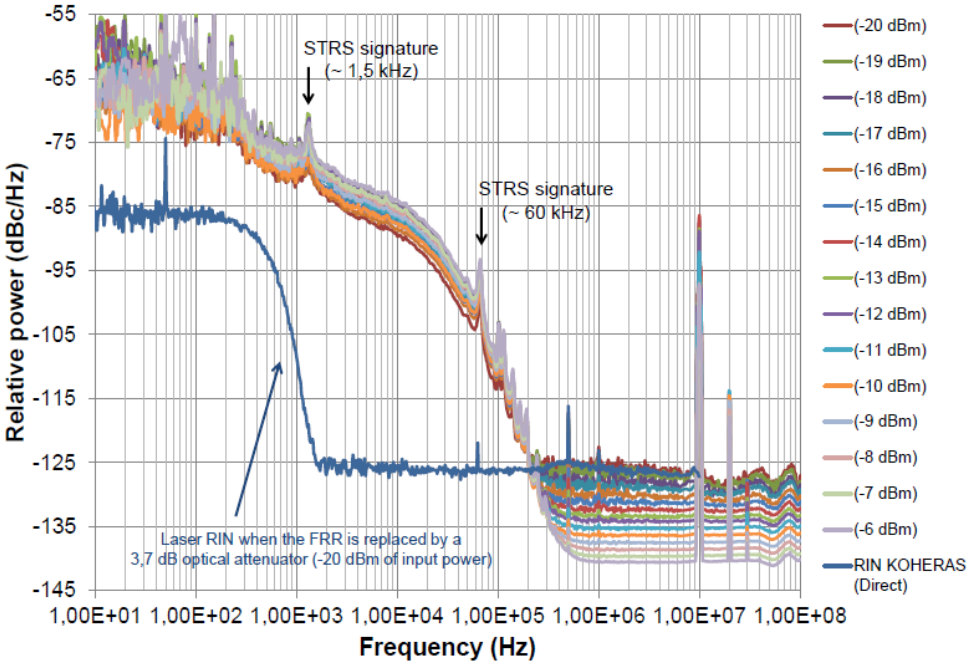

Figure III-4 [18] RIN spectra at the transmission output of a 20m long FRR, versus input optical power: -20 to -6 dBm.

III.2.a.iii Raman scattering

The Raman scattering (SRS) is another form of the inelastic scattering (like the Brillouin scattering). The main difference between the two is that optical phonons participate in SRS while acoustic phonons participate in SBS. In addition, in single-mode fibers, the SBS occurs only in the backward direction, while SRS can occur in both directions.

In contrast to the SBS, the spectral linewidth of the Rayleigh gain spectrum is as broad as several THz (up to 40 THz in silica fibers). Thanks to this feature, the Raman scattering was employed to develop new types of fiber optic amplifiers, especially the ones used in modern telecommunication systems [3]. However, this scattering can severely limit the performance of multichannel optical links by transferring energy from one channel to the neighboring channels.

However, the Raman threshold is the highest between the presented nonlinear effects (typically few watts). In our optoelectronic systems, such as OEOs, the stimulated Raman scattering will not occur because the input optical power levels are typically in the range of 10 mW.

III.2.a.iv Four-wave mixing

Four-wave mixing (FWM) is an optical parametric interaction, in which there is no net change in the energy and momentum. It occurs when photons from one or more waves are annihilated and new photons are created at different frequencies [3]. A specific choice of input

wavelengths and fiber parameters are needed to satisfy the phase-matching condition between the waves, so as to get a highly efficient FWM process.

Interestingly, the FWM process can be initiated from only a single pump wave. This is known as a degenerate FWM, where a strong pump wave at w_p creates two sidebands waves, upshifted (w_2) and downshifted (w_1) in frequency with a frequency shift Δ given by

$$\Delta = w_p - w_1 = w_2 - w_p \tag{III.2}$$

where the low-frequency sideband w_1 and the high-frequency sideband w_2 are referred to as the signal waves (or Stokes) and idler waves (or anti-Stokes), respectively.

In the general case, referring to the nondegenerate FWM, two pump waves at w_{p1} and w_{p2} are annihilated, and due to the mixing process two photons at frequencies w_1 and w_2 are created simultaneously, such that

$$w_{p1} + w_{p2} = w_1 + w_2 \tag{III.3}$$

where the frequency shift Δ is fixed by the frequency difference between w_{p1} and w_{p2} such that: $\Delta = w_{p2} - w_{p1} = w_2 - w_{p2}$.

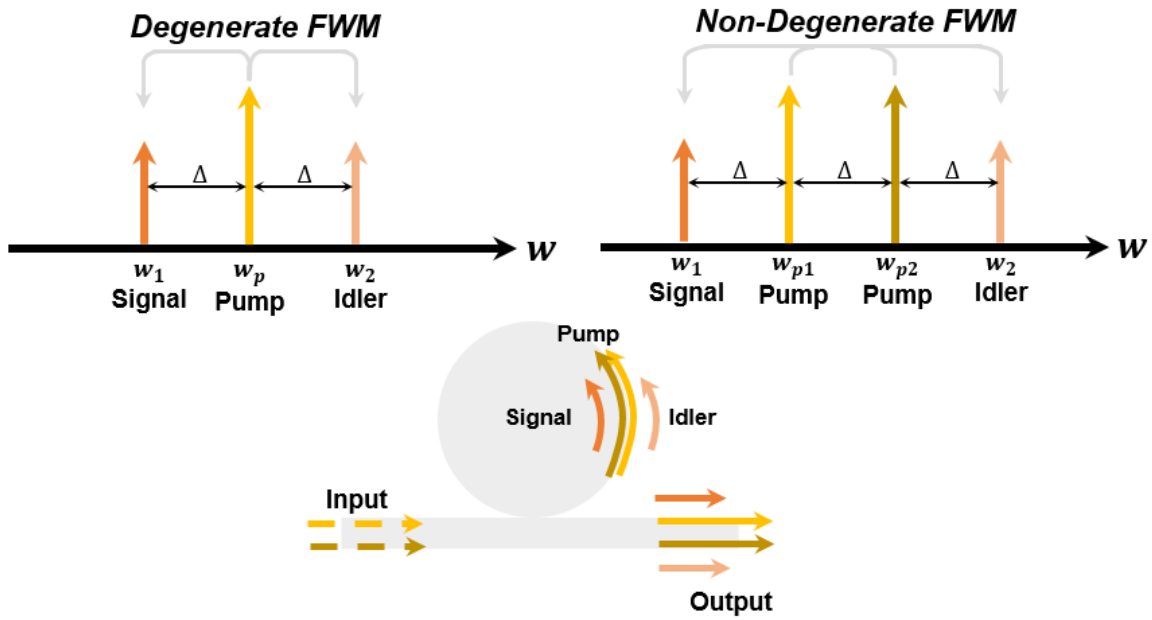

Figure III-5 Illustration of the mechanisms of the Four-wave mixing (both type degenerate and non-degenerate process) in a ring optical resonator. All signals co-propagate with the pump. FWM process generates both Stokes and anti-Stokes with a frequency shift (Δ) of the resonator.

It has been shown that the fiber chromatic dispersion plays an important role in FWM behavior [30]. In fact, the efficiency of this nonlinear interaction strongly depends on the phase-matching condition, bearing in mind that the chromatic dispersion is the key parameter

that determines the phase-matching in optical fibers. It has been demonstrated that the FWM efficiency decreases as the fiber dispersion increases. Thus, in a uniform zero-dispersion fiber, the phase-matching condition is completely satisfied, and hence the efficiency of this process reaches its maximum.

The importance of this condition is that depending on the used application, the presence of this nonlinear process can be either harmful or beneficial. For instance, in the optoelectronic oscillator case, the FWM process in resonators generates optical frequency harmonics that are useful for producing spectrally pure microwave signals [31]. Yet, in all the fiber ring resonator tested, this process was not generated even with high input optical power. This may be due to the start up of the stimulated Brillouin scattering, which limits the available power for the FWM process. This can be due also to the dispersion parameters of our fiber ring resonators.

New ring resonators are under study at this time at LAAS to try to generate FWM. These resonators are realized with highly nonlinear fiber (small core diameter). Unfortunately, the first resonators of this type realized were subject to SBS generation, and no FWM has been observed. New resonators are currently being developed and modelled. These resonators are the main subject of an on-going PhD thesis [Napoleon Gutierrez].

III.2.b Laser amplitude and frequency noise conversions

The laser is affected by amplitude and frequency fluctuations, which both feature a $1/f$ like shape at low frequency, noting that the shape can vary largely from pure $1/f$ spectrum to a spectrum with various and complex slopes, depending on the physical processes involved in the laser. Numerous researchers have explored the effects of these fluctuations on the RF phase noise or, in another words, they have investigated the different means by which the laser AM and FM noise are converted to RF phase noise [32-34].

III.2.b.i The fiber chromatic dispersion

In delay line based OEOs, the laser's wavelength fluctuations (Δf_{opt}) are converted into delay fluctuations (ΔT) through a dispersion mechanism, and therefore into RF phase noise ($\Delta\phi_{RF}$), and this conversion increases with the chromatic dispersion (D_λ) of the delay optical fiber and with the physical optical fiber length (L) [33-35]. This noise conversion relation can be expressed as:

$$\Delta\phi_{RF} = -2\pi\, f_0\, \Delta T = 2\pi\, f_0\, \lambda_{Laser}^2\, D_\lambda \frac{L}{c}\, \Delta f_{opt} \qquad \text{(III.4)}$$

A significant improvement can be obtained by stabilizing the laser or by using a zero-dispersion fiber or even by using a laser wavelength near the zero-dispersion point of signal mode optical fibers. Volyanskiy *et al.* [33] have shown that the use of a zero-dispersion

fiber enables a 10 dB reduction in the phase noise spectrum. It has been also proven, in this case, that low frequency laser RIN has a minor influence on the phase noise.

In the case of the fiber ring resonator, this conversion process cannot be avoided or even reduced by a zero-dispersion fiber, due to the fact that using these fibers in a FRR will intensify the nonlinear optical phenomena which can severely degrade the OEO phase noise [36].

III.2.b.ii The interferometric phenomenon

The optical frequency noise can also be converted to close-in RF phase noise, due to the interferometric phenomenon [32]. Interferometric noise arises from one or more pairs of reflection, which is caused by the refractive index discontinuities in the optical fiber (splices, connectors, coupler…), and/or from fiber nonlinear effects, like the stimulated Brillouin scattering, Rayleigh scattering [37,38] or the Fresnel back-reflection, which is often due to the index change from the glass-air interfaces at the fiber connections. The latter phenomenon can be avoided by using optical fibers with cleaved connectors (i.e. cleaving angle ~8º) [39], or by using index matching gel between the fibers' connectors. It has been also demonstrated that the insertion of an optical amplifier in the optical link of an OEO increases the interferometric noise [40].

III.2.b.iii The locking method

A precise alignment and a good mode-matching between the laser frequency and one of the transmission peaks of the optical resonator are a key requirement for high performance OEO and an excellent short-term stability. That is to say that any frequency shift between the laser frequency and the resonance results in the degradation of the phase noise of the output microwave signal.

In fact, it has been shown experimentally and confirmed by a software simulation (Agilent ADS) [36] that the laser frequency shift results in a deformation in the output RF amplitude (i.e. a splitted resonance) and phase responses (i.e. the phase transition at the resonance becomes less sharp, with two phase transitions corresponding to the two resonances of the splitted resonance). The consequence is firstly a reduction of the Q factor of the OEO and, secondly, a possible conversion of the laser FM noise into amplitude noise because the laser is no longer locked at a maximum of the amplitude curve.

Thus, the used stabilization technique should be chosen carefully of sufficient quality and controlled strictly in order to properly stabilize the laser carrier onto the center of the optical resonance, and to maintain this matching condition over time.

III.2.b.iv The photodiode nonlinearity

The laser intensity noise, known as the relative intensity noise, can be converted to microwave amplitude and phase noise via the optical link's nonlinearities. The photodiode seems to be the main device responsible for these conversions [34]. It has to be noted that

the nonlinear behavior of other components, such as the Mach-Zehnder modulator and the optical fiber, becomes significant at much higher optical power level compared with that of the photodiode.

Analytical and experimental studies of the photodiode nonlinear behavior, in function of the received optical power level at the photodiode input, are detailed in the next section.

III.3 Conversion of AM laser noise to RF phase noise

III.3.a Analytical study

The fluctuations in laser intensity are typically characterized by the laser relative intensity noise (RIN), which can limit the maximum signal-to-noise ratio (SNR), and thus can severely degrade the performance of any system based on fiber optic link. It is expressed as:

$$RIN(f) = \frac{\Delta P_{opt}^2(f)}{P_{opt}^2} \tag{III.5}$$

where $\Delta P_{opt}(f)$ and P_{opt} are the spectral density of the laser intensity fluctuations at frequency f and the laser average optical power, respectively [41].

On top of that, the low frequency components of the RIN can be up-converted to RF amplitude and phase noises through the devices nonlinearities, especially the photodiode, as it has been reported in delay line based OEOs by Eliyahu *et al.* [34].

In fact, for low optical power levels, below the photodiode saturation power, the number of carriers in the photodiode increases with the increase of light power. The RF power increases as well following a square-law detection of the photodiode [41]:

$$P_{RF} \sim P_{opt}^2 \tag{III.6}$$

where P_{RF} is the RF power at the photodiode output, and P_{opt} is the average optical power at the photodiode input.

Since the propagation speed of the RF signal depends on the number of carriers and their transit-time in the semiconductor, the RF amplitude and phase will change as well. Therefore, small laser amplitude fluctuations will transfer into RF amplitude and phase fluctuations, in a way that can be described by the following qualitative equations:

$$S_\alpha(f) = RIN(f) \cdot P_{opt}^2 \cdot \left({}^{da}/_{dP_{opt}} \right)^2 \quad \frac{w}{Hz} \tag{III.7}$$

$$S_{\Phi}(f) = RIN(f) \cdot P_{opt}^2 \cdot \left({}^{d\Phi}/_{dP_{opt}}\right)^2 \qquad \frac{rad^2}{Hz} \qquad \text{(III.8)}$$

where $S_{\alpha}(f)$ is the spectral density of the normalized RF amplitude fluctuation α, $S_{\Phi}(f)$ is the RF phase noise spectral density at offset frequency f from the carrier, ${}^{da}/_{dP_{opt}}$ is the normalized RF amplitude-to-optical power slope, and ${}^{d\Phi}/_{dP_{opt}}$ is the RF phase-to-optical power slope.

The evolution of the ${}^{d\Phi}/_{dP_{opt}}$ parameter has been followed firstly by an experimental measurements of the RF phase at the output of a high-speed photodiodes, and secondly by a modeling approach.

III.3.b Experimental set-up

To understand this conversion process, the study of the nonlinear behavior of a photodiode started with the measurements of the RF power and the relative RF phase at the output of a Discovery *DSC30S* photodiode as a function of the modulated optical power at the input of the photodiode [42].

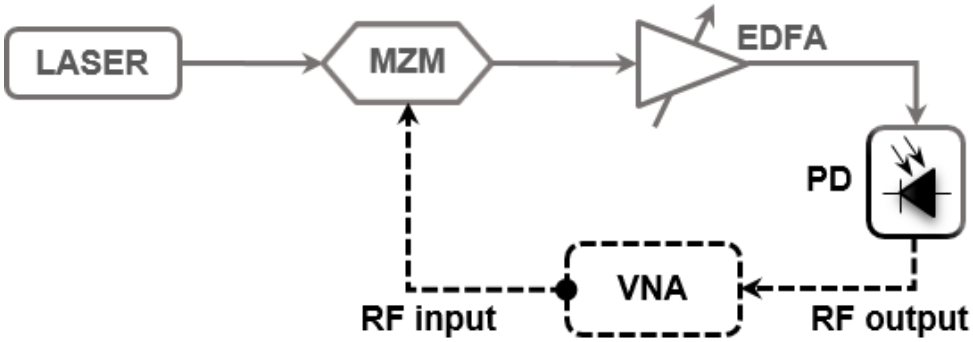

Figure III-6 Characterization bench of the photodiode's amplitude and phase response; MZM: Mach-Zehnder modulator, EDFA: Erbium doped fiber amplifier in a gain control mode, PD: photodiode.

Therefore, the experimental set-up, which is presented in Figure III-6, has been realized with a 20 mW telecommunications laser module (1550 nm), temperature controlled and externally modulated at 10 GHz by means of a Mach-Zehnder modulator (MZM - EOspace 20Gbits/s). The MZM was biased at $V_{\pi/2}$ in order to get a linear modulation (LM), which is less likely to generate additional disturbances (especially in phase). It was also passively thermalized with a large piece of brass in contact with the modulator. The microwave signal (i.e. the RF frequency) comes from a calibrated vector network analyzer (VNA) working in a continuous wave (CW) mode.

An Erbium Doped Fiber Amplifier (EDFA) has been also included in the set-up just before the photodiode under test, so as to get a higher optical power on the photodiode. The amplitude and phase responses of the S_{21} (transmission) parameter were accurately measured while changing the received optical power at the photodiode input. To this purpose, the automatic gain control mode of the EDFA has been activated so that the optical power at the photodiode input can be varied, and therefore the MZM nonlinearity versus the optical power can be discarded. Some experiments have also been performed using an optical variable attenuator before the photodiode (in place of the EDFA gain control), in order to be sure that the RF phase fluctuations do not come from any delay process in the optical amplifier.

III.3.c Experimental results

The experimental results, presented in Figure III-7, clearly show the nonlinear behavior of the phase response of a Discovery *DCS30S* photodiode and its ability to convert the laser RIN into RF phase noise.

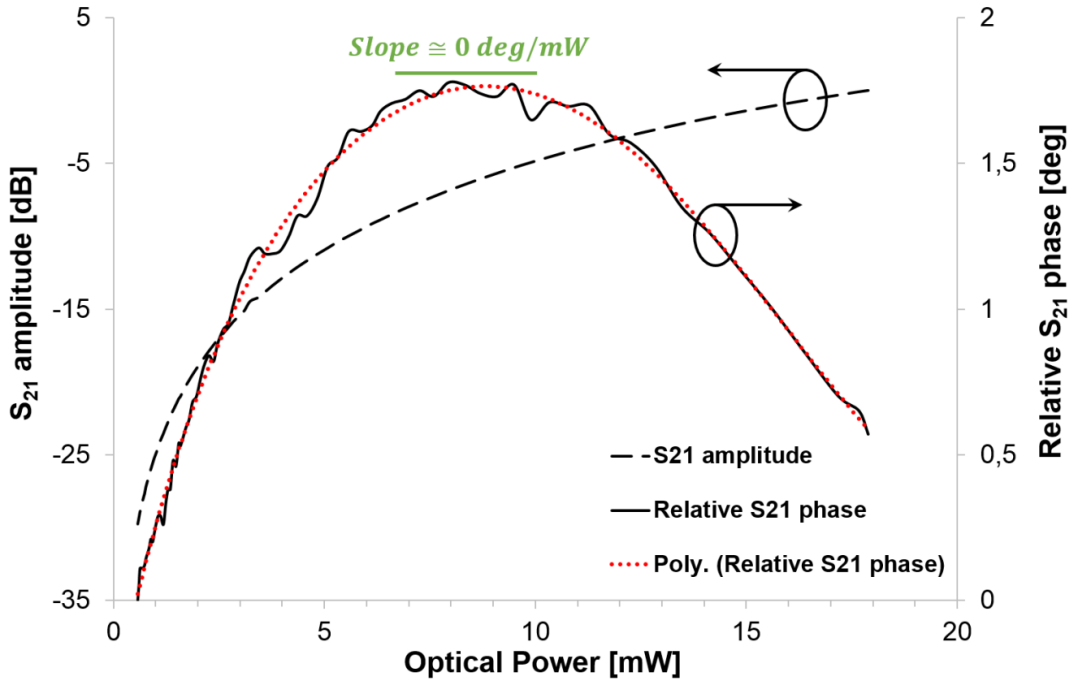

Figure III-7 S_{21} RF amplitude (dashed) and phase (solid) responses of the Discovery DCS30S photodiode versus the input optical power, at 10 GHz of RF frequency. The measured phase data is fitted with a sixth order polynomial fit (dotted).

This behavior is well documented in the literature, and related to the screening effect phenomenon (known as the space charge effect) [43-46]. Broadly speaking, when the optical power increases from low values, it is converted into a large number of electron-holes pairs in the photodiode intrinsic region. The polarization bias field results in the separation of photogenerated electron-hole pairs, and followed by a recombination phenomenon via the electronic circuit load. This enhances the photodiode response which reflects the decrease in

the carrier transit-time (steeper slope in Figure III-7). However, as the optical power approaches the photodiode saturation power, the electric field induced by the carriers opposes the externally applied bias field, and results in an increase of the carrier transit-time (i.e. reduction in carrier velocities), which consequently causes a slow current response.

More interestingly, this slow transit-time near saturation might explain the zero slope in the photodiode's relative RF phase at optical input power of about 8-10 mW and then a fast phase decrease at higher optical power. However, strong saturation on the RF amplitude is only visible at much higher power. That is probably due to the fact that the thermal effects contribute in the saturation response level. This zero slope is particularly interesting in the context of low microwave phase noise [47], since at this specific point, the conversion of the laser amplitude noise is negligible or even absent.

Furthermore, a good fit to the measured RF phase was obtained with a sixth order polynomial fit. At this point, it is useful to calculate the RIN-to-SSB phase noise conversion level or factor, which could estimate numerically the contribution of the RIN in the RF phase noise. In fact, it can be computed from equation (III.8) together with the derivative of the polynomial fit of the RF phase versus the optical power [34]. This conversion factor is given by

$$\mathcal{F}(P_{Opt}) = \frac{P_{opt}^2}{2} \cdot \left(\frac{d\Phi}{dP_{opt}} \right)^2 \tag{III.9}$$

Figure III-8 illustrates the RIN-to-SSB RF phase noise conversion factor in dB. Clearly more than -50 dB reduction is observed near the photodiode saturation, more precisely during the screening effect phenomenon; where the RF phase-to-optical power slope is equal or close to zero. For instance, in the case of a DFB laser, a high frequency RIN level of around -160 dB/Hz will be converted to RF phase noise below -200 dBc/Hz. However, in a lot of applications, this noise level is below the shot and thermal noise.

Thus, based on the measurements and the calculated conversion factor, it is fair to say that the optimal working optical power, at the photodiode's input, lies in the range of 8 to 10 mW, where the laser RIN noise conversion is negligible.

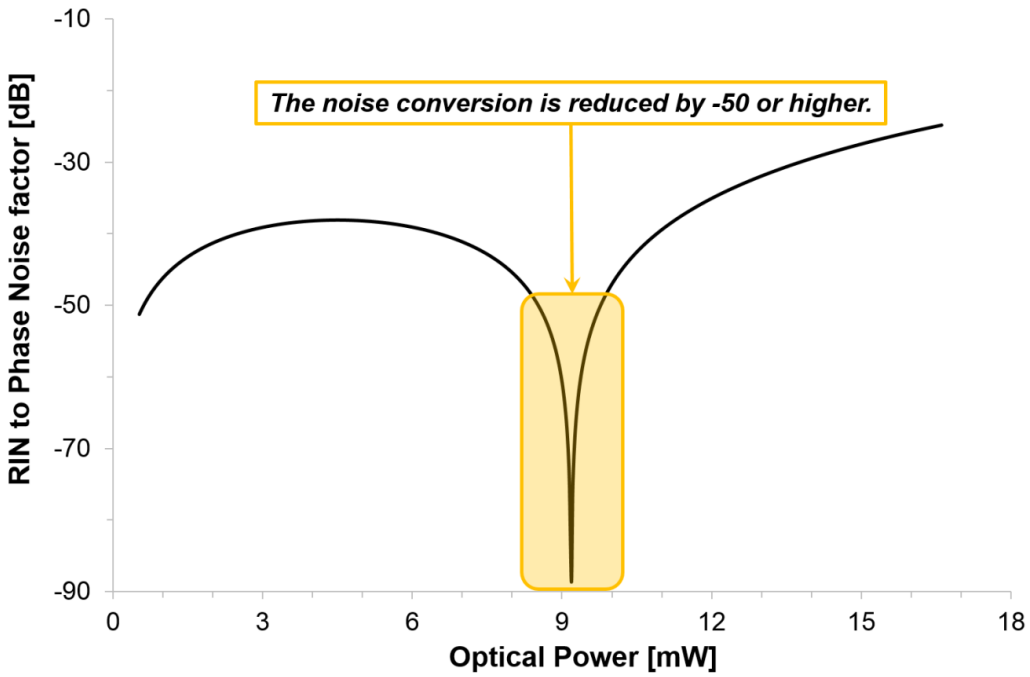

Figure III-8 The RIN-to-SSB RF phase noise conversion factor versus optical power of a Discovery PD.

On the other hand, the low frequency component of the laser RIN $(1/f)$ may have a critical impact on the RF close-in phase noise, especially when the optical power levels are far from the optimal power range.

Moreover, the measurements were performed for three different modulation frequencies: 2, 5 and 10 GHz (Figure III-9). They show that the relative RF phase increases with the increase of the modulation frequency. That is to say that when the application is at higher frequencies, the photodiode RF output power is more sensitive to the response time variation, and thus, this noise conversion phenomenon will be more critical. It is worthy also to point out that the zero slope of the relative RF phase is independent of the modulation frequency as is seen in Figure III-9, where it is clear that this zero slope occurs always for the same optical power range (between 8-10 mW).

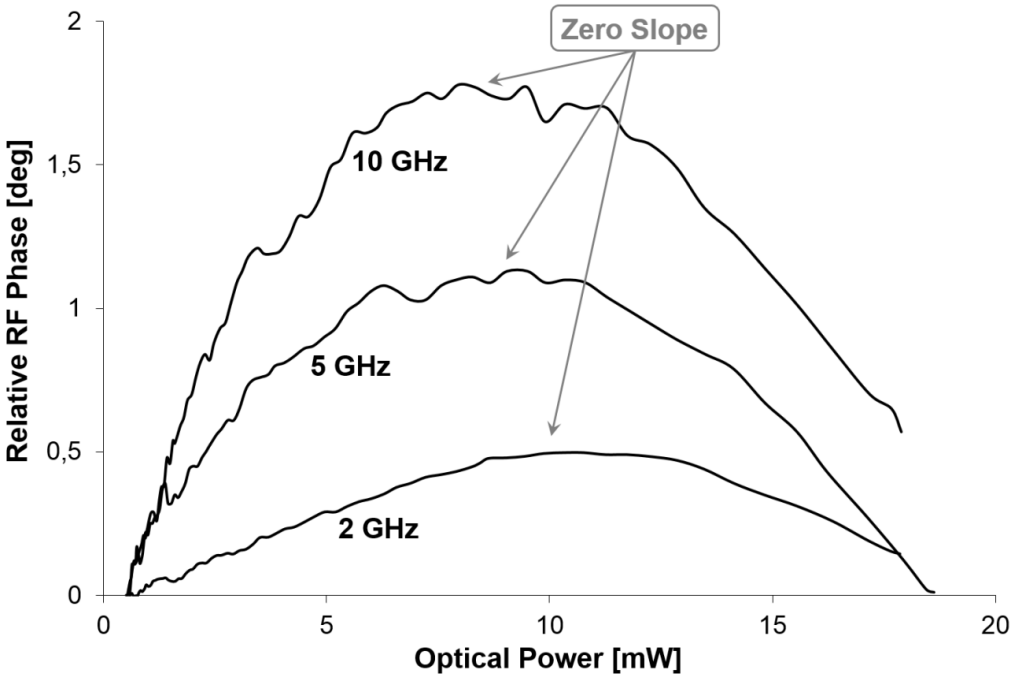

Figure III-9 Relative RF phase of a Discovery DSC30S fast photodiode, versus the received optical power, for three different RF frequencies: 2, 5 and 10 GHz.

It was also found during the experimental screening that this phase parameter also varies with the temperature fluctuations of the Mach-Zehnder modulator, which change slightly its bias point. For this reason, the MZM temperature has been controlled by fixing it on a thick brass plate with foam insulation. Another alternative, which has also been used for some of the experiments, was to take benefit of an active MZM bias locking system, in this case, a Photline MBC-AN controller was used to control the MZM bias point and to guarantee proper linear modulation.

At this stage, it must be stated that, even though this nonlinear behavior of the photodiode came mainly from the carrier transit-time, it could be also a result of a variation of its output capacitance. Nevertheless, after an experimental study of a high speed InGaAs/InP PIN photodiode chip (*PDCS32T*), it has been confirmed that this behavior only comes from the carrier transit-time. In fact, by taking advantage of the photodiode chip, the output reflection coefficient S_{22} has been measured at several input optical powers using the same experimental bench described in the above section. Figure III-10 shows the measured real and imaginary parts of S_{22} versus frequency (from 40 MHz up to 20 GHz) for several optical powers ranging from 0.5 to 8.2 dBm. It is clearly visible that the real and the imaginary components of S_{22} are constant versus the optical power, so consequently the output capacitance is constant as well.

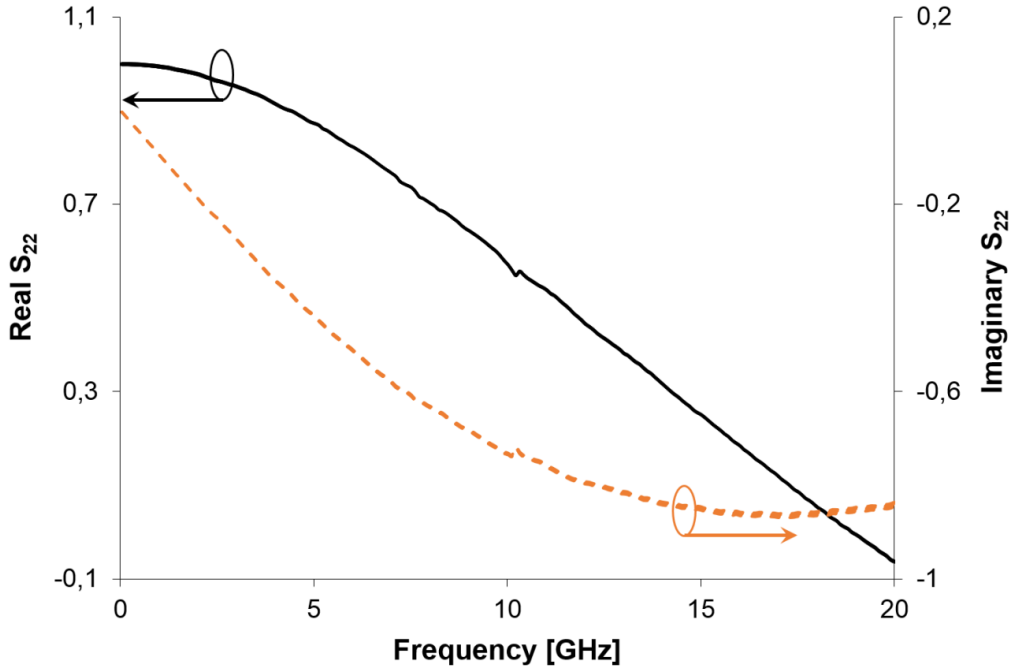

Figure III-10 Measured real (solid) and imaginary (dotted) parts of the S_{22} versus frequency from (40 MHz up to 20 GHz) of a InGaAs/InP PIN photodiode chip for several optical powers ranging from 0.5 to 8.2 dBm.

III.4 Equivalent circuit of a fast photodiode

To quantify and investigate the noise conversion phenomenon in the photodiode, it could be relevant to implement an equivalent circuit model of the device in a microwave circuit simulator, such as Agilent Advanced Design System (ADS).

In previous works, several equivalent electrical circuit models have been proposed for fast photodiodes [48-53]. To name only a few, G. Wang *et al.* have developed a time-delay equivalent-circuit model (Figure III-11 (a)) which includes both the carrier transit-induced time-delay effect and stored charge effect of p-i-n photodiodes in high-power operation [49]. These effects were represented as linear R_tC_t circuit and capacitance C_{sc}, respectively, both combined in parallel to a voltage-controlled current source. All these time-delay circuit elements R_t, C_t and C_{sc} were treated as voltage-dependent components. The presented approach provides a method that directly predicts and analyses the high-power properties of ultrafast p-i-n photodiodes using a full electrical equivalent circuit.

In addition, M. Piels *et al.* have presented a new method for simulating the photodiode nonlinearities (Figure III-11 (b)), with a model including the effects of non-uniform three dimensional absorption, self-heating, and is compatible with circuit components defined in the frequency domain, such as transmission lines [51]. It has been demonstrated the accuracy of the simulation technique to predict the linear and nonlinear behavior of photodiodes, enabling

direct quantitative comparison of the effects of different design decisions on the figure of merit of interest.

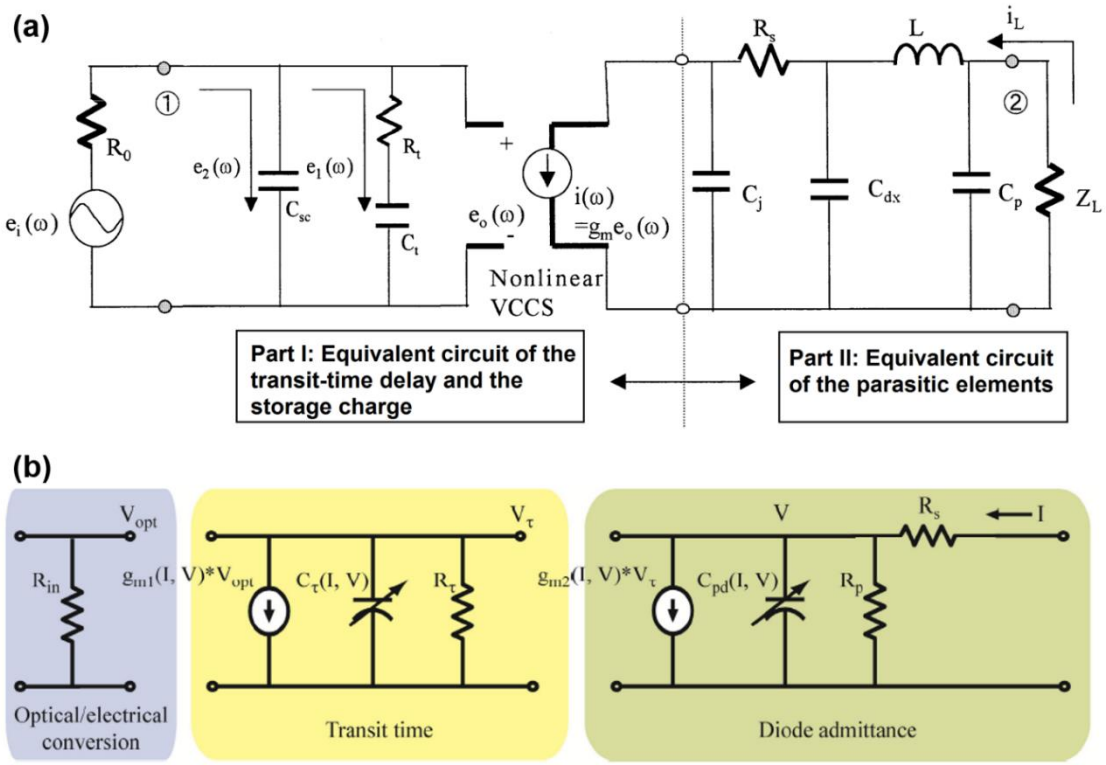

Figure III-11 (a) [49] High-power equivalent-circuit model of the side-illuminated WG p-i-n PD; (b) [51] Nonlinear model of waveguide photodetectors.

However, none of the previously proposed models treated completely the nonlinear behavior of the photodiode, especially the conversion of the amplitude laser noise to RF phase noise. The combination of the experimental results and the analysis presented above, along with the physical understanding of this behavior, were utilized to provide a more realistic modeling of this nonlinearity. The new equivalent circuit model of a fast photodiode, which has been implemented in a microwave circuit simulator Agilent ADS, is represented and detailed below.

III.4.a Photodiode new nonlinear model description

Even though ADS library does not include models of any optical or optoelectronic devices, these components have been described using electrical equivalent models or mathematical equations, thanks to the symbolically defined devices module of ADS, or a mix between these two approaches.

The new nonlinear equivalent-circuit model of the photodiode [42] is presented in Figure III-12.

As it is known, the photodiode is used as an optical receiver. It operates by converting the light signal into electrical current. The photocurrent (i_{PD}) generated in the photodiode is linearly related to the received light beam power:

$$i_{PD} = R_{PD} \cdot P_{opt} \tag{III.10}$$

where R_{PD} is the responsivity of the photodiode in A/W, and P_{opt} is the power of the light beam in W.

The Optical/Electrical conversion of the photodiode is therefore described as a quadratic detector using a nonlinear voltage controlled current source (NonlinVCCS). Its output current I_{out} is defined as a function of the input voltage V_{in} as follow:

$$I_{out} = \frac{R_{PD}}{R} V_{in}^2 \tag{III.11}$$

where R is the load resistance at the MZM output.

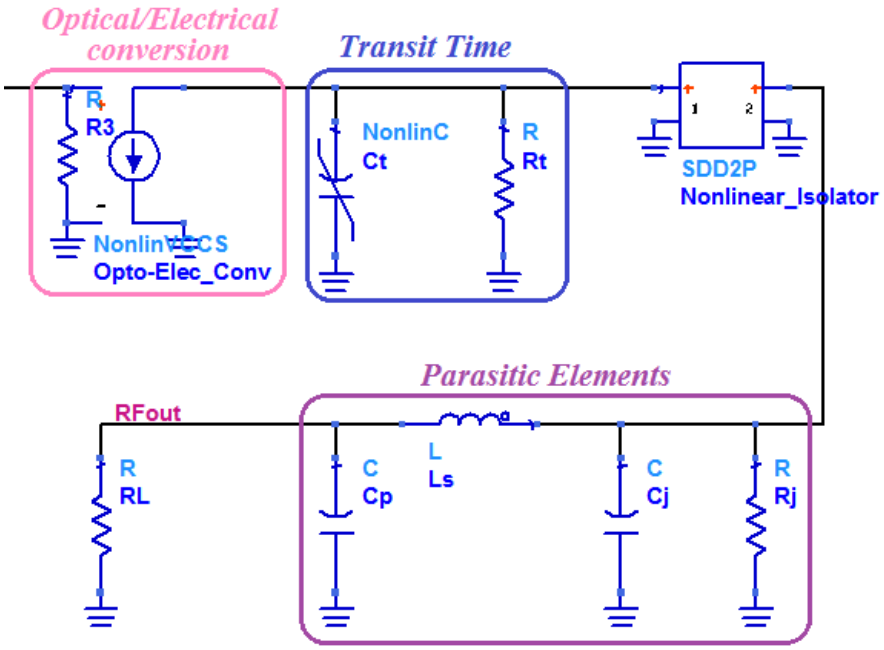

Figure III-12 A nonlinear equivalent-circuit model of a photodiode.

To describe precisely the behavior of a photodiode, the screening effect should be taken into account. To this purpose, the center section of this model deals with the carrier transit-time effects, which is represented by a parallel $R_t C_t$ nonlinear circuit, where the capacitance C_t is a nonlinear function of voltage. It is defined as

$$C_t(V) = \alpha_1 + \alpha_2 \cdot V + \alpha_3 \cdot V^2 \quad \text{(III.12)}$$

where V is the voltage across the capacitance, and α_1, α_2 and α_3 are the polynomial coefficients.

The parallel $R_t C_t$ circuit is fed by the current source from the NonlinVCCS (I_{in}, input current of the $R_t C_t$ circuit), the transfer function of this transit-time circuit can be written as:

$$\frac{V_{out}}{I_{in}} = \frac{R_t}{1 + jw\tau_t} \quad \text{(III.13)}$$

where V_{out} is the transit-time circuit output voltage, and τ_t, which is equal to $C_t(V) \cdot R_t$, represents the nonlinear delay time.

This nonlinear time-delay equivalent circuit is separated from the parasitic elements by a nonlinear isolator (SDD2P) where the output current is assumed to be linearly proportional to the input power (low input optical power), and where the current compression is allowed for high optical power (close to the saturation threshold). This isolator is defined as:

$$I(V) = Isat \cdot \tanh\left(\frac{V}{R \cdot Isat}\right) \quad \text{(III.14)}$$

where I and V are the output current and input voltage of the isolator, $Isat$ is the current saturation, which is defined as the dc photocurrent at which the ac output power is compressed from the linear response by 1 dB. Its value is based on experimental studies of the Discovery photodiode.

Finally, the parasitic parameters were added to the model, where R_j and C_j are the junction resistance and capacitance, respectively. C_p is the parasitic capacitance, and L_s is the series inductance.

As for this parasitic elements model, it is in fact a simplified model that depict the parasitic components of a Discovery photodiode. However, the availability of a high speed photodiode on chip (*PDCS32T*) and the access to its output reflection coefficient S_{22} measurement make it possible to apply a complete parasitic equivalent circuit model that is related to the physical parameters of the p-i-n photodiode [53] and to extract the circuit components values for the various elements (R, C, L) in the equivalent circuit. This model is depicted in Figure III-13 (a), where R_j is the resistance representing the dark current leakage, C_d is the capacitance between p- and n- contact metallization which is significant at low frequencies, R_s is the p- and n- electrode contact resistance, L_s is the inductance of the p/n contacts to signal/ground electrodes, R_{sh} and C_{sh} are the shunt resistance and capacitance of coplanar waveguide which take into account the electric energy storage inside the transmission line and the losses caused by the transverse component and C_p is the open circuit at the end of the coplanar waveguide transmission line.

All the parameters for the elements included in the equivalent circuit model were extracted by fitting the measurement-based S_{22} parameter up to 20 GHz using Agilent ADS "parameter Tuning procedure". The parasitic equivalent model has been validated by reasonable agreement with the measured output reflection coefficient (S_{22}) of the PIN photodiode, as demonstrated in Figure III-13 (b).

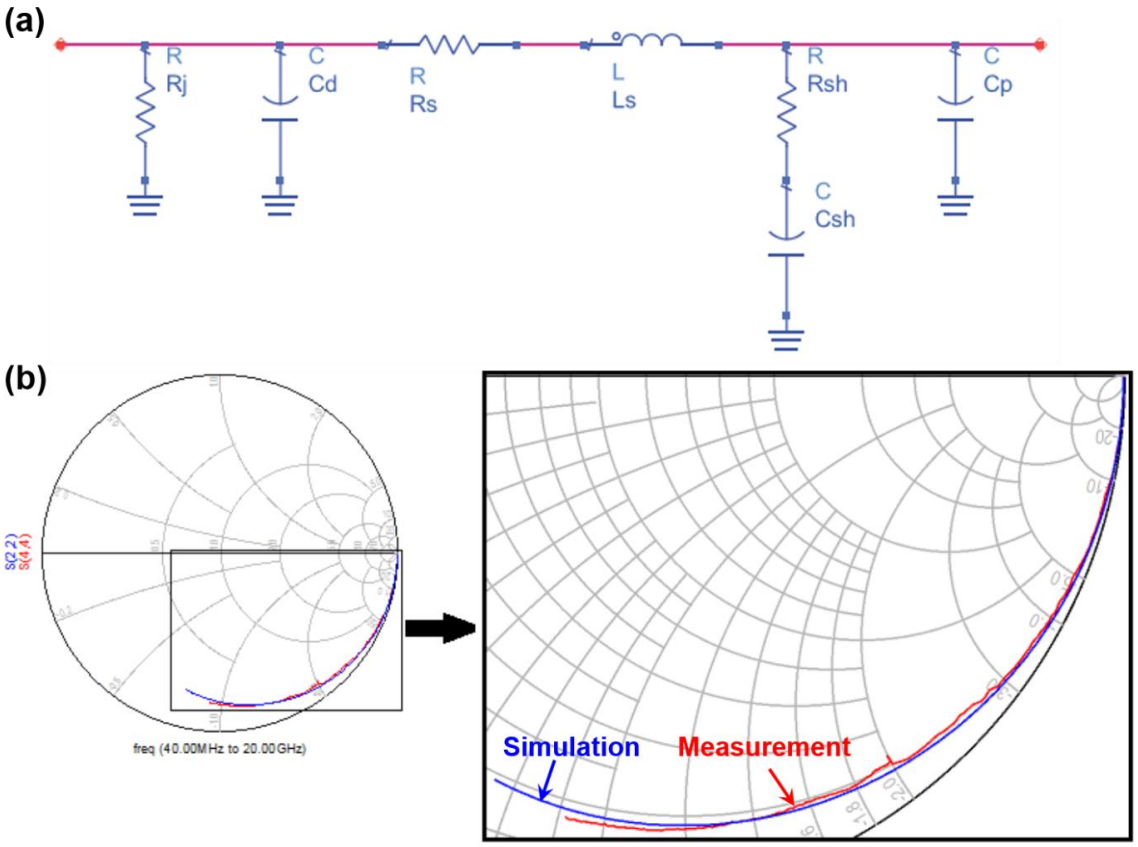

Figure III-13 (a) Parasitic elements model of a high speed InGaAs/InP photodiode on chip. (b) Measured and fitted reflection coefficient S_{22} versus frequency (from 40 MHz up to 20 GHz) of a pin photodiode on Smith Chart.

III.4.b Simulation of the PD's nonlinearity

Despite the fact that Agilent ADS is a pure microwave circuit simulator, it was chosen primarily because it includes the harmonic balance approach, which is a frequency-domain analysis technique [54,55]. The interest of this approach lies in its ability to simulate the noise conversions in nonlinear devices, between different carrier frequencies, even if these frequencies are as far apart as DC, microwave signal (10 GHz) and optical carrier (200 THz). Using this approach, nonlinear devices are computed in the time-domain and then converted to frequency-domain via the Fast Fourier Transform (FFT).

To validate the performance of this photodiode's new model, it has been implemented in an ADS description of a microwave-optical link that was already suggested by

H. Brahimi *et al.* [56]. Figure III-14 depicts the microwave-optical link model including the new photodiode's model.

III.4.b.i Optical components modeling

The laser is described using an RF power source (P_1Tone), where the optical carrier is considered like the RF carrier but at an extremely higher frequency. In our case the frequency has been fixed at 200 THz (Fr_HF). In this phase of the study, the laser relative intensity noise has not been included in the laser model, since the main focus here was on the photodiode nonlinearity. In addition, an "attenuator" has been placed between the MZM and the photodiode model to allow for variations in the optical power, received by the photodiode. In fact, the RIN was included later on, in order to simulate the RF phase noise of the whole system.

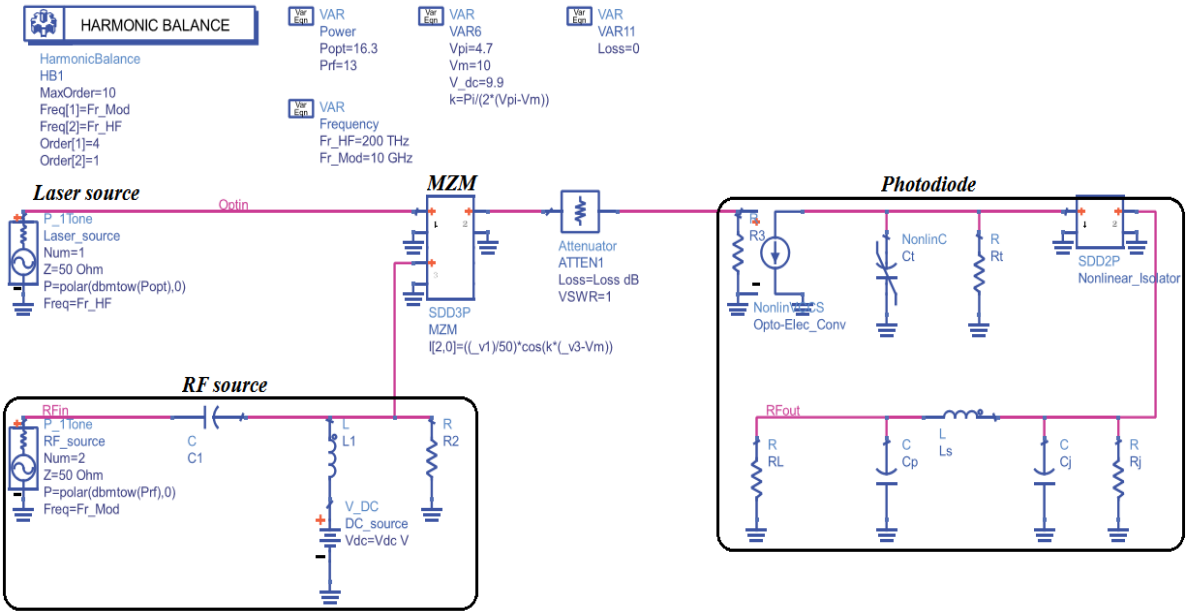

Figure III-14 ADS model of a microwave optical link, including an optical source (Laser) and a Mach-Zehnder modulator (MZM).

The Mach-Zehnder modulator [56-58] is represented by a symbolically defined device (SDD), including its $1 + \cos x$ response:

$$P_{Out\_MZM} = \frac{P_{opt}}{2}(1 + \cos \varphi_{MZM}(t)) \tag{III.15}$$

where P_{opt} is the laser optical power and $\varphi_{MZM}(t)$ is the phase difference between the waves propagation through the MZM two arms, it is expressed as:

$$\varphi_{MZM}(t) = \pi \frac{V_{RF}(t) + V_{dc} - V_m}{V_\pi - V_m} \tag{III.16}$$

where $V_{RF}(t)$ is the RF modulation signal voltage, V_{dc} is the MZM DC bias voltage, V_m is the MZM maximum voltage, and V_π is the MZM extinction voltage. Using formulas (III.15) and (III.16), the SDD current and voltage relation is defined as follow:

$$I_{out} = \frac{V_{opt}}{R} \cos\left(\pi \frac{V_{RF}(t) + V_{dc} - V_m}{2(V_\pi - V_m)}\right) \tag{III.17}$$

III.4.b.ii Simulation versus experimental results

In Figure III-15, the comparison between the measured and simulated relative RF phase data of a Discovery photodiode are presented for three different RF frequencies: 2, 5 and 10 GHz.

By carefully choosing the values for the carrier transit-time components $R_t C_t$, and especially the polynomial coefficients (α_1, α_2 and α_3) of the nonlinear capacitance C_t, the simulated relative RF phase results are in satisfactory agreement with the measured results, with a maximal error level in the relative phase difference below 0.3º. Interestingly also, the zero phase slope appears in almost the same range of optical power as for the measurements.

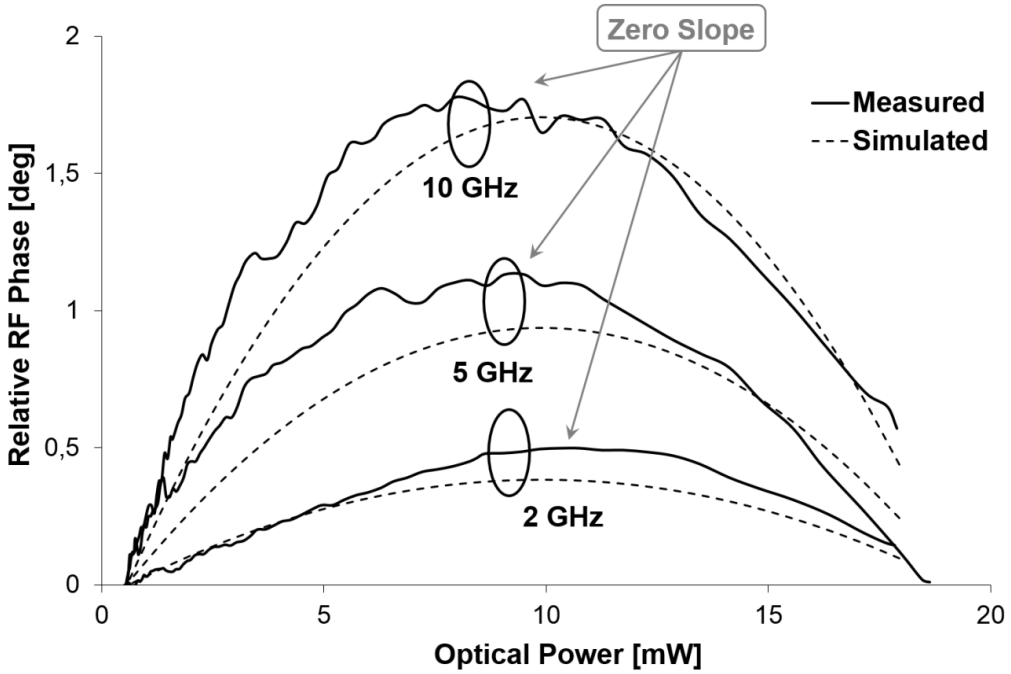

Figure III-15 Simulated (dashed) and experimental (solid) relative RF phase of a discovery photodiode versus input optical power, for three different frequencies: 2, 5 and 10 GHz.

The amplitude of the forward transmission frequency response S_{21} versus frequency (from 40 MHz up to 20 GHz) of the Discovery photodiode has also been measured and

simulated for several optical power, ranging from 0.6 to 7.4 dBm. The results are presented in Figure III-16, where a relatively good agreement is again obtained. It is notable that the amount of optical power received does not change the frequency response, but the RF output power increases with the optical power with a 2 dB RF gain every 1 dB optical gain, up to the photodiode saturation threshold power.

Taking into account the difficulties and the precision of the measurements, particularly because of their temperature sensibility, this new nonlinear equivalent model of a photodiode can be considered as a good predictor of the nonlinearity behavior of a fast photodiode, and especially when it comes to represent the conversion of the laser amplitude noise into RF phase noise.

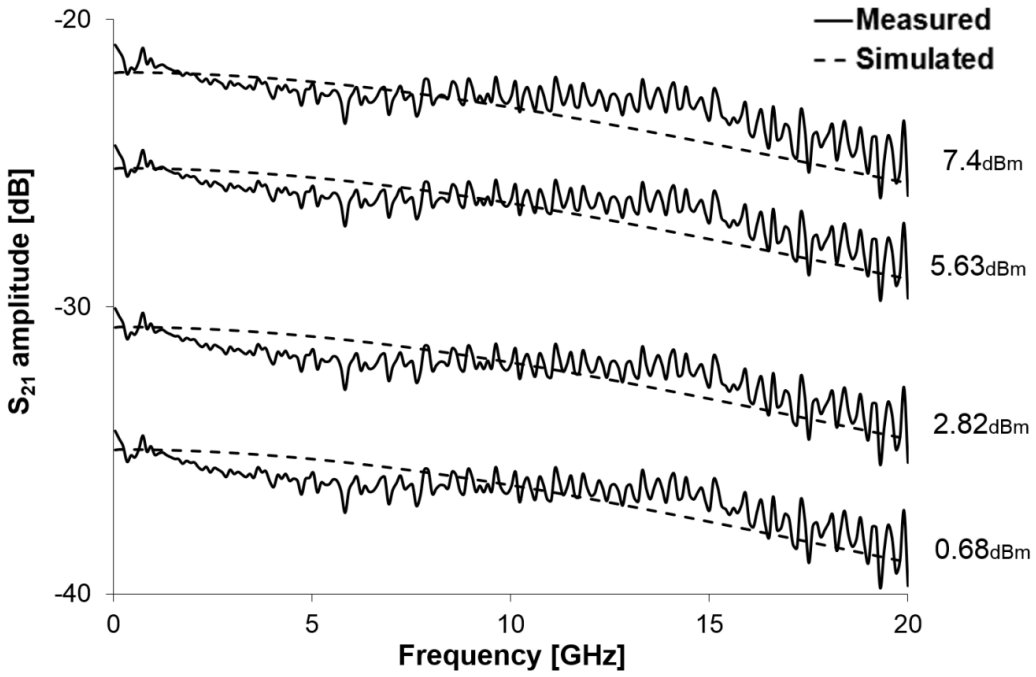

Figure III-16 Simulated (dashed) and experimental (solid) forward transmission gain S_{21} of a Discorvery PD versus the RF frequency (from 40 MHz up to 20 GHz), for different optical power levels.

III.5 RF phase noise simulation

Accurate modeling of this nonlinear conversion phenomenon is an essential requirement in OEOs applications. It also complete the modeling approach of microwave optical systems suggested by H. Brahimi [56], which was not able to compute the optical link close-to-the-carrier $(1/f)$ phase noise. In the case of OEOs, it results in a 30 dB/dec slope of the close-to-carrier spectrum which is always observed experimentally.

In fact, simulating directly the phase noise of an OEO, in a closed-loop configuration, is rather difficult because an OEO is an autonomous system, in which the oscillation start-up has to be managed independently from the optical signal, contrary to the open-loop

configuration, where the oscillation frequency is externally selected (i.e. by means of the RF input of the Mach-Zehnder modulator). Fortunately, the closed-loop performance of the OEO can be computed analytically from its open-loop phase noise [59]; hence, for this reason, the first step was to be able to properly simulate the phase noise performance of an open-loop optical link, especially close-to-the-carrier, and then the expected OEO closed-loop phase noise can be determined.

Concerning the noise simulation, the harmonic balance approach includes a specific module which is able to compute the effect of a small perturbation at a given frequency on any other simulation frequencies, in amplitude and phase. This technique is known as the conversion matrix technique for nonlinear noise computation [55]. This module not only allows the description of a quasi-static perturbation, but is also able to take into account a possible frequency dispersion in a small frequency bandwidth around any of the simulation frequencies. In other words, it is the perfect tool to compute the conversion of a noise at a given frequency towards another frequency of the analysis (in this case, the RF frequency). The phase noise simulation results are presented by the ADS noise variable “pnmx” (in dBc/Hz), which stands for phase noise from mixing analysis.

III.5.a.i Open-loop phase noise simulation

In the model depicted in Figure III-17, the noisy devices are the laser and the photodiode, whereas the Mach-Zehnder modulator was considered as a nonlinear noiseless device. The laser is described by its amplitude noise (RIN), thanks to the amplitude modulator (AM_ModTuned) fed by a voltage noise source (V_noise). This noise source is simply described by the sum of a $1/f$ noise and a noise floor. The parameters of the noise source feeding the AM modulator are adjusted such that the laser RIN simulated around DC on the photodiode can fit the measured low-frequency RIN of a semiconductor DFB laser.

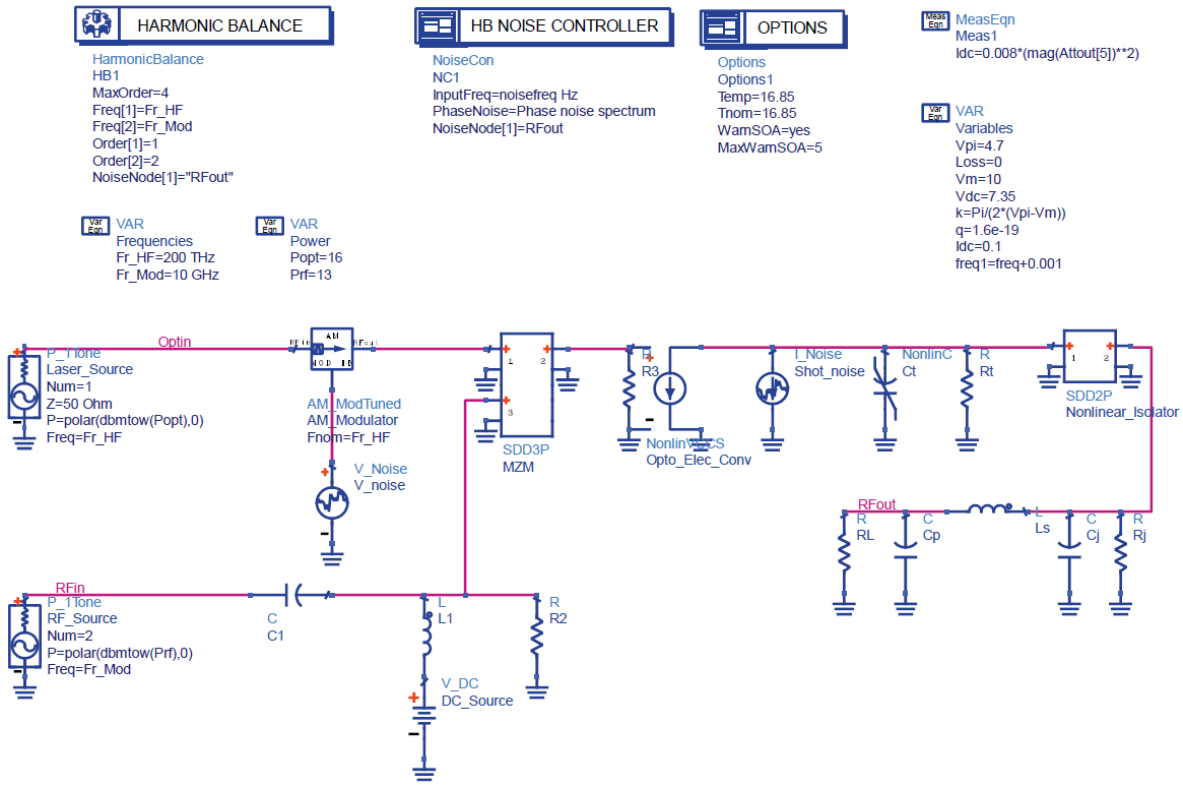

Figure III-17 Model of an optical link on ADS including an optical source with amplitude noise (AM modulator) and a Mach Zehnder modulator (MZM).

Note that, the phase noise of the laser could be also included in the model. However, there is no element in this model able to perform a conversion of such noise (such as an optical delay line). In a near future, a model of a dispersive optical fiber will be included in this approach, and in this case the laser frequency noise will be of interest.

In addition, a shot noise source is added to the photodiode model, presented as a noise current source (Shot_noise) [60]. The current output is expressed as square root of the current white noise spectral density:

$$I_{Shot\_noise} = \sqrt{2qI_0} \tag{III.18}$$

with q being the electron charge and I_0 the DC photocurrent.

Figure III-18 depicts the simulated RIN at the photodiode output around DC frequency, for three optical power levels: 9.1, 13.6 and 18.6 dBm. These results corresponds to measurements spectra which have been obtained on a high power EM4 semiconductor DFB laser, similar to the measurements described in [61] for the same device. It is clear that the laser RIN improves with the increase of the optical power, for both the $1/f$ components and the noise floor.

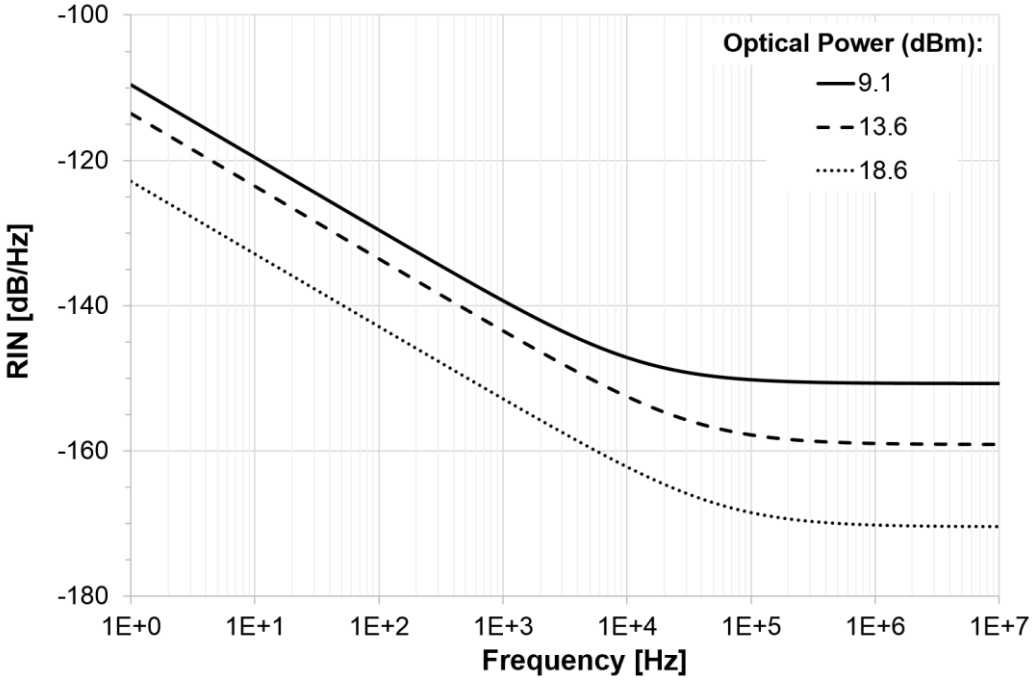

Figure III-18 RIN simulated with ADS at the photodiode output around DC frequency (fitted to a semiconductor DFB laser measured data), for three optical power levels.

Then, in an open-loop configuration, the 10 GHz phase noise of the optical link has been simulated with ADS using the dedicated variable for nonlinear noise simulation “pnmx”, for three optical power levels. The results are presented in Figure III-19. As shown in this figure, the only important $1/f$ contribution which appears in the simulated data is at high optical power level (>12 dBm), and this noise decreases as the optical power approaches the optimal optical power (~ 9 dBm), where the RIN to phase noise conversion is at its lowest levels.

For high offset frequencies (above 1 kHz), the phase noise is most probably limited and dominated by the high frequency component of the laser RIN, especially at low optical power, as it is evident from Figure III-18. That explains why the phase noise level at 9.1 dBm optical power is higher than the phase noise level at higher optical power.

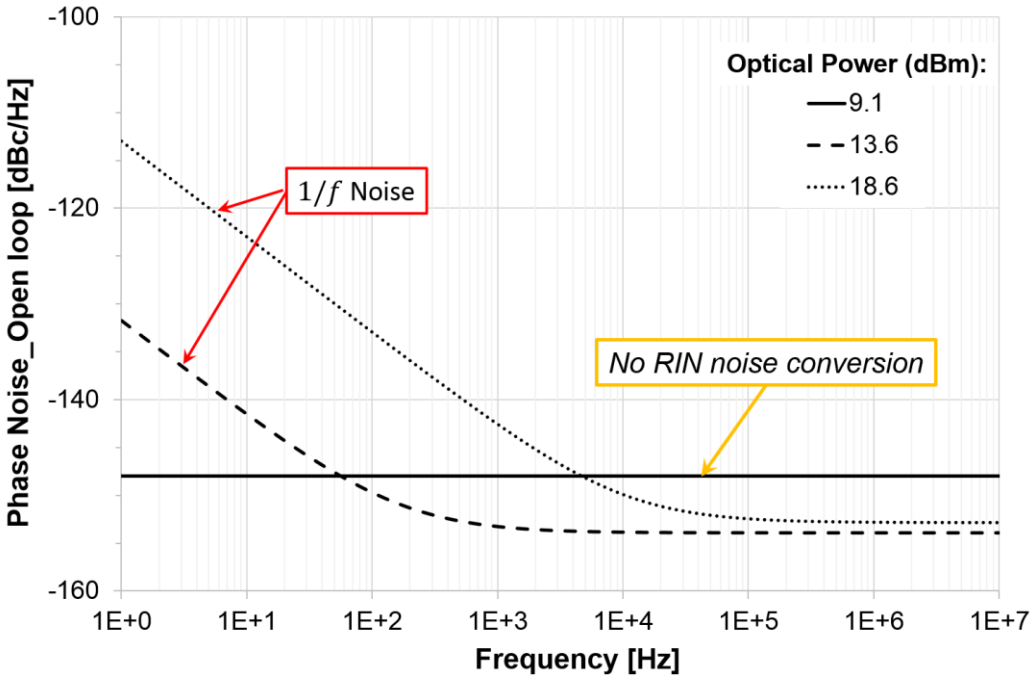

Figure III-19 Simulated phase noise (pnmx) around the RF carrier (10 GHz) on an open loop configuration optical link, at three optical power levels.

Considering that the laser is perfectly locked to the peak of a resonator's resonance, the simulated phase noise (Figure III-19) represents the RF phase noise performance of an optoelectronic oscillator in an open-loop configuration.

III.5.a.ii Close-loop phase noise of an OEO

Up until now, it is still difficult to simulate an optoelectronic oscillator phase noise in its closed-loop configuration, directly using ADS. However, based Lesson's models [59], the closed-loop phase noise is related to the open-loop phase noise, and thus it can be calculated using the following formula:

$$L_{OEO}(f_m) = 10 \cdot Log\left(\frac{f_{opt}^2}{8\,Q_{opt}^2\,f_m^2} + 1\right) + L_{OEO\_OL} \qquad \text{(III.19)}$$

where $L_{OEO}(f_m)$ is the oscillator single-sideband phase noise in dBc/Hz, f_{opt} is the optical frequency (200 THz), Q_{opt} is the optical quality factor of the used resonator, and L_{OEO_OL} is the oscillator open-loop single-sideband phase noise in dBc/Hz.

Figure III-20 illustrates the computed closed-loop phase noise of an 100m long fiber ring resonator based OEO using the simulated phase noise presented above (Figure III-19) for three different optical power levels. This figure shows an excellent phase noise performance for these type of oscillators.

However, two noise sources were not taken into account in the present modeling and simulation processes. These noise sources include the RF amplifier phase noise and the nonlinear optical effects generated inside the fiber resonator. In fact, at these optical power levels, the nonlinear optical effects contribute significantly in the degradation of the OEO phase noise, especially close-to-the-carrier.

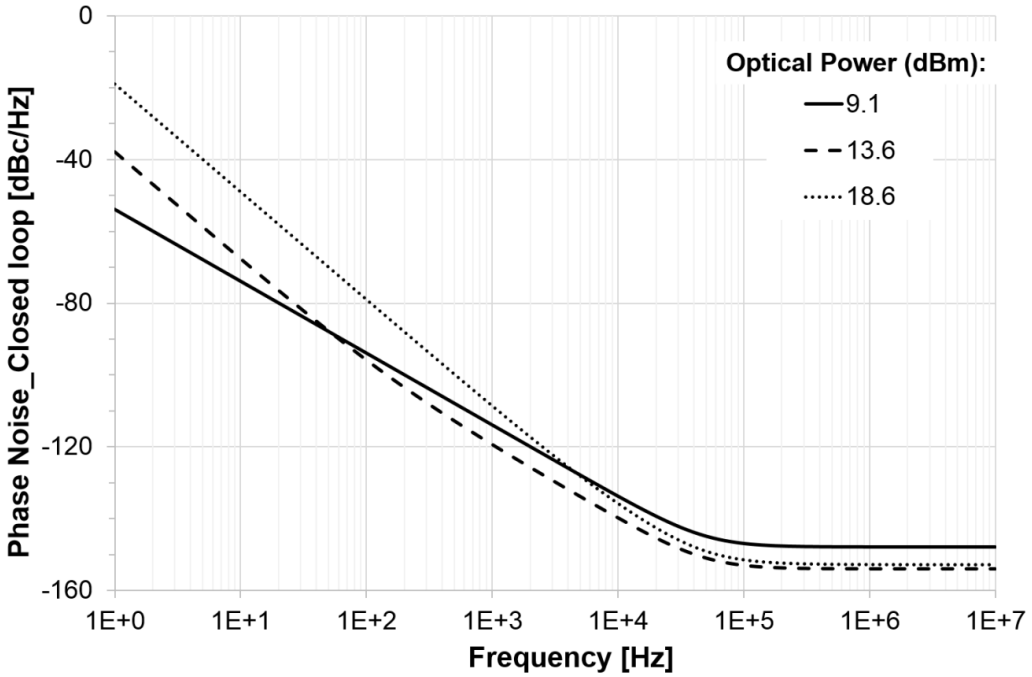

Figure III-20. Calculated 100m long FRR based OEO closed-loop phase noise using the simulated OEO open-loop phase noise, based on Lesson's model.

Further improvement should be done regarding the simulation of the OEO phase noise, where all the noises sources and the nonlinearity behavior that could contribute to the oscillator short-term stability should be modeled in order to be able to predict realistic performance.

III.6 Conclusion

In this chapter, an overview is provided on the main different factors that have significant impact on the overall performance of an OEO system. These factors include the amplitude and phase noises of the various components in the loop, the different noise conversion processes that can take place in the OEO setup, and the nonlinear optical effects generated inside an optical resonator.

A large part of this chapter was dedicated to study the conversion process of the laser relative intensity noise into microwave amplitude and phase noise via the photodiode nonlinearity. This nonlinear behavior of the photodiode has been attributed mainly to the dependency of the carrier transit-time inside the photodiode on the received optical power and the related screening effect phenomenon. Based on experimental findings, an optimal optical

power has been identified, at which the laser RIN-to-RF phase noise conversion could be negligible.

A new nonlinear equivalent circuit model of a fast photodiode, which takes into account the transit-time delay effect, was proposed and modeled using a microwave circuit simulator, Agilent ADS. This conversion is realized through a nonlinear RC circuit. The validity of this model has been confirmed by a good match between the simulation and experimental results of the microwave phase data at different microwave frequencies. These studies have been of major importance for modeling realistically the physical behavior of a photodiode and for optimizing the contribution of the laser noise on the OEO short-term stability.

Furthermore, this new model has been included in a model describing a complete optical link and has been used to simulate the residual phase noise of this link. This approach is found to be able to simulate the RF phase noise of an open loop optical link, and especially its close-to-the-carrier component ($1/f$ noise) at high optical power. It was confirmed through simulation that this noise decreases as the optical power approaches the optimal optical power, where the RIN to phase noise conversion was at its lowest levels.

As for the case of an OEO in its closed-loop configuration, the open-loop phase noise data of an optical link has been used to calculate the closed-loop RF phase noise, based on Leeson's approach. However, the results obtained so far do not represent the real performance of an OEO, since some noise sources were not taken into account in this model.

So as a conclusion, to predict and reduce the phase noise of an OEO and especially its $1/f$ noise, additional noise modeling investigations are required, on one hand for accurately compute the OEO $1/f$ phase noise at low optical power (i.e. lower than the photodiode's input optimal optical power), which was a main drawback of this approach even with the presence of the new photodiode nonlinear model. On the other hand, for including the other noise sources, for instance, the nonlinear optical scattering inside the optical fibers and the optical resonators, since at a specific optical power, these optical effects may degrade severely the phase noise of an OEO system.

III.7 References

1. Stolen, R. H. Nonlinearity in fiber transmission. *Proc. IEEE* **68**, 1232-1236 (1980).
2. Chraplyvy, A. R. Limitations on lightwave communications imposed by optical-fiber nonlinearities. *J. Lightwave Technol.* **8**, 1548-1557 (1990).
3. Agrawal, G. P. *Nonlinear fiber optics* (Academic Press 2007).
4. Ruffin, A. B. Stimulated Brillouin scattering: an overview of measurements, system impairments, and applications. *NIST Symposium on Optical Fiber Measurements, Technical Digest*, 23-28 (2004).
5. Brillouin, L. Diffusion de la lumière et des rayons X par un corps transparents homogène. Influence de l'agitation thermique. *Ann. Phys.* **17**, 88-122 (1922).
6. Rastogi, P. K. *Photomechanics*. p.286 (Springer Science & Business Media, 2003).
7. Tkach, R. W., Chraplyvy A. R. & Derosier, R. M. Spontaneous Brillouin scattering for single-mode optical-fibre characterization. *IEE Electron. Lett.* **22**, 1011-1013 (1986).
8. Chiao, R. Y., Townes, C. H. & Stoicheff, B. P. Stimulated Brillouin scattering and coherent generation of intense hypersonic waves. *Phys. Rev. Lett.* **12**, 592-595 (1964).
9. Ippen, E. P. & Stolen, R. H. Stimulated Brillouin scattering in optical fibers. *Appl. Phys. Lett.* **21**, 539-541 (1972).
10. Jenkins R. B., Sova, R. M. & Joseph R. I. Steady-state noise analysis of spontaneous and stimulated Brillouin scattering in optical fibers. *J. Lightwave Technol.* **25**, 763-770 (2007).
11. Chen, L. & Bao, X. Analytical and numerical solutions for steady state stimulated Brillouin scattering in a single-mode fiber. *Opt. Commun.* **152**, 65-70 (1998).
12. Ferreira, M. F. Limitations imposed by stimulated Brillouin scattering on uni- and bi-directional transmission systems using active fibers. *Electron. Lett.* **31**, 1182-1183 (1995).
13. Niklès, M., Thévenaz, L. & Robert, P. A. Brillouin gain spectrum characterization in single-Mode optical fibers. *J. Lightwave Technol.* **15**, 1842-1851 (1997).
14. Yeniay, A., Delavaux, J-M. & Toulouse, J. Spontaneous and stimulated Brillouin scattering gain spectra in optical fibers. *J. Lightwave Technol.* **20**, 1425-1432 (2002).
15. Lee, J. H., Tanemura, T., Kikuchi, K., Nagashima, T., Hasegawa, T., Ohara, S. & Sugimoto, N. Experimental comparison of a Kerr nonlinearty figure of merit including the stimulated Brillouin scattering threshold for state-of-art nonlinear optical fibers. *Opt. Lett.* **30**, 1698-1700 (2005).
16. Kobyakov, A., Sauer, M. & Chowdhury, D. Stimulated Brillouin scattering in optical fibers. Adv. Opt. Photon. **2**, 1-59 (2010).
17. Hirano, M., Nakanishi, T., Okuno, T. & Onishi, M. Silica-based highly nonlinear fibers and their application. *IEEE J. Sel. Topics Quantum Electron.* **15**, 103-113 (2009).
18. Saleh, K., Llopis, O. & Cibiel, G. Optical scattering induced noise in fiber ring resonators and optoelectronic oscillators. *J. Lightwave Technol.* **31**, 1433-1446 (2013).

19. Okusaga, O., Cahill, J., Zhou, W., Docherty, A., Carter, G. M. & Menyuk, C. R. Optical scattering induced noise in RF-photonic systems. *2011 Joint Conference of the IEEE international Frequency Control and the European Frequency and Time Forum (FCS) Proceedings*, San Francisco, CA, 1-6 (2011).
20. Stépien, L., Randoux, S. & Zemmouri, J. Intensity noise in Brillouin fiber ring lasers. *J. Opt. Soc. Am. B* **19**, 1055-1066 (2002).
21. Geng, J., Staines, S., Wang, Z., Zong, J., Blake, M. & Jiang, S. Highly stable low-noise Brillouin fiber laser with ultranarrow spectral linewidth. *IEEE Photon. Technol. Lett.* **18**, 1813-1815 (2006).
22. Li, J., Lee, H. & Vahala, K. J. Low-noise Brillouin laser on a chip at 1064 nm. *Opt. Lett.* **39**, 287-290 (2014).
23. Smith, S. P., Zarinetchi, F. & Ezekiel, S. Narrow-linewidth stimulated Brillouin fiber laser and applications. *Opt. Lett.* **16**, 393-395 (1991).
24. Saleh, K., Merrer, P. H., Llopis, O. & Cibiel, G. Optical scattering noise in high Q fiber ring resonators and its effect on optoelectronic oscillator phase noise. *Opt. Lett.* **37**, 518-520 (2012).
25. Zhu, T., Bao, X., Chen, L., Liang, H. & Dong, Y. Experimental study on stimulated Rayleigh scattering in optical fibers. *Opt. Express* **18**, 22958-22963 (2010).
26. Smith, A. V. & Smith, J. J. Spontaneous Rayleigh seed for stimulated Rayleigh scattering in high power fiber amplifiers. *IEEE. Photon. J.* **5**, 7100807 (2013).
27. Boyd, R. W. *Nonlinear optics* (Academic Press, 2008).
28. Li, T. *Optical Fiber Communications: Fiber Fabrication*. Vol. 1 (Academic Press, 1985).
29. Okusaga, O., Cahill, J., Docherty, A., Zhou, W. & Menyuk, C. R. Guided entropy mode Rayleigh scattering in optical fibers. *Opt. Lett.* **37**, 683-685 (2012).
30. Inoue, K. Four-wave mixing in an optical fiber in the Zero-dispersion wavelength region. *J. Lightwave Technol.* **10**, 1553-1561 (1992).
31. Savchenkov, A. A., Matsko, A. B., Strekalov, D., Mohageg, M., Ilchenko, V. S. & Maleki, L. Low threshold optical oscillations in a whispering gallery mode CaF2 resonator. *Phys. Rev. Lett.* **93**, 243905 (2004).
32. Shieh, W. & Maleki, L. Phase noise of optical interference in photonic RF systems. *IEEE Photon. Technol. Lett.* **10**, 1617-1619 (1998).
33. Volyanskiy, K., Chembo, Y. K., Larger, L. & Rubiola, E. Contribution of the laser frequency and power fluctuations to the microwave phase noise of optoelectronic oscillators. *J. Lightw. Technol.* **28**, 2730-2735 (2010).
34. Eliyahu, D., Seidel, D. & Maleki, L. RF amplitude and phase noise reduction of an optical link and an opto-electronic oscillator. *IEEE Trans. Microw. Theory Techn.* **56**, 449-456 (2008).

35. Brahimi, H. Etude en bruit de systèmes optiques hyperfréquences modélisation, caractérisation et application à la métrologie en bruit de phase et à la génération de fréquence. *Ph.D. Thesis*, Toulouse University, Paul Sabatier University, Toulouse, France (2003).
36. Saleh, K. High spectral purity microwave sources based on optical resonators. *Ph.D. Thesis*, Toulouse University, Paul Sabatier University, Toulouse, France (2012).
37. Attard, J. C., Mitchell, J. E. & Rasmussen, C. J. Performance analysis of interferometric noise due to unequally powered interferers in optical networks. *J. Lightwave Technol.* **23**, 1692-1703 (2005).
38. Atlas, D. A. Nonlinear optical crosstalk in WDM CATV systems. *Nanostructures and Quantum Dots/WDM Components/VCSELs and Microcavaties/RF Photonics for CATV and HFC Systems, 1999 Digest of the LEOS Summer Topical Meetings,* San Diego, CA, USA, IV23-IV24 (1999).
39. Filipenko, A. I. End face nonperpendicularity analysis in fiber connectors. *Laser and Fiber-Optical Networks Modeling, 2001 Proceedings of LFNM 2001. 3rd International Workshop on,* Kharkiv, 53-55 (2001).
40. Way, W. I., Lin, C., Zah, C. E., Curtis, L., Spicer R. & Young, W. C. Multiple-reflection-induced intensity noise studies in a lightwave system from multichannel AM-VSB television signal distribution. *IEEE Photon. Technol. Lett*. **2**, 360-362 (1990).
41. Cox, C. H., III, *Analog Optical Links: Theory and Practice*. (Cambridge, U.K.: Cambridge Univ. Press, 2004).
42. Abdallah, Z., Rumeau, A., Fernandez, A., Cibiel, G. & Llopis, O. Nonlinear equivalent-circuit modeling of a fast photodiode. *IEEE Photon. Technol. Lett.* **26**, 1840-1842 (2014).
43. Kuhl, D., Hieronymi, F., Böttcher, E. H., Wolf, T., Bimberg, D., Kuhl, J. & Klingenstein, M. Influence of space charges on the impulse response of InGaAs metal-semiconfuctor-metal photodetectors. *J. Lightwave Technol*. **10**, 753-759 (1992).
44. Williams, K. J., Esman, R. D. & Dagenais, M. Effects of high space-charge fields on the response of microwave photodetectors. *IEEE Photon. Technol. Lett.* **6**, 639-641 (1994).
45. Williams, K. J. Comparisons between dual-depletion-region and uni-travelling-carrier p-i-n photodetectors. *IEE Proc.-Optoelectron.* **149**, 131-137 (2002).
46. Tulchinsky, D. A., Williams, K. J., Li, X., Li, N. & Campbell, J. C. High-power photodetectors. *IEEE LEOS Newslett*. **19**, 16-17 (2005).
47. Zhang, W., Li, T., Lours, M., Seidelin, S., Santarelli G. & Le Coq, Y. Amplitude to phase conversion of InGaAs pin photodiode for femto second lasers microwave signal generation. *Appl. Phys. B* **106**, 301-308 (2012).
48. Wang, G., Tokumitsu, T., Hanawa, I., Sato, K. & Kobayashi, M. Analysis of high speed p-i-n photodiodes S-parameters by a novel small-signal equivalent circuit model. *IEEE Microw. Compon. Lett*. **12**, 378-380 (2002).

49. Wang, G., Tokumitsu, T., Hanawa, I., Yoneda, Y., Sato, K. & Kobayashi, M. A time-delay equivalent circuit model of ultrafast p-i-n photodiodes. *IEEE. Trans. Microw. Theory Techn.* **51**, 1227-1233 (2003).
50. Jou, J. J., Liu, C. K., Hsiao, C. M., Lin, H. H. & Lee, H. C. Time-delay circuit model of high-speed p-i-n photodiodes. *IEEE Photon. Technol. Lett.* **14**, 525-527 (2002).
51. Piels, M., Ramaswamy, A. & Bowers, J. E. Nonlinear modeling of waveguide photodetectors. *Opt. Express* **21**, 15634-15644 (2013).
52. Jiang, H. & Yu, P. K. L. Equivalent circuit analysis of harmonic distortions in photodiode. *IEEE Photon. Technol. Lett.* **10**, 1608-1610 (1998).
53. Nikoufard, M., Leijtens, X. J. M., Zhu, Y. C., Kwaspen, T. J. J., Bente, E. A. J. M., Groen, F. H. & Smit, M. K. Modelling and characterization of InP-based high-speed pin-photodiode. *Proc. IEEE/LEOS Symp.* 2003, 149-152 (2003).
54. Nakhla, M. & Vlach, J. A piecewise harmonic balance technique for determination of periodic response of nonlinear systems. *IEEE Trans. Circuits Syst.** **23**, 85-91 (1976).
55. Rizzoli, V., Mastri, F. & Masotti, D. General noise analysis of nonlinear microwave circuits by the piecewise Harmoni-Balance Technique. *IEEE Trans. Microw. Theory Techn.* **42**, 807-819 (1994).
56. Brahimi, H., Martinez-Reyes, H. L., Merrer, P. H., Bouchier, A. & Llopis, O. A CAD approach of microwave optical systems including noise performance. *Proc. Eur. Microw. Conf. (EuMC)*, Rome, Italy, 1642-1645 (2009).
57. Hilt, A. Microwave harmonic generation in fiber-optical links. *13th International Conference on Microwave, Radar and Wireless Communication (MIKON-2000)* **2**, Wroclaw, Poland, 693-698 (2000).
58. Le Guennec, Y., Maury, G. & Cabon, B. Performance of interferometric systems for optical processing of microwave signals: influence of laser- and microwave- phase noise. *IEEE Photon. Technol. Lett.* **16**, 2120-2122 (2004).
59. Leeson, D.B. A simple model of feedback oscillator noises spectrum. *Proc. IEEE* **54**, 329-330 (1966).
60. Abdallah, Z., Rumeau, A., Fernandez, A., Maxin, J., Pillet, G., Cibiel, G. & Llopis, O. Photodiode nonlinear modeling and its impact on optical links phase noise*. IEEE 28th European Frequency and Time Forum*, Neuchâtel, Switzerland (2014).
61. Brahimi, H., Lacroix, P. & Llopis, O. Optimization of a microwave frequency discriminator based on an optical delay line*. IEEE Int. Topical Meeting on Microwave Photonics (MWP)*, Valencia (2009).

Chapter IV: OEO based on FRR – Experiment

IV.1 Introduction

Increasing the quality factor of an optical resonator tends to increase their sensitivity to the incident optical power. That is to say, when the incident optical power is absorbed inside the resonator, the circulating intra-cavity power can be tens to hundreds of times higher than the absorbed optical power, depending on the resonator optical quality factor (Q_{opt}). Thus, this high intra-cavity power will heat up the cavity of the resonator, leading to a strong thermal variation which causes a thermal drift of the resonator's optical resonances. Consequently, the optical carrier will not be sufficiently coupled to the resonator.

Furthermore, this frequency shift between the resonance of the resonator and the laser frequency may also be caused by the aging of the components of the optoelectronic oscillator and by the changes of the environmental conditions, such as temperature fluctuations, stress, or other disturbances.

Thus, the difference between the laser's frequency and the resonator's resonant frequency must be continually controlled in order to maintain a desirable and stable performance of an OEO in the high-end applications, where self-sustaining highly stable oscillators are required. This can be accomplished by either actively locking the laser frequency to the respective resonance peak (by altering the laser frequency for instance), or alternatively, actively locking the resonator to the laser (by changing the cavity's length to alter the resonant mode, for instance). The choice of these two locking techniques depend on the components used and on the intended application.

Three common locking techniques are presented and detailed in the first section of this chapter: the optical self-injection locking, the thermal locking technique and the Pound-Drever-Hall radio frequency sideband approach. A special focus is given to the latter approach, the PDH technique, as it has been used in numerous experimental studies during this thesis, on different optical resonators and with various lasers and electronic feedback circuits.

Even a frequency stabilization technique could play a critical role in limiting the short-term performance of an OEO. In order to identify and address the shortcomings of the PDH stabilization loop, a study has been carried out on the low-frequency electrical part of the PDH loop, known as a servo controller. Many different circuits have been realized and tested in order to improve the system for a better long-term stability and faster time response, and to try to reduce its effect on the OEO phase noise.

Finally, a study has been carried out to replace a DFB fiber laser with a narrow linewidth, small size and high performance semiconductor laser (RIO laser). The breakthrough was in being able to stabilize this semiconductor laser to a very high-Q resonator, with a small free spectral range (FSR order of MHz). The results are presented in the final section of this chapter.

IV.2 Stabilization techniques

Various techniques and methods have been developed in order to overcome the difficulties of maintaining frequency locking between the laser and the optical resonator. These methods are based on either an optical feedback, thermal approach, or electrical feedback, or even a combination between these techniques.

IV.2.a Optical feedback locking technique

Optical feedback technique [1-3], known as well as self-injection locking technique, is widely employed method since it is used for two essential purposes: firstly, to narrow the laser's linewidth, and secondly to stabilize its frequency optically to the cavity resonance. It has been demonstrated that the instantaneous linewidth of the locked laser could be at least 10^4 times smaller than the linewidth of the free running device along with a good short- and long-term stability [4,5].

The key concept is that part of the signal induced inside the resonator should be fed-back to the laser in order to lock its frequency to one of the resonator's resonance. This could be achieved by different feedback mechanisms. Three examples of feedback techniques are given below.

The first one is based on the counter-propagating waves circulating inside the resonator through the Rayleigh scattering [6-8]. The light caused by the Rayleigh scattering will be moving in an opposite direction of the original optical wave and it will travel from the resonator back into the laser. The second feedback mechanism is based on using an external reflector, for instance a partially transparent mirror. The external reflector is placed at the output of the resonator in order to reflect part of the resonator output beam back into the resonator as a counter-propagating wave and then fed-back toward the laser [9]. A combination of these two mechanisms, the Rayleigh scattering with the external reflector, may also be used (see Figure IV-1 (a)).

In the third presented technique, the light beam from the laser is injected into the resonator through a three ports optical circulator. An optical coupler is placed after the resonator, and its output is connected to the circulator's port 1 in order to direct part of the resonator output beam back toward the laser (Figure IV-1 (b)) [10].

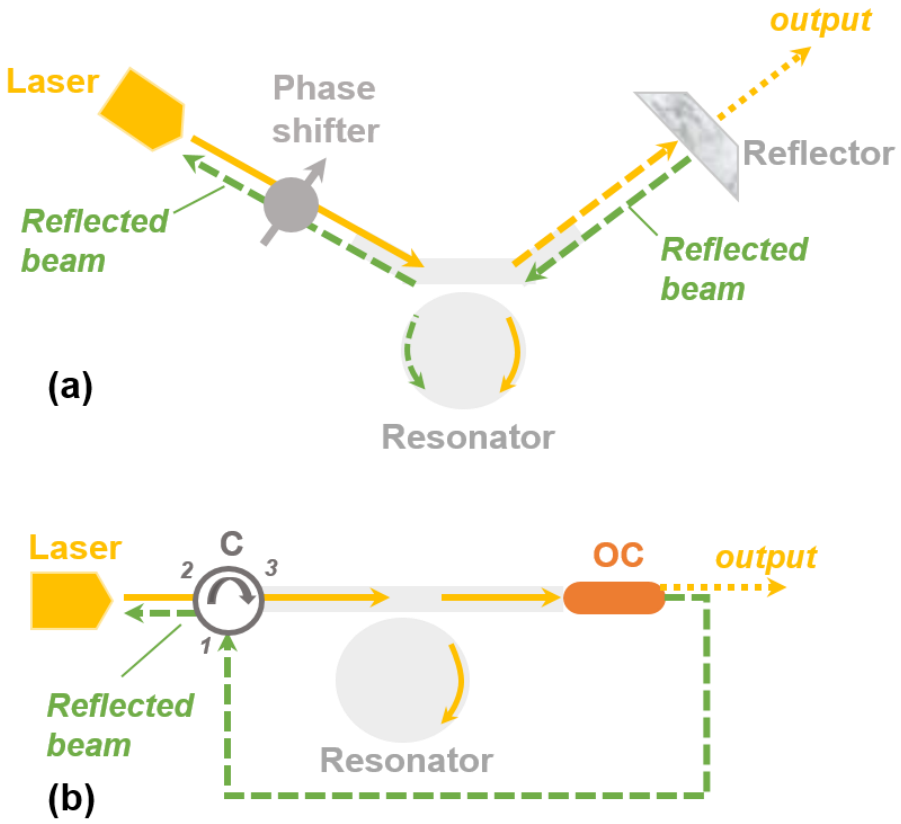

Figure IV-1 Example of a self-injection locking technique, using an external ring resonator (a) with an external reflector; (b) with an optical circulator (C) and an optical coupler (OC).

The optical phase of the feedback light must meet a phase-matching condition for a proper injection locking phenomenon. This could be reached, for example, by introducing a phase shifter between the resonator and the laser or between the external reflector and the resonator, or by controlling accurately the distance between the laser and the resonator or the distance between the resonator and the reflector to adjust the optical phase of the feedback signal. Another option, if it is available, is to tune slightly the resonator temperature in order to change the optical frequency, and thus the phase shift between the laser and the resonator. A slight adjustment of the laser temperature may also help in finding the proper locking conditions.

Various successful self-injection locking experiences of several types of lasers to an external optical resonator have been previously reported. Most frequently used resonators are the confocal Fabry-Perot resonators [1,11,12], whispering gallery mode resonators [4,5,13] and fiber ring resonators [14,15].

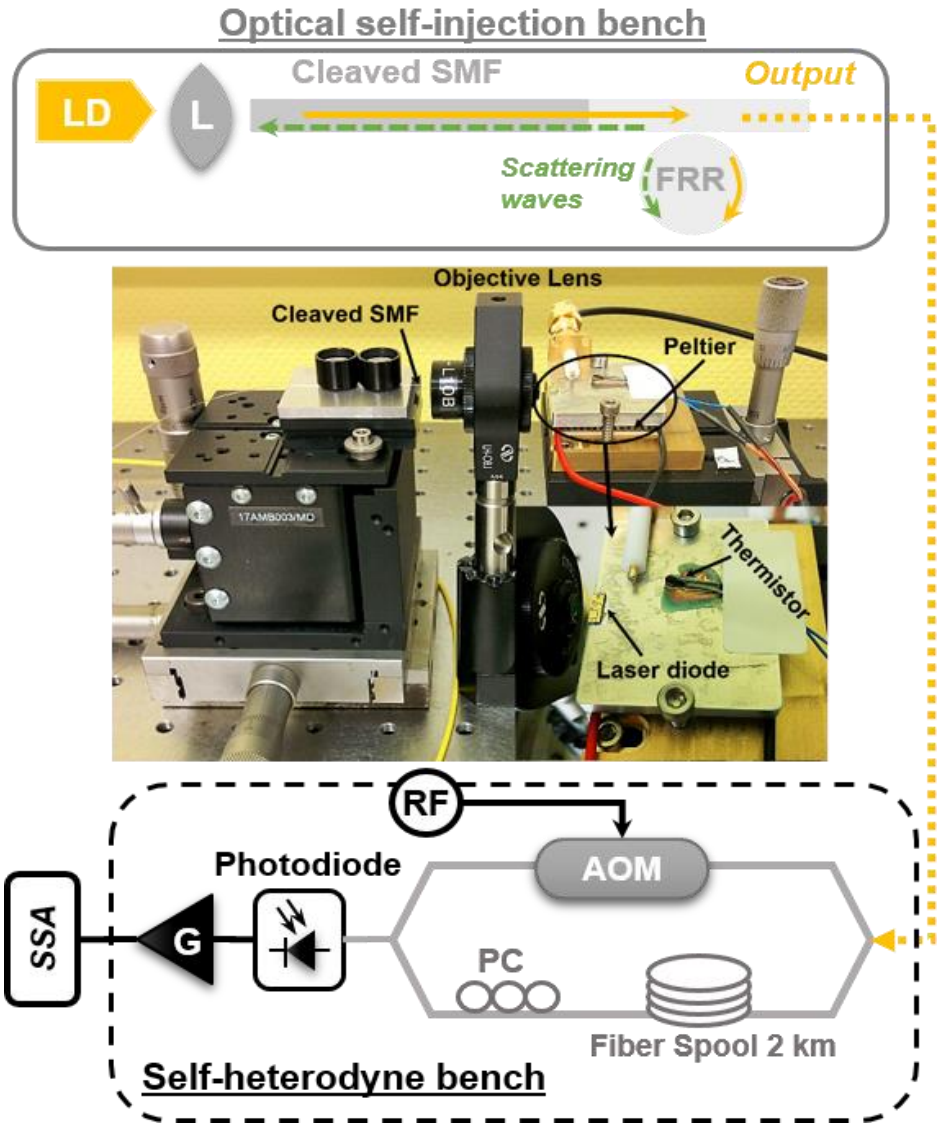

Figure IV-2 Schematic diagram of: (1) The optical self-injection technique, which based on the counter-propagation waves inside a fiber ring resonator (FRR) through the Rayleigh scattering. LD: DFB-laser diode; L: laser diode objective lens; SMF: single-mode fiber. (2) The self-heterodyne approach. AOM: acousto-optic modulator; PC: polarization control; G: amplifier gain; SSA: signal source analyzer.

A self-injection locking technique has been set up in LAAS-CNRS using the counter-propagation of the Rayleigh scattering inside a fiber ring resonator (FRR). A light source from a DFB laser diode (1550 nm), thermally controlled, has been collected and collimated by a laser diode objective lens and focused onto the tip of a cleaved single-mode optical fiber, to be finally delivered to a passive 20m long fiber ring resonator of high quality factor ($Q_{opt} = 1.6\ 10^9$). The locking bench is presented in Figure IV-2.

Once the laser is locked, its spectral purity is enhanced thanks to the high Q factor of the external resonator. To check this behavior, the linewidth of the DFB laser has been measured in two different states, i.e. when the laser is free running without any feedback and when the laser is optically locked onto the FRR. These measurements have been performed

with a self-heterodyne approach [16-19]. The laser signal is split in two paths. On one path, an acousto-optic modulator shifts the laser frequency of 80 MHz. On the other path, the signal is delayed using a fiber spool of 2 km, and then recombined to the first path. The beat frequency is recovered using a fast photodiode, amplified and finally the microwave output signal has been measured by means of an Agilent E5052B signal source analyzer (see Figure IV-2). It is worthy to note that this self-heterodyne approach is basically dedicated to the phase noise characterization of high spectral purity lasers.

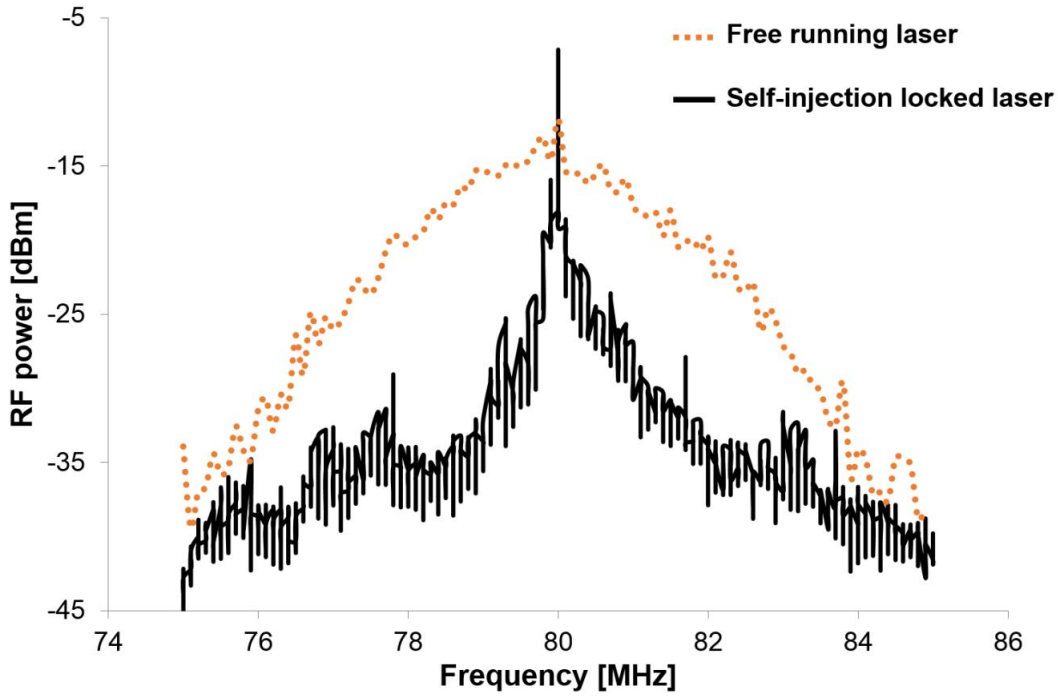

Figure IV-3 RF power spectra of the beat note signal for the free running DFB-laser (dotted) and with optical feedback using an external 20m length fiber ring resonator (solid). (Measured by A. Ali Slimane).

Figure IV-3 depicts the RF power spectra of the beat note signal for the DFB-laser, in its two different states for the same laser optical power level. In its free running state, and based on these measurements data, the DFB-laser has a linewidth of around 2 MHz. Once optically locked, the instantaneous linewidth of this laser has harshly narrowed to an order of kHz. The width of the displayed beat note is limited by the RF spectrum analyzer's resolution bandwidth (spectrum monitoring down to 25 kHz of resolution bandwidth (RBW) in a real-time mode).

This experimental observation clearly demonstrate that self-injection locking technique can improve the laser linewidth by nearly several orders of magnitude by purely optical means, without any electronic control. It also features a large frequency bandwidth and can stabilize lasers with a linewidth much larger than the 3-dB bandwidth of the resonator on which they are locked. However, the locked laser is not stable enough for our applications. Unless the optical path between the laser and the resonator is well fixed and the temperature of the system is well controlled, the lock will shift from one mode of the resonator to another. This is

visible on the locked linewidth which flashes sometimes, revealing locking/unlocking processes. Therefore, for low phase noise OEO applications, or more generally for time & frequency applications, this technique should be combined to other techniques to ensure a more robust locking behavior.

IV.2.b Thermal locking technique

Thermal fluctuation in optical resonator is one of the major obstacles that can affect the frequency stability of an OEO. In fact, optical absorption of the light power inside the resonator during the optical pumping or a change of the ambient temperature lead to a significant variation of the cavity's temperature, and owing to the thermal dependency, the refractive index (n) and the thermal expansion will change as well, proportionally to the temperature shift. These variations will lead to a thermal nonlinearity inside the resonator [20-23], and therefore may induce frequency shift of the resonance.

In a silica optical fiber, for instance, the thermo-optic coefficient (α_n in K^{-1}) and the thermal expansion coefficient (ε in K^{-1}) for L fiber length [20, 24-26] are given by:

$$\alpha_n = \frac{1}{n}\frac{dn}{dT} = 6.3 \cdot 10^{-6} \tag{IV.1}$$

$$\varepsilon = \frac{1}{L}\frac{dL}{dT} = 0.5 \cdot 10^{-6} \tag{IV.2}$$

It is noticeable that the value of the thermal expansion coefficient in silica fiber was found to be much lower than that for the average thermo-optic coefficient.

The resonance-frequency can now be expressed as a function of the temperature [23], as follow:

$$f_r = f_0\,[1 - (\alpha_n + \varepsilon)\,\Delta T] \tag{IV.3}$$

where f_0 is the cold resonance-frequency and n_0 is the cavity index of refraction.

This thermal instability has a detrimental effects on the stability and continuous operations of the optoelectronic oscillator.

However, one can take benefit of the thermal instability in order to realize a thermal locking of the laser frequency onto a corresponding resonance. Carmon *et al.* [23] have demonstrated a self-stable thermal equilibrium solution for a pump-microcavity system. The principle is to reach a stable warm-equilibrium region where the laser frequency is higher than the cold-cavity resonance frequency. In this region, a small pump power decrease will cool down the cavity temperature and push the cavity frequency closer to the laser frequency. This will increase the absorbed power and hence will compensate for the pump reduction by increasing the intra-cavity power. As a result, the cavity stays warm and loaded as perturbations are self-compensated, and therefore, the locking is achieved. This thermal

self-locking allows for tuning ranges of tens of gigahertz without losing the resonance of the microcavity [23, 27].

Over relatively long time-scale, this technique alone may drift due to external perturbations, translating into resonant frequency fluctuations. Thereby, a combination of the optical and the thermal lock has been reported [28]. A semiconductor laser was thermo-optically locked to a toroid optical microresonator, and its linewidth was reduced from 1.4 MHz to 300 kHz. Briefly speaking, the optical feedback locking was used to optimize the laser frequency with respect to the microtoroid resonance in order to maximize the constructive interference between the feedback and intracavity laser fields; whilst the thermal locking was used to optimize the microtoroid resonance frequency with respect to the laser frequency to balance the optical heating and the thermal heat loss. The lock using this technique was demonstrated to be maintained for time periods exceeding several hours [28].

However, in a fibered system and in real applications environment (far from an optical table), it seems difficult to rely on this approach for long term operation.

IV.2.c Electrical feedback technique

The electrical feedback technique provides an interesting alternative to the previous locking techniques. Many electrical feedback approaches [29-37] have been developed and aimed for continuous locking purposes. Among these locking approaches are those which track the variations in either the transmitted or reflected intensity of some probe beam, and those which are based on interferometry. Yet, they are all based on the same concept, which is the generation of an error signal proportional to the difference between the laser frequency and the cavity resonance frequency. To name only a few of these techniques, one could mention the transmission locking [29], fringe side locking [30], Hänsch-Couillaud locking [31], mode interference locking [32], Pound-Drever-Hall locking [33,34] and tilt locking [35].

In this section, a specific focus is devoted to the Pound-Drever-Hall (PDH) stabilization loop that is the most widely used method currently. Thanks to its potential advantage of preventing laser intensity fluctuations from coupling directly into the frequency (phase) error signal, the PDH technique detects only the fluctuations in the laser's frequency.

As mentioned before, the locking technique can be used either to lock the laser to a stable cavity or to lock a cavity to a stable laser. The latter method is very useful in some application, such as precisely measuring the length noise in the cavity. In this case, the laser is stable and its frequency is unmodified, while the length of the cavity is adjusted until the light is resonant [38]. Concerning the first method, it is the most used one in the PDH technique since many modern lasers nowadays are frequency tunable, i.e. they come with some input port into which an electrical signal can be fed and adjust the laser frequency. This case will be considered for the rest of this manuscript.

Moreover, depending on the technology and configuration of the optical resonator, it is possible to use its reflective or transmission properties to measure the difference between the laser's frequency and the cavity's resonant frequency, noted Δf, and more specifically the sign

of Δf so that it can be used to appropriately cancel this difference with an electrical feedback signal. At this stage, it has to be noted that the conceptual explanation and the analytical model will be based on the transmission transfer function (detailed in chapter II) of the fiber ring resonator, the corresponding transmission coefficient is noted $A(w)$. The math maintains its similarity for any other resonator used.

IV.2.c.i PDH conceptual overview

At the core of the PDH loop is the optical resonator. On resonance, the incident light will experience constructive interference with the circulating waves inside the cavity, and consequently minimum transmission intensity results at the resonator's output (case 1 in Figure IV-4 (d)). If the laser is outside the resonator resonance, there will be no power circulating inside the resonator, thus, the incident light will be almost completely transmitted (destructive interference), the cavity appears almost transparent, and therefore the transmission intensity is at a maximum (case 2 in Figure IV-4 (d)).

As it is evident from Figure IV-4 (d), the transmission intensity is symmetric about resonance frequency. So by just taking into account the intensity spectrum, one wouldn't be able to tell which side of the resonance the laser's frequency is on. In contrast to the intensity case, the phase of the transmitted light is antisymmetric across the resonator resonance frequency (Figure IV-4 (e)). For this reason, the PDH system relies on the phase information of the transmitted light to determine the exact correction needed to adjust the laser's frequency. Here comes the importance of the phase modulator.

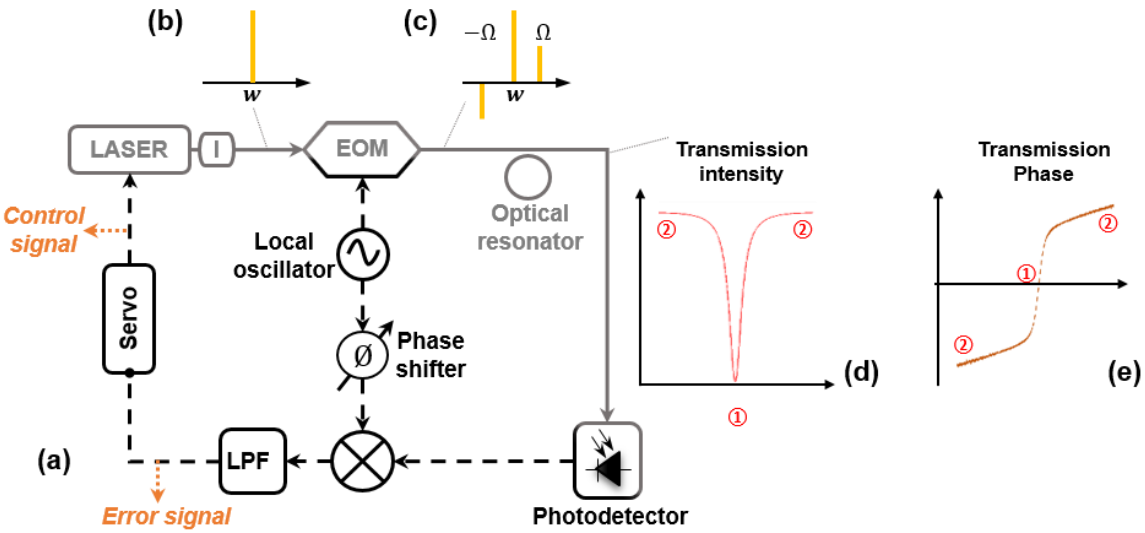

Figure IV-4 (a) Experimental layout for PDH technique. Solid gray lines are the optical paths and dashed black lines are the electrical paths. I: isolator; LPF: low-pass filer. (b) Optical spectrum. (c) Phase modulated optical spectrum. (d)-(e) Magnitude and phase of the transmission spectrum as a function of frequency, near resonance (where 1 represents the case on resonance and 2 out of resonance).

Figure IV-4 (a) shows a basic Pound-Drever-Hall setup. The incident light from a laser passes through an electro-optic modulator (EOM), to modulate its phase before being

transmitted by the resonator. The phase modulated is driven by a radio-frequency signal generator. The modulated beam then passes through an optical resonator, and the transmitted beam is collected and detected by a photodetector. Mixing the output of the photodetector with the local oscillator (LO) signal gives access to signals at both low frequency and twice the modulation frequency.

The interesting signal is the low frequency one since it contains the required phase information. In fact, it is the error signal that is proportional to the frequency difference between the laser and the resonator, indicating on which side of the resonance is the laser. A low-pass filter on the output of the mixer is used to isolate this error signal, which is then fed into a servo controller to adjust the laser frequency by means of a control signal, locking the laser to the resonator's resonance.

The optical isolator (I in Figure IV-4) is essential in order to eliminate any feedback to the laser, which may destabilize it. In addition, the phase shifter is necessary in the PDH loop to compensate for unequal delays in the signal paths, in order to produce two pure sine terms at the inputs of the mixer. If the inputs of the mixer do not have appropriate relative phase, the error signal can be damaged or lost [39]. Another solution to get a proper phase relationship is to change the value of the modulation frequency from the LO. However, this latter method is less accurate than the phase shifter solution and depends on the length of the cables used in the experiment (in a compact experiment, it cannot work).

IV.2.c.ii Analytical overview

The electric field of the light passing through the EOM can be written as:

$$E_{EOM} = E_0 e^{i(wt+\beta \sin \Omega t)} \tag{IV.4}$$

where β represents the modulation index and Ω is the phase modulation frequency. Using the Jacobi-Anger expansion, this equation can be reformulated as a sum of Bessel function [40]:

$$E_{EOM} = E_0\left[J_0(\beta)e^{iwt} + J_1(\beta)e^{i(w+\Omega)t} - J_1(\beta)e^{i(w-\Omega)t} \right] \tag{IV.5}$$

This form shows the three different beams: the carrier with frequency w and the two sidebands with frequencies $w \pm \Omega$ (Figure IV-4 (c)). The modulation index, which is controlled by the power of the modulation signal, will limit the power to the carrier and the sidebands. Equation (IV.5) is only valid if the modulation index is small ($\beta < 1$), since in this case almost all of the incident power (P_0) is in the carrier (P_c) and the first-order sidebands (P_s), while the greater orders are nearly subtracted:

$$P_0 \approx P_c + 2P_s \tag{IV.6}$$

With $P_c = J_0^2(\beta)$ and $P_s = J_1^2(\beta) = J_{-1}^2(\beta)$. As mentioned before, the PDH approach uses the low frequency components when analyzing the phase, so any higher orders of sidebands

will not add any phase information to the error signal. Plus, if further orders of sidebands are added, the carrier signal will have less power.

When the modulated beam passes through the resonator, each frequency component of equation (IV.5) will be multiplied by the resonator's transfer function $A(w)$, resulting in a resonator's output electric field of:

$$E_{out} = E_0\left[\, A(w)J_0(\beta)e^{iwt} + A(w+\Omega)J_1(\beta)e^{i(w+\Omega)t} - A(w-\Omega)J_1(\beta)e^{i(w-\Omega)t}\,\right] \qquad \text{(IV.7)}$$

The photodetector, placed after the resonator, will detect the power (intensity) of the optical signal:

$$\begin{aligned} P_{out} = |E_{out}|^2 = {} & P_c|A(w)|^2 + P_s\{|A(w+\Omega)|^2 + |A(w-\Omega)|^2\} \\ & + 2\sqrt{P_cP_s}\,\{Re[A(w)A^*(w+\Omega) - A^*(w)A(w-\Omega)]\cos\Omega t \\ & + Im[A(w)A^*(w+\Omega) - A^*(w)A(w-\Omega)]\sin\Omega t\} + (2\Omega\ terms) \end{aligned} \qquad \text{(IV.8)}$$

It is evident that the resonator's output power contains several frequency components: the DC intensity from the carrier, the Ω components arising from the interference between the carrier and the sidebands, and the higher-order components 2Ω from the interactions between the sidebands.

However, to get the phase information of the resonator's output, the only two interesting components are the ones that oscillate at the modulation frequency Ω. That is what is accomplished by the mixer and the low-pass filter after the photodetector. The oscillating components from the photodetector will be mixed with a local oscillator signal from the signal generator, which has the same RF frequency as the EOM.

IV.2.c.iii Error signal

In equation (IV.8), there are two oscillating components, a sine term and a cosine term. However, at the mixer's output, only one of them will remain and the other will vanish, depending on both the modulation frequency and the full-width at half-maximum of the resonator ($FWHM$). It exist two cases to modulate the laser light, i.e. with a slow modulation, or with a fast modulation.

- ***Slow modulation:***

The phase modulator sweeps the phase of the laser carrier at a frequency much lower than the $FWHM$ of the resonator, i.e. $\Omega \ll FWHM$. In this case, only the cosine term in equation (IV.8) remains. The PDH error signal can be expressed as:

$$\epsilon = 2\ \sqrt{P_c\,P_s}\ \ Re[A(w)\,A^*(w+\Omega) - A^*(w)\,A(w-\Omega)] \qquad \text{(IV.9)}$$

The shape of this error signal is represented in Figure IV-5. It illustrates the extremely narrow capture range of the Pound-Drever-Hall error signal.

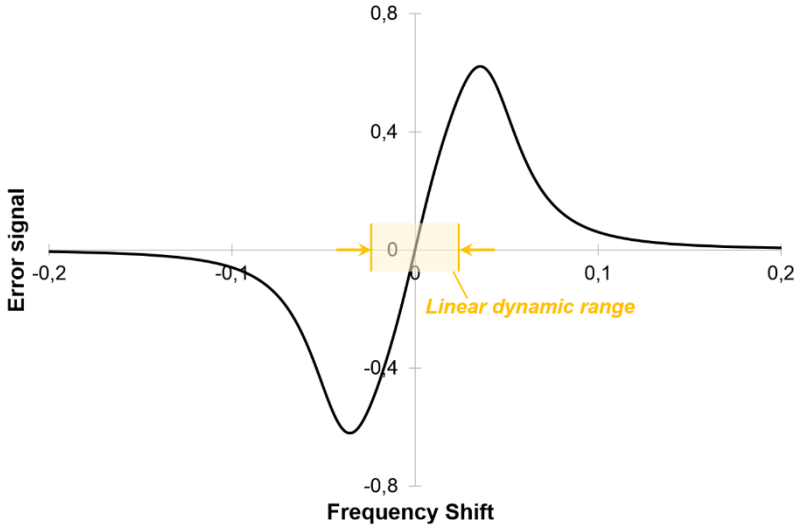

Figure IV-5 The Pound-Drever-Hall error signal versus w/FSR, when the modulation frequency is low ($\Omega \ll FWHM$).

- ***Fast modulation:***

The phase modulator sweeps the phase of the laser carrier at a frequency much higher than the resonator $FWHM$, i.e. $\Omega \gg FWHM$. In another words, the laser carrier is near resonance and the modulation frequency is high enough that the sidebands are not, so they are totally transmitted at the resonator's output. In this case, the cosine term in equation (IV.8) is cancelled, and only the sine term is left. Therefore, the expression of the error signal can be written as:

$$\epsilon = -2\sqrt{P_c P_s}\ Im[A(w)A^*(w+\Omega) - A^*(w)A(w-\Omega)] \qquad \text{(IV.10)}$$

Figure IV-6 shows the plot of this error signal. It is evident that in this case, the locking capture range (~2* Ω) is larger, and consequently the detuning between the laser frequency and the resonant frequency will be reduced.

It is worth to point out that in both cases of modulation, the error signal is linear near resonance and is centered about zero when the laser's frequency is locked exactly at the resonator resonance frequency. Yet, the error signal can be zero at frequencies other than the resonant frequency of the resonator. Using a PDH technique with relatively narrow capture range will result in a cavity lock at frequencies other than the resonant frequency. That is more likely be occur in the slow modulation case than the fast one. For this reason, in practice, modulating with a high Ω (fast modulation) is the one chosen when using the PDH approach. In fact, as it is evident from Figure IV-6, in the capture range zone, the only solution to get an error signal at zero, or close to zero, is at the center of the curve, i.e. at the resonance. During the set up process, the modulation frequency and the phase shifter are adjusted until the presented error signal shape is obtained (Figure IV-6).

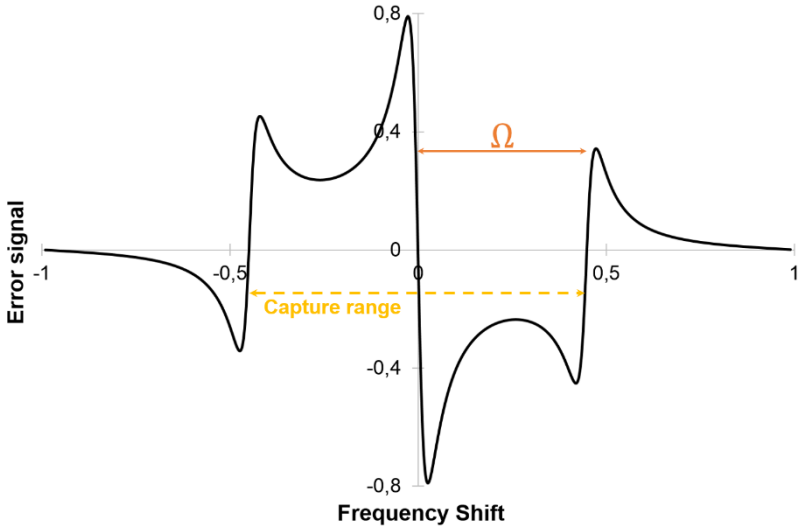

Figure IV-6 The Pound-Drever-Hall error signal versus w/FSR, when the modulation frequency is high ($\Omega \gg FWHM$).

- ***Slope of the error signal***

It has to be noted also that it is necessary to maximize the slope of the linear range of the error signal around the resonance, to obtain a large gain in the feedback loop. In this steep linear region, defined as linear dynamic range, the servo controller would operate ideally and with a fast response time.

However, when the capture range becomes much wider, the slope of the linear range of the error signal becomes less steep. Therefore, the chosen modulation frequency of the EOM is a compromise of the steepness of the error signal slope and the width of the capture range.

In addition, the sign of the slope of the PDH error signal depends on the phase condition between the output of the photodetector and the LO, and on the modulation frequency. So, if the sign is not chosen correctly, the correction signal will not be able to lock the laser's frequency on the peak transmission of the resonator.

- ***RAM of the phase modulator***

As it is clear, the phase modulator is one fundamental component in the PDH technique. But, many mechanisms may reduce the purity of the phase modulation, producing an amplitude modulation, which is often known as residual amplitude modulation (RAM).

Many effects can give rise to RAM [41,42]. In fact, if there is a misalignment between the polarization of the laser beam and one of the principle axes of the electro-optic crystal, each polarization component experiences different phase shifts, and thus will be converted into RAM. Briefly, the residual amplitude modulation arises when the modulation sidebands are unequal in magnitude, or not exactly in phase, or both [43].

Unfortunately, in the PDH system, RAM results in an introduction of frequency offset noise to the error signal, after being detected by the photodiode, and thus in a degradation of

the laser stability. In other words, it degrades the short- and long-term stability of the PDH system.

Various techniques have been developed to cancel out the RAM [43-45]. However, in all experimental setup explained in this thesis, a simple method was used to suppress the RAM effects, by maintaining the correct polarization between the laser and the EOM.

IV.3 New simplified servo controller

Once a proper error signal is obtained, the next step is to process this signal to determine the appropriate correction signal, which is fed back to the laser's actuator to close the loop and to complete the PDH system. Several methods have been developed to get the correction signal. Nevertheless, they all include some type of servo controller, an electronic technique that monitor and alter the laser frequency, in order to maintain the error signal at zero and, consequently, to align the laser frequency at the peak of the resonator's resonance.

A common type of servo is the PID device, which stands for proportional-integral-derivative controller. The proportional term produces the negative feedback, attempting to zero its input. In fact, the proportional controller reduces the error but does not eliminate it entirely, that is to say an offset between the actual and the desired value will exist, and here comes the role of the integral controller. The integral term eliminates the residual offsets that are accumulated over time with the pure proportional controller. Therefore, after a given time, the error signal will be forced to the zero level. The derivative term is used to improve the settling time (dynamic response) and the stability of the system. However, most lasers respond fast to the frequency changes, and due to the sensitivity of the derivative term to noises, the proportional-integral (PI) controller is more suitable to be used without the derivative action since it may behave more steadily in case of noisy signal.

Up until now, in all the previous investigations done by our team, a commercial servo controller has been frequently used in the PDH feedback loop to stabilize an extremely narrow linewidth DFB fiber laser (Koheras laser) onto a fiber ring resonator. The control signal from a PI controller is sent to the laser's piezoelectric actuator (PZT) and thus alter its wavelength. However, this PI controller with its complexity and the electronics behind, may contribute in the degradation of the OEO phase noise, in addition to its poor long-term stability. In addition, using this commercial controller, an unsuccessful attempt was made to stabilize a semiconductor laser onto a high-Q fiber ring resonator. For this reason, new simplified servo controllers have been realized, using low noise active devices, in order to replace the commercial controller.

IV.3.a Description and test with fiber laser

Several different servo controller circuits were realized and tested, ranging from simple to a more sophisticated circuit. In this section, a description of a best three controller feedback circuits that were used successfully to stabilize a Koheras laser, featuring an extremely narrow linewidth (1 kHz), onto a fiber ring resonator, will be presented.

- ***First circuit***

Figure IV-7 represents the simplest possible circuit that is able to replace the commercial PI controller. It was designed with a summing amplifier, preceded and followed by passives low-pass filters. The adder, which is realized with an ultra-low noise operational amplifier AD797, is designed to set the offset voltage required for a proper operation of the laser's piezoelectric actuator. The output voltage and the gain of the adder are adjustable via two variable resistors, Rvar and Rvar2 in Figure IV-7.

The first low-pass filter (530 Hz) is used to ensure that the error signal from the mixer is a low noise signal and contains only the low frequency components, i.e. the ones that oscillate at the modulation frequency Ω. The output low-pass filter (10 Hz) is used to ensure the stability of the feedback loop.

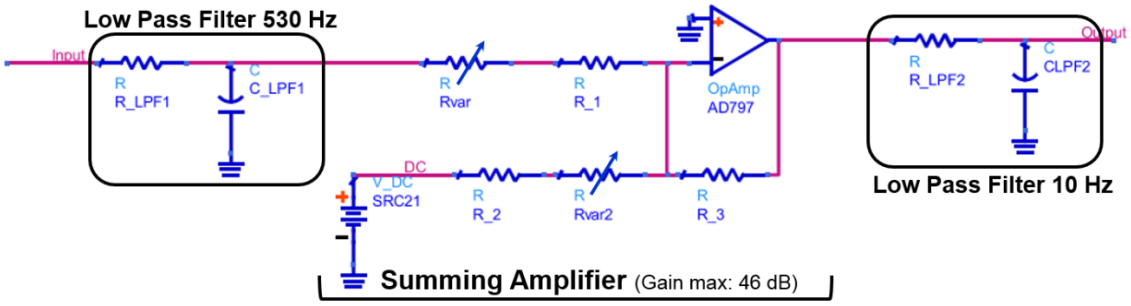

Figure IV-7 First functional configuration of a simple servo controller circuit.

The locking process was easier and more stable, once the gain of the summing amplifier was set to its maximum (46 dB). The Pound-Drever-Hall technique including this simple servo circuit has been proved stable and capable of operating continuously for several minutes at a time. However, a long-term stability was not ensured according to the preliminary experiments. It was reasonable, thus, to modify this circuit by adding another controller that guarantee more stability.

- ***Integrator-Adder circuit***

In this configuration, depicted in Figure IV-8 (a), an integrator followed by an inverter were added to the previous servo circuit, between the first filter and the adder. The inverter is essential in some cases to have the appropriate error sign and it can be easily shorted if it is not needed. In this case, the gain of the summing amplifier was set at this minimum level for more stability, since the gain of the integrator is relatively high, and an unstable operation occurs with too much feedback loop gain.

Based on experimental observations and results, the locking mechanism is highly stable with a PDH using this circuit. A laser has been demonstrated to be stabilized to a high-Q fiber ring resonator (20m long fiber, Q = 1.3 10^9) for more than 20 minutes (see Figure IV-8 (b)). Most importantly, it has been demonstrated also a tendency for the laser to relock automatically, without any exterior interference, to the cavity transmission peak, in case of any

locking problem. In fact, a high bandwidth PDH system could detect an unlock condition and react with a high response time to apply the proper correction to the laser's wavelength.

It is noteworthy at this stage that the parameter or the components in the PDH loop, and especially the components of the servo controller, must be carefully chosen and adjusted to, on one hand, determine the proper gain and bandwidth conditions and, on the other hand, prevent any noise conversion in the OEO oscillation loop. It has been observed that if the PDH loop bandwidth is too low, it may considerably degrade the OEO phase noise. Yet, if the bandwidth is too high, the performance of the PDH system decreases with a very poor stability.

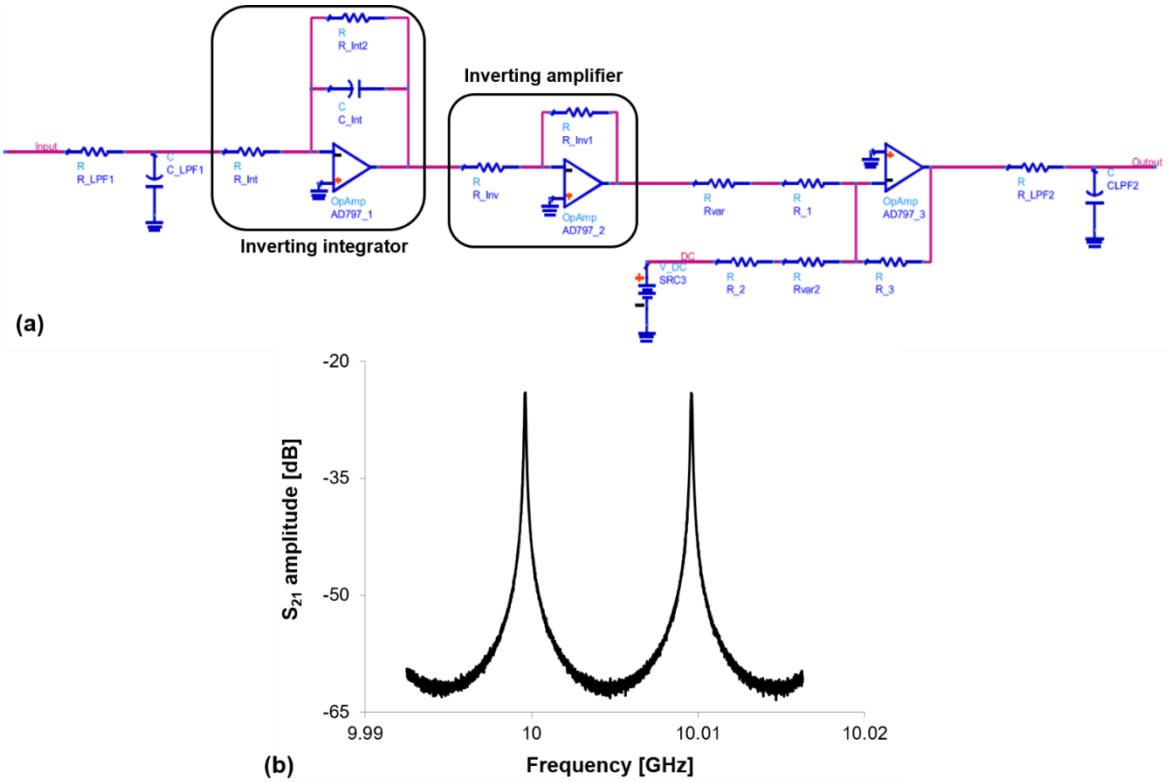

Figure IV-8 (a) Integrator-Adder circuit used as a servo controller. (b) RF transmission intensity (uncalibrated) of a fiber laser locked onto a 20m long fiber ring resonator using the Adder-integrator controller.

- ***Integrator-Adder controller vs. commercial servo controller***

To deeply assess the performance of the proposed servo circuit, it was relevant to compare it with the commercial PI controller. The measurements of the laser frequency noise in three different configurations were performed: free running state, locked using the commercial servo controller (CS) and locked using the new servo controller (NS). It is evident from Figure IV-9 that a very slight improvement of the laser frequency noise is found when the Koheras laser is locked using the PDH technique with the integrator-adder circuit, compared to the commercial one. However, the remaining noise may not be caused by the electronic circuit. It is rather due to the vibrations sensitivity of both the measurement system (and particularly the fiber 2 km spool) and the fiber ring resonator.

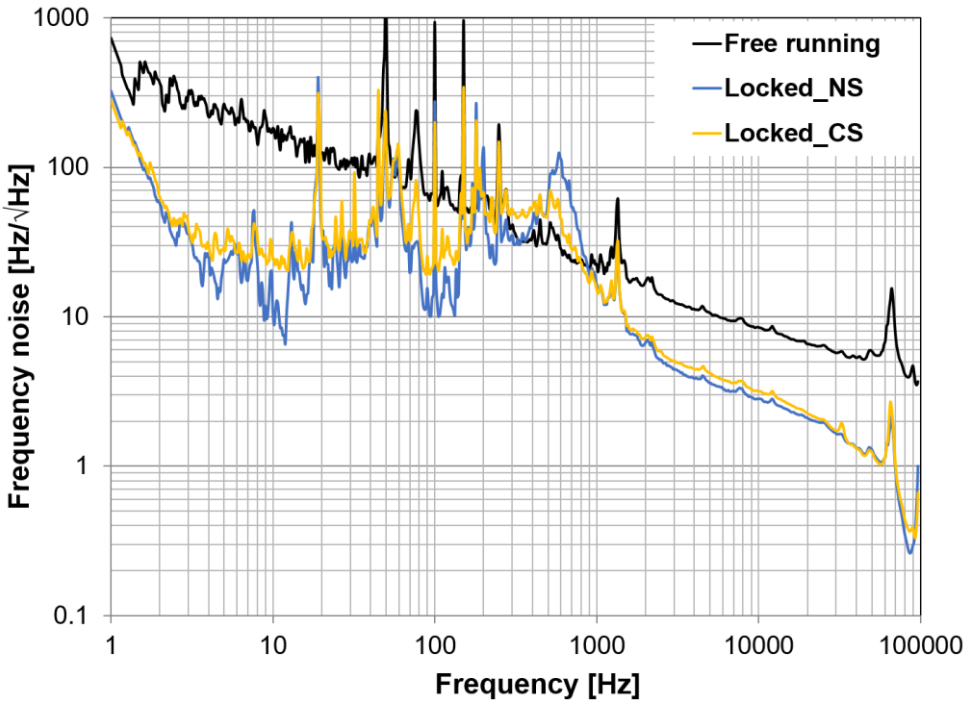

Figure IV-9 Frequency noise measurements of the Koheras laser in three different states: Free running state, locked with the new servo controller (NS) and locked with the commercial servo (CS).

- ***New PDH circuit***

So far, in Pound-Drever-Hall system, the commercial servo controller was just replaced with homemade one. But in this section, a new PDH system was designed from scratch for high performance, starting from the mixer to the final corrector (controller).

In this configuration, a voltage ramp was applied to the laser PZT input to sweep the laser frequency, while the transmitted intensity by the resonator, as detected by the photodiode, and the error signal were observed by an oscilloscope. When the laser frequency is near a resonance frequency, the voltage ramp from the signal generator was automatically turned off, and the feedback loop, which means the PZT controller, was then engaged to acquire the lock. A temperature controller (TEC) was added to the circuit in order to monitor the PZT controller feedback voltage and to prevent any over-voltage or negative voltage to be apply to the PZT from the control signal. When engaged, this TEC controller will regulate the temperature of the PZT in such a way that the piezo voltage remain in its mid-position. Both of the PZT- and the TEC- controller have been developed with PI circuit.

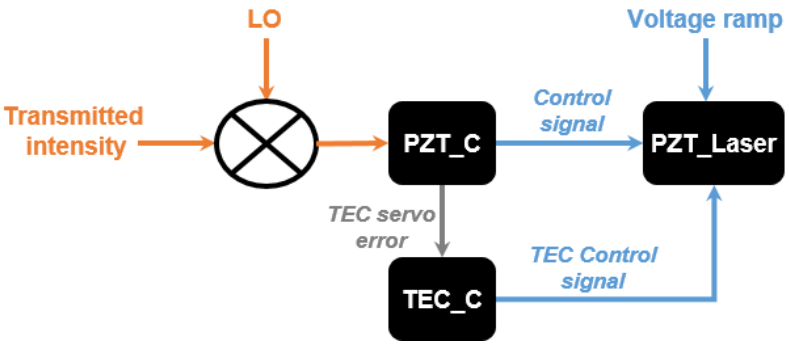

Figure IV-10 New Pound-Drever-Hall loop, using a piezoelectric actuator controller (PZT_C) along with a piezoelectric actuator temperature controller (TEC_C). LO: local oscillator.

The frequency stabilization acquisition was straightforward, and once it was done, the system stayed locked and stable for several hours even when subjected to external noise events. The total Pound-Drever-Hall feedback loop had a 3-dB bandwidth smaller than 10 kHz.

These features have been demonstrated and validated by locking the DFB fiber laser (Koheras) to a 100m long fiber ring resonator with a very high-Q.

IV.3.b Semiconductor laser

Semiconductor lasers are ideal and widely used light sources for multiple commercial and military fiber optics applications, such as security and smart structure systems. For this reason, and regardless of the extremely narrow linewidth and ultra-low phase noise of a fiber laser, which was used up until now in many of our investigation studies, an attempt was made to replace this fiber laser with a RIO semiconductor laser.

This laser combines high performance, with the low cost, simplicity, small size (in a butterfly package) and reliability of a semiconductor laser, while retaining a narrow linewidth (around 15-30 kHz) and low frequency and phase noise.

IV.3.b.i Wavelength variation vs. temperature and current

Since the locking system is based on altering the wavelength of the laser tested, the first step was to assess the wavelength behavior of the RIO laser regarding the temperature and the bias current. Figure IV-11 (a) depicts the hysteresis in the RIO laser's wavelength versus the laser temperature characteristics. The same hysteresis behavior has also been observed in the output power of the laser versus laser temperature. So, first of all, it is essential to determine the optimal operating temperature range to avoid any hysteresis or mode-hopping during the stabilization process. This optimal temperature range has been found to be about 27-34°C.

In addition, Figure IV-11 (b) shows the RIO laser's wavelength versus the applied bias current, where no hysteresis behavior is observed. The magnitude of the bias current will alter slightly the wavelength of the laser. Furthermore, the wavelength versus bias current tuning coefficient was measured to be around ~0.8 pm/mA, which is much smaller than the change induced by the temperature with a typical tuning coefficient of about 12 pm/°C.

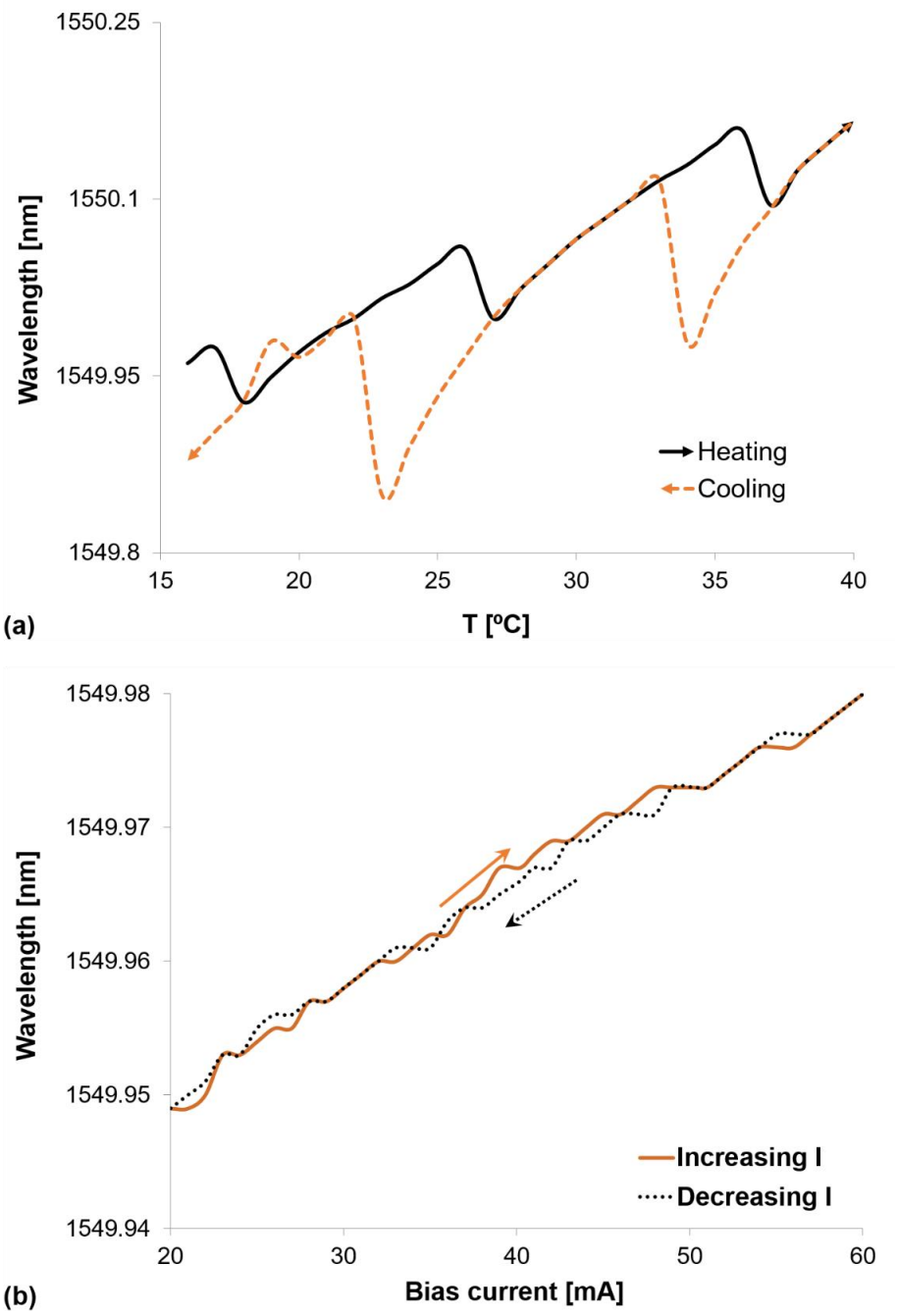

Figure IV-11 Measurements of the RIO laser's wavelength vs. (a) TEC temperature and (b) Bias applied current, when tuning up and down the temperature and the current.

Briefly, the wavelength has a lower sensitivity to the bias current than to the temperature. However, the temperature tuning is a slow tuning motion, which will be unable to lock in case of vibrations or which will not be able to reduce the laser free running noise. Therefore, the laser will be current controlled while the temperature will be maintained within the optimal operating range, to prevent any mode-hopping behavior and to ensure a stable and low noise performance over time.

IV.3.b.ii Locking with the previous controllers

A basic voltage-to-current converter has been designed and used as an output stage after the Integral-Adder feedback controller in the PDH loop (Figure IV-8 (a)), the control current is added to the bias current from the external current source in order to adjust the wavelength of the laser and therefore stabilize it to the optical resonator.

Using this configuration, locking the RIO laser onto a long fiber ring resonator (L > 10m long) was still limited by the mode-hopping of the laser and the lack of stable operation, even though the laser temperature was well controlled. In fact, during the entire investigation, the laser frequency was dithering too fast in such a way that the light resonating inside the cavity couldn't have enough time to completely build up or settle down.

However, a successful lock acquisition has been demonstrated by stabilizing the laser to a 2m long highly nonlinear fiber (HNLF) ring resonator featuring a Q-factor of 4 10^7, as it is shown in Figure IV-12.

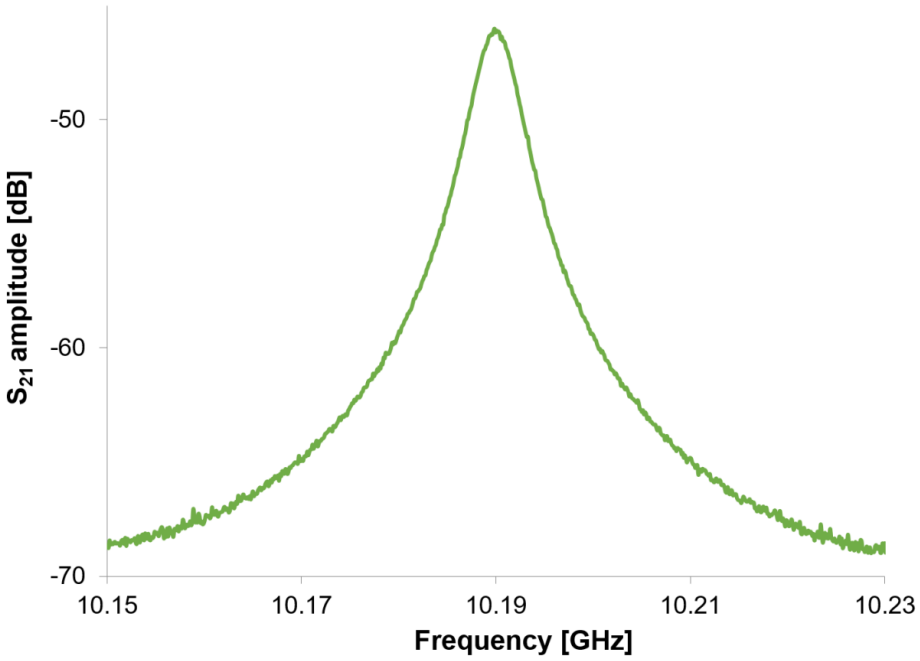

Figure IV-12 Resonance of a 2m long HNLF ring resonator with a Q factor of 4 10^7, using the PDH loop including the Integral-Adder servo controller with a voltage-to-current converter.

As mentioned before the bandwidth of PDH loop, with this configuration, is smaller than 10 kHz, so replacing this system with a wider bandwidth one could solve the shortcomings of this laser. The new circuit is detailed and presented next.

In a second configuration, a commercial standard PI controller has been used after the mixer, followed by the voltage-to-current converter, which was designed to play also the role of a lead compensator, in order to increase the bandwidth of PDH system.

Fortunately and as opposed to the previous case, locking the RIO laser to a long length fiber ring resonator (L = 100m), featuring a very high-Q 1.4 10^9, was successfully accomplished with the presented circuit, as it evident from Figure IV-13 (a).

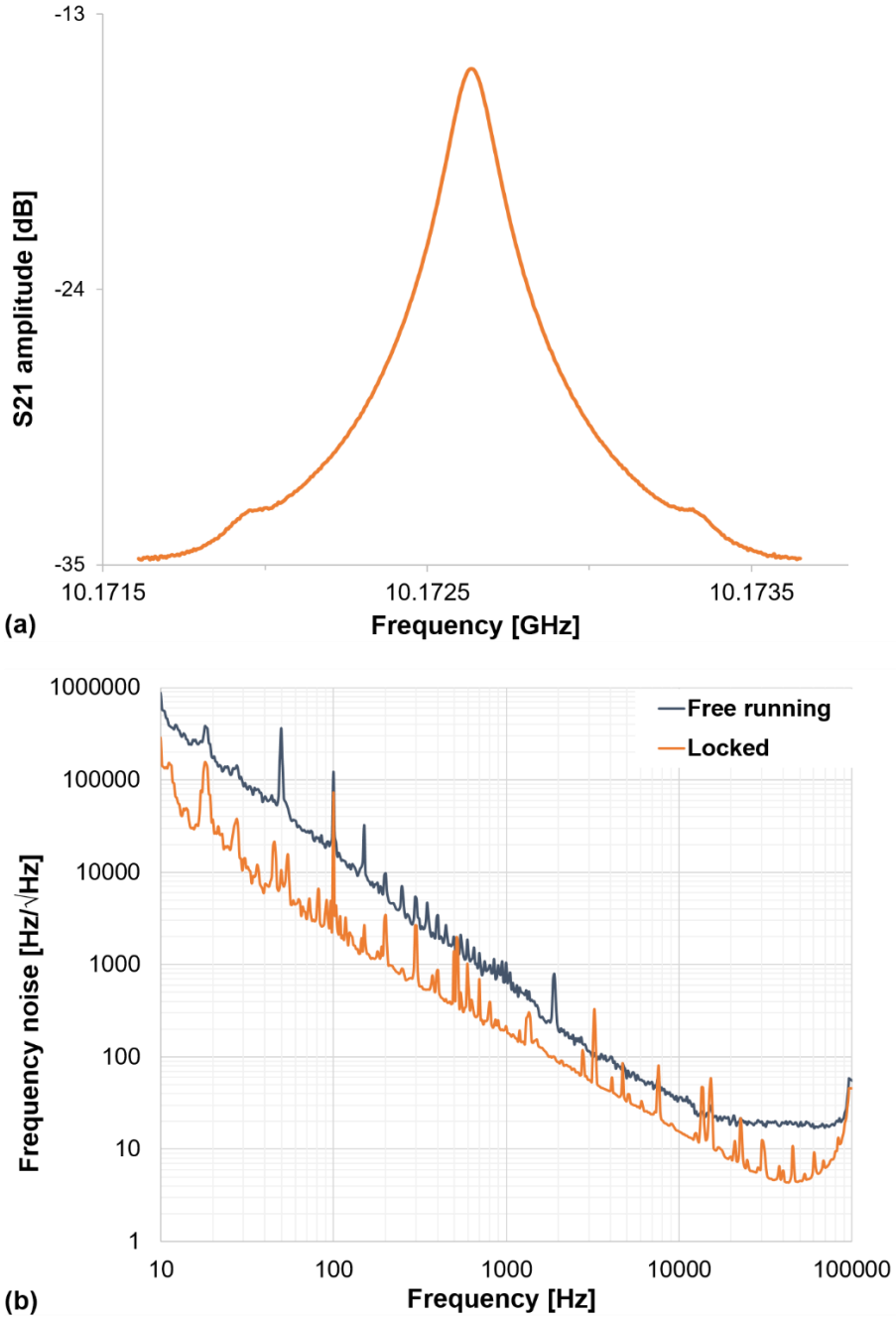

Figure IV-13 (a) Resonance of a 100m long fiber ring resonator of a high-Q equal to 1.4 10^9, using the last PDH loop. (b) Frequency noise of the RIO laser in its free running state and when it is locked to the 100m FRR.

Thanks to the relatively wide bandwidth of the PDH loop, which was measured close to 1 MHz (100 times higher than the previous one), the response of the PDH system kept the laser from losing lock under external environmental factors, for a long period of time (several hours).

Basically, the laser frequency noise should decrease when the laser is properly stabilized to a high-Q resonator. So in order to assess the performance the new PDH loop, a measurement of the RIO laser frequency noise has been performed when it is locked to the 100m IFRR, and then it has been compared to the free running laser frequency noise. Figure IV-13 (b) depicts the data results, where a decrease in the locked laser frequency noise is shown.

It is noteworthy to point out that during these studies and tests on the RIO laser, it has been found that there is an excess noise stemming from the external bias current source, and which contribute severely in the degradation of the phase noise of the laser. So to circumvent this drawback, the external bias current source has been replaced by a home-made battery based current source.

So far, the PDH system, using the latter configuration, has shown a very promising results and performance regarding various problems faced during the locking process with the semiconductor RIO laser.

IV.4 OEO phase noise

Once the laser is duly stabilized at the transmission peak of the resonator resonance, the OEO system can be set up (as described in Figure IV-14). The RF gain is adjusted, using a VNA, in order that the RF amplifier will not saturate too much when the loop will be closed (a loop gain of 3 or 4 dB is chosen to this purpose). Then, the RF phase shifter is tuned to start the oscillation. The RF oscillation starts on a single mode, multiple of the resonator FSR, thanks to the RF filter included in the loop. The tuning of the RF loop phase is an essential step, not only to start the oscillation, but also to get a low phase noise performance in steady state regime.

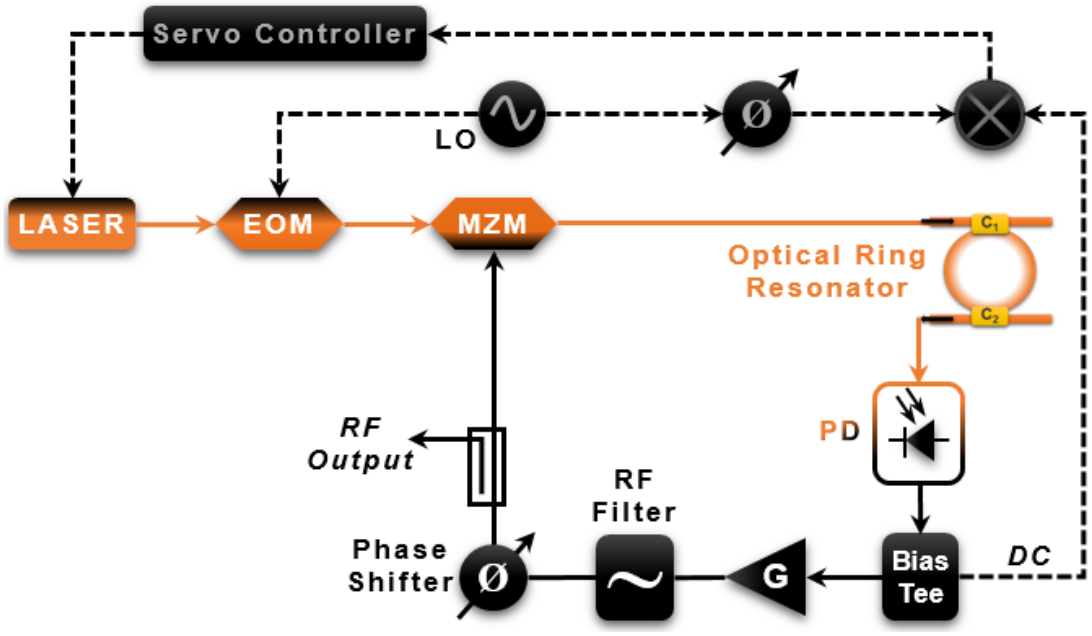

Figure IV-14 OEO configuration. A closed loop with microwave amplification.

Once the steady state oscillation has been obtained, it can be analyzed using a signal source analyzer. The phase noise results obtained on two different fiber ring resonators based OEO are presented and discussed below. Both oscillators use the Koheras laser locked to the resonator frequency. The oscillator and measurement setup have been described in chapter I in detail, and the phase noise spectrums have been measured using the Agilent E5052B signal source analyzer (SSA).

IV.4.a 100m long FRR

The 100m long P-M fiber ring resonator, presented in chapter II (II.6.b), features a full-width-at-half-maximum ($FWHM$) of 21.9 kHz and very high loaded Q factor of 8.9 10^9, which is equivalent to a Q_{RF} of 4.6 10^5 at 10 GHz. The phase noise spectrum of the OEO based on this resonator is depicted in Figure IV-15.

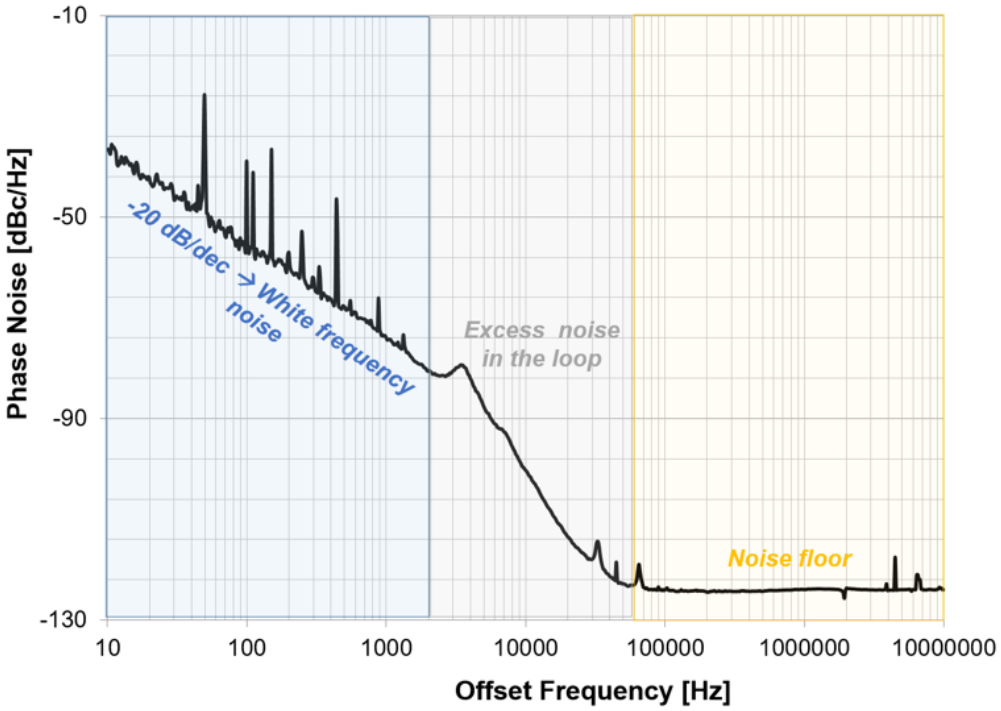

Figure IV-15 Phase noise spectrum of the 100m long FRR based 10 GHz OEO.

In this spectrum, one can identify three different parts: the white frequency noise part that occupies the 10 Hz to 2 kHz offset frequency band, characterized by its -20 dB/dec noise slope, the phase noise floor that appears above 60 kHz offset frequency, and a steep noise slope between these two regions. If adjusted with a Leeson like model, this curve reveals that a high level of open loop phase noise, featuring a Lorentzian shape with a ~3 kHz cut-off frequency, is involved in the system. This noise contribution degrades the performance of the OEO, which is not at the level expected taking into account the ultra-high Q factor of the resonator. The origin of this noise is still difficult to understand. However, due to the extreme Q factor, many nonlinear optical effects inside the resonator may be generated. To reduce these effects, this measurement has been performed with a -7dBm of optical power at the FRR input, but this power level may not be sufficiently low to prevent the starting up of some

of these effects. The locking technique used to stabilize the laser onto one resonance may also affect the RF phase noise. In fact, the noise between 3 and 60 kHz offset frequency band may be related to the frequency stabilization loop, and especially its bandwidth and its gain.

It has to be pointed out also that such a high level of excess noise close-to-the-carrier has been observed on other OEOs realized with ultra-high Q factor resonators (Q ~ 10^{10}) made with SMF fiber instead of P-M fiber. This problem has to be studied more deeply in order to understand if it is due to the PDH set up or if it is a fundamental limitation of the approach due to the increase of the nonlinearity of the fiber with the one of the Q factor.

IV.4.b 100m long immunized FRR

During the thesis of K. Saleh [45], a 100m long fiber ring resonator immunized from SBS effect was designed and used in an OEO setup. The best phase noise performance had been obtained for this type of OEO with this resonator: -128 dBc/Hz noise level at 10 kHz offset frequency and a -150 dBc/Hz noise floor for a 10.2 GHz oscillation.

New phase noise measurements have been performed in OEO configuration with this resonator, using different Pound-Drever-Hall configurations: a commercial servo-controller (CS) and a new PDH configuration that was presented in Figure IV-10. In addition, two different signal generators involved in the PDH set-up have been tested: an HP 8662A low phase noise synthesizer and a Tektronix AFG3022B dual output signal generator. Only the Tektronix generator allows the tuning of the phase of the interrogation signal, thanks to the dual output, and this is a critical feature to get a proper error signal. However, the HP synthesizer features a much lower phase noise level.

The phase noise spectrum of these measurements are presented in Figure IV-16.

It is evident from these data that the phase noise level has significantly increased compared to the results presented before, around -100 dBc/Hz at 10 kHz and -140 dBc/Hz noise floor. A first explanation may be in a degradation of the resonator performance. The recently measured Q factor of this resonator has shown a reduction from 2 10^9 (K. Saleh thesis data) to 1.3 10^9, but this relatively small reduction in Q would only degrade the phase noise of about 4 dB. More significant is the degradation of the transmission losses through the resonator, which have increased from about 4 to 7.7 dB. In these conditions, a higher optical power is required to lock the laser to the resonator, and this may explain the observed degradation of the noise. However, other parameters may have contribute to this result, and particularly the PDH loop parameters (including the noise of the PDH loop).

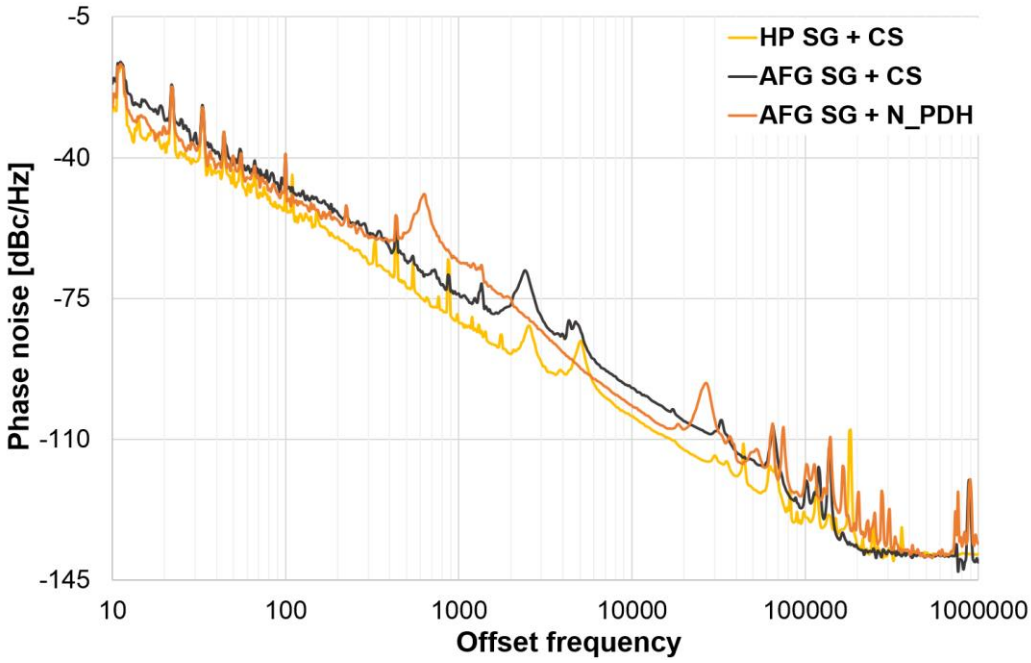

Figure IV-16 Phase noise spectrum of the 100m-IFRR based OEO in three different PDH configurations. HP SG: HP signal generator; AFG SG: Tektronix dual output generator; CS: commercial servo controller; N_PDH: new PDH configuration.

Regarding the different configurations tested, two observations may be made from these results. In the first cases, where the signal generators have been used in the PDH loop including the same commercial servo controller, it is clear that the use of the HP signal generator has a lower excess noise or contributes less in the degradation of the OEO phase noise than the AFG one. In the second case, where the same signal generator has been employed in two different PDH configurations, the phase noise performance with the new PDH loop has been reduced compared to the PDH loop with a commercial servo controller. This reduction can be explained by the longer stability of the locking mechanisms that has been observed with the new PDH configuration.

These findings have important implications for understanding some causes of the phase noise degradations. As a result, the study roadmap has been adjusted and several steps have been included. The improvement of the homemade PDH system is fixed as the first step in addressing the effects of this stabilization loop on the OEO short-term stability.

IV.5 Conclusion

Various methods for stabilizing a laser to an optical resonator have been widely studied and developed. Three of these methods that are commonly used in many applications, have been presented in this chapter, the optical feedback, the thermal and the electrical feedback locking technique. A special emphasis was dedicated to the Pound-Drever-Hall frequency feedback stabilization technique.

Regardless of its indubitable usefulness and effectiveness through many several previous demonstrations, the PDH system could potentially influence the stability of the system, and it may degrade the overall phase noise of the overall system. The use of the PDH loop in critical applications necessitates extensive mastering of its various parameters and characteristics, especially its gain and its 3-dB bandwidth, since it has been demonstrated that these two parameters can play a fundamental role in the short-term stability results. Furthermore, using a very-low noise components is another means of solving the noise and stability shortcomings.

In the purpose to achieve a long-term sustainable performance, different PDH loop circuits and configurations have been deeply studied, designed and tested with two different types of laser, a DFB fiber laser (Koheras) and the semiconductor RIO laser. As documented in this chapter, these lasers have been successfully locked to various fiber ring resonators, featuring a high-Q factor ranging from several 10^7 to several 10^9.

While circumventing some weakness in the locking process with the PDH system, particularly using a semiconductor laser, further requirements are necessary to be fulfilled to design an adjustable PDH system and more specifically its servo controller that can be used with different lasers and cavities.

Finally, several phase noise measurements performed on two different fiber ring resonators based OEO have been presented. The results were not as good as expected, since a high phase noise level has been observed, leading to various possible new hypotheses on the origin of the noise sources, such as the excess noise caused by the low frequency signal generator which can degrade the system phase noise. This finding among other may create a virtuous cycle of improvements.

IV.6 References

1. Dahmani, B., Hollberg, L. & Drullinger, R. Frequency stabilization of semiconductor lasers by resonant optical feedback. *Opt. Lett.* **12**, 876-878 (1987).
2. Hollberg, L. & Ohtsu, M. Modulatable narrow-linewidth semiconductor lasers. *Appl. Phys. Lett.* **53**, 944-946 (1988).
3. Hemmerich, A., Zimmermann, C. & Hänsch, T. W. Compact source of coherent blue light. *Appl. Opt.* **33**, 988-991 (1994).
4. Liang, W., Ilchenko, S., Savchenkov, A. A., Matkso, A. B. Siedel, D. & Maleki, L. Whispering gallery mode resonator based ultra-narrow linewidth external cavity semiconductor laser. *Optics Lett.* **35**, 2822-2824 (2010).
5. Zhao, Y., Li, Y., Wang, Q., Meng, F., Lin, Y., Wang, S., Lin, B., Cao, S., Cao, J., Fang, Z., Li, T. & Zang, E. 100-Hz linewidth diode laser with external optical feedback. *IEEE Photon. Technol. Lett.* **25**, 1795-1798 (2012).
6. Gorodetsky, M. L. & Ilchenko, V. S. Thermal nonlinear effects in optical whispering-gallery microresonators. *Laser Phys.* **2**, 1004-1009 (1992).
7. Weiss, D. S., Sandoghbar, V., Hare, J., Lefevre-Seguin, V., Raimond, J. M. & Haroche, S. Splitting of high-Q Mie modes induced by light backscattering in silica microspheres. *Opt. Lett.* **20**, 1835-1837 (1995).
8. Gorodetsky, M. L., Prymikov, A. D. & Ilchenko, V. S. Rayleigh scattering in high-Q microspheres. *J. Opt. Soc. Am. B* **17**, 1051-1057 (2000).
9. Maleki, L., Matsko, A. B., Savchenkov, A., Ilchenko, V. & Seidel, D. Low-noise RF oscillation and optical comb generation based on nonlinear optical resonator. *Patent US 8111722 B1* (2012).
10. Ilchenko, V & Maleki, L. Tunable balanced opto-electronic filters and applications in opto-electronic oscillators. *Patent US 7187870 B2* (2007).
11. Laurent, Ph., Clairon, A. & Breant, Ch. Frequency noise analysis of optically self-locked diode lasers. *IEEE J. Quantum Electron.* **25**, 1131-1142 (1989).
12. Lewoczko-Adamcyzk, W., Pyrlik, C., Häger, J., Schwertfeger, S., Wicht, A., Peter, A., Erbert, G. & Tränkle, G. Ultra-narrow linewidth DFB-laser with optical feedback from a monolithic confocal Fabry-Perot cavity. *Opt. Express* **23**, 9705-9709 (2015).
13. Vassiliev, V. V., Velichansky, V. L., Ilchenko, V. S., Gorodetsky, M. L., Hollberg, L. & Yarovitsky, A. V. Narrow-line-width diode laser with a high-Q microsphere resonator. *Opt. Commun.* **158**, 305-312 (1998).
14. Bulushev, A. G., Dianov, E. M., Kuznetsov, A. V. & Okhotnikov, O. G. Reduction in the line width of an injection laser by resonant Rayleigh scattering in a fiber ring interferometer. *Sov. J. Quantum Electron.* **19**, 479 (1989).
15. Paul, T. J. & Swanson, E. A. Narrow-linewidth diode laser using a fiber-optic ring resonator. *Opt. Lett.* **18**, 1241-1243 (1993).
16. Camatel, S. & Ferrero, V. Narrow linewidth CW laser phase noise characterization methods for coherent transmission system applications. *J. Lightwave Technol.* **26**, 3048-3055 (2009).

17. Kéfélian, F., Jiang, H., Lemonde, P. & Santarelli, G. Ultra low frequency noise laser by locking to an optical fiber delay line. *Opt. Lett*. **34**, 914-916 (2009).
18. Llopis, O., Merrer, P. H., Brahimi, H., Saleh, K. & Lacroix, P. Phase noise measurement of a narrow linewidth CW laser using delay line approaches. *Opt. Lett.* **36**, 2713-2715 (2011).
19. Llopis, O., Abdallah, Z., Auroux, V. & Fernandez, A. High spectral purity laser characterization with a self-heterodyne frequency discriminator. *2015 Joint Conference of the IEEE International Frequency Control Symposium and European Frequency and Time Forum*, Denver, United States (2015).
20. Ghosh, G. Temperature dispersion of refraction indexes in some silicate fiber glasses. *IEEE Photon. Technol. Lett*. **6**, 431-433 (1994).
21. Il'chenko, V. S. & Gorodetsky, M. L. Thermal nonlinear effects in optical whispering gallery microresonators. *Laser Phys.* **2**, 1004-1009 (1992).
22. Fomin, A. E., Gorodetsky, M. L., Grudinin, I. S., Ilchenko, V. S. Nonstationary nonlinear effects in optical microspheres. *J. Opt. Soc. Am. B* **22**, 459-465 (2005).
23. Carmon, T., Yang, L. & Vahala, K. J. Dynamical thermal behavior and thermal self-stability of microwavities. *Opt. Express* **12**, 4742-4750 (2004).
24. Choi, H. S., Taylor, H. F. & Lee, C. E. High-performance fiber-optic temperature sensor using low-coherence interferometry. *Opt. Lett.* **22**, 1814-1816 (1997).
25. Wynne, R., Daneu, J. L. & Fan, T. Y. Thermal coefficients of the expansion and refractive index in YAG. *Appl. Opt.* **38**, 3282-3284 (1999).
26. Chang, S., Hsu, C. C., Huang, T. H., Chuang, W. C., Tsai, Y. S., Shieh, J. Y. & Leung, C. Y. Heterodyne interferometric measurement of the thermo-optic coefficient of single mode fiber. *Chinese Journal of Physics* **38**, 437-442 (2000).
27. Del'Haye, P., Arcizet, O., Schliesser, A., Holzwarth, R. & Kippenberg, T. J. Fill stabilization of a microresonator-based optical frequency comb. *Phys. Rev. Lett.* **101**, 053903 (2008).
28. McRae, T. G., Lee, K. H., McGovern, M., Gwyther, D. & Bowen, W. P. Thermo-optic locking of a semiconductor laser to a microcavity resonance. *Opt. Express* **17**, 21977-21985 (2009).
29. White, A. D. Frequency stabilization of gas lasers. *IEEE J. Quantum Electron.* **1**, 349-357 (1965).
30. Barger, R. L., Sorem, M. S. & Hall, J. L. Frequency stabilization of a CW dye laser. *Appl. Phys. Lett.* **22**, 573-575 (1973).
31. Hansch, T. W. & Couillaud, B. Laser frequency stabilization by polarization spectroscopy of a reflecting reference cavity. *Opt. Commun.* **35**, 441-444 (1980).
32. Wieman, C. E. & Gilbert S. L. Laser-frequency stabilization using mode interference from a reflecting reference interferometer. *Opt. Lett.* **7**, 480-483 (1982).
33. Drever, R. W. P., Hall, J. L., Kowalski, F. V., Hough, J., Ford, G. M., Munley, A. J. & Ward, H. Laser phase and frequency stabilization using an optical resonator. *Appl. Phys. B* **31**, 97-105 (1983).
34. Black, E. D. An introduction to Pound-Drever-Hall laser frequency stabilization. *Am. J. Phys.* **69**, 79-87 (2001).

35. Shaddock, D. A., Gray, M. B. & McClelland, D. E. Frequency locking a laser to an optical cavity using spatial mode interference. *Opt. Lett.* **24**, 1499-1501 (1999)
36. Yao, X., Maleki, L. & Ilchenko, V. Opto-electronic oscillators having optical resonators. *Patent US 6567436 B1* (2003).
37. Maleki, L., Matsko, A. B., Savchenkov, A., Ilchenko, V., Liang, W., Seidel, D. & Byrd, J. Optical locking based on optical resonators with high quality factors. *Patent US 7869472 B2* (2011).
38. Black, E. D. Notes on the Pound-Drever-Hall technique. *LIGO Technical Report T980045*, California Institute of Technology, 1-12 (1998).
39. Bjorklund, G. C., Levenson, M. D., Lenth, W. & Ortiz, C. Frequency modulation (FM) spectroscopy: Theory of lineshapes and Signal-to-Noise analysis. *Appl. Phys. B* **32**, 145-152 (1983).
40. Cantrell, C. D. *Modern mathematical methods for physicists and engineers*. Cambridge University Press, Cambridge, UK, 692-693 (2000).
41. Wong, N. C. & Hall, J. L. Servo control of amplitude modulation in frequency-modulation spectroscopy: demonstration of shot-noise-limited detection. *J. Opt. Soc. Am. B* **2**, 1527-1533 (1985).
42. Whittaker, E. A., Gehrtz. M. & Bjorklund, G. C. Residual amplitude modulation in laser electro-optic phase modulation. *J. Opt. Soc. Am. B* **2**, 1320-1326 (1985).
43. Zhang, W., Martin, M. J., Benko, C., Hall, J. L., Ye, J., Hagemann, C., Legero, T., Sterr, U., Riehle, F., Cole, G. D. & Aspelmeyer, M. Reduction of residual amplitude modulation to $1x10^{-6}$ for frequency modulation and laser stabilization. *Opt. Lett.* **36**, 1980-1983 (2014).
44. Li, L., Liu, F., Wang, C. & Chen, L. Measurement and control of residual amplitude modulation in optical phase modulation. *Rev. Sci. Instrum.* **83**, 043111 (2012).
45. Silander, I., Ehlers, P., Wang, J. & Axner, O. Frequency modulation background signals from fiber-based electro-optic modulators are caused by crosstalk. *J. Opt. Soc. Am B* **29**, 916-923 (2012).
46. Saleh, K. High spectral purity microwave sources based on optical resonators. Thesis delivered by Paul Sabatier University, Toulouse III, Toulouse-France (2012).

General Conclusion

From its birth in the 1990's until its present state, the optoelectronic oscillator has been employed in numerous applications in the RF domain, or even as a clock recovery technique in the digital domain. This has provided a great motivational push for the microwave and optical scientists to increase their efforts to improve the compactness, the stability and the phase noise performance of this device. Our research group in LAAS-CNRS has been engaged for the past few years in this innovation process through several PhD thesis and collaborations with different national and international industries and laboratories.

This thesis has focused on an original configuration of this system: the optoelectronic oscillator referenced on an optical resonator, which is supposed to be more compact than the delay line oscillator if the control electronics can be integrated. The system performance has been tackled by means of multidisciplinary approaches, including circuit development, characterization, modeling and simulations. Adjustments of these approaches have been considered, depending on the priorities given to the study cases or to the new (unexpected) results.

This type of oscillator can be realized either using small size whispering gallery mode resonators or fiber ring resonators. The fiber ring resonator is the easier to set up. It is larger in size than the WGM resonator, but its 2D shape makes it easy to include in a system. Prior to any system development with these resonators (either WGM or fiber ring), it is essential to accurately characterize and model their performance. To this purpose, the RF spectrum technique developed at LAAS has been optimized, in order to be able to extract all the extrinsic and intrinsic parameters of the resonator. Taking into account the phase information, available on the vector network analyzer, together with a model of the resonator, it is possible to extract the resonator coupling conditions (under or over-coupling), the resonator intrinsic and extrinsic Q factors, the resonator losses and the intra-cavity power enhancement factor.

System modelling of the oscillator is another important step to set up if the phase noise performance has to be improved. Once again, during a previous PhD thesis, a model had been developed on a microwave simulator (Agilent ADS), but this model was not able to predict some important noise conversion effects, and particularly the conversion of the $1/f$ amplitude noise of the laser. Actually the photodiode, through its nonlinearity, seems to be the main cause of the conversion of the optical amplitude noise into microwave phase noise. As a result of the importance of this noise conversion process on the OEO performance, a new nonlinear equivalent circuit model of a fast photodiode has been proposed for ADS platform. It takes into account the carrier transit-time delay, which is directly related to the nonlinear behavior of the photodiode, by means of a nonlinear RC circuit. Some OEO simulations have been performed using this new model, revealing that this noise conversion process could be dominant at high optical power. However, this model still not include the locking circuit between the laser and the resonator.

Indeed, for an oscillation to start in this system, the very first step is to duly lock the laser's frequency onto one of the resonator resonance frequencies. This can be achieved through various techniques. Two methods have been tackled by our research group, the optical self-injection locking technique and the Pound-Drever-Hall stabilization technique, but this thesis highlights mainly the Pound-Drever-Hall one. Some experimental findings have confirmed our hypothesis that the PDH loop could degrade the phase noise performance of an OEO, by showing different phase noise performance levels when modifying the components of the stabilization loop or its parameters. Several new circuits have been designed and tested with two different lasers, a fiber laser and a semiconductor one. The breakthrough here was to be able to maintain as long as possible the stability of the laser's frequency to a resonance, and also to reduce the system size thanks to the semiconductor laser. The OEO long-term or medium-term stability has been greatly improved. However, the short-term stability (phase noise) has degraded and further work is required for a better understanding of this degradation.

Work is thus still in progress on these locking system, particularly for the semiconductor laser case for which a new low noise electronic locking circuit is under development. Another issue is the mechanical stability of the system, which limits the optical phase noise performance of the laser locked on the resonator. New resonators will be designed, featuring a more rigid optical path and, hopefully, these resonators will be more robust versus external mechanical or acoustic vibrations. Finally, these OEO systems could be used to generate ultra-high frequencies (in the millimeter wave or terahertz range) or could be used as a link between microwave and Terahertz ranges thanks to the frequency division process which can be set-up with these multi-mode resonators.

All these works take part of a collaboration research project, hence when gathering all these skills with the other partners of the project, this will lead to gain an improved understanding of the different components in the optoelectronic oscillator loop and their link with the phase noise performance of the overall system.

List of Publications

Scientific reviews:

- **Abdallah, Z.**, Boucher, Y. G., Fernandez, A., Balac, S., Llopis, O. Radio frequency spectral characterization and model parameters extraction of high Q optical resonators. *Scientific Reports* **6**, 27208 (2016).
- **Abdallah, Z.**, Rumeau, A., Fernandez, A., Cibiel, G., Llopis, O. Nonlinear equivalent-circuit modeling of a fast photodiode. *IEEE Photon. Technol. Lett*. **26**, 1840-1842 (2014).

International Conferences:

- **Abdallah, Z.**, Boucher, Y. G., Fernandez, A., Balac, S., Llopis, O. Optical resonators metrology using an RF-spectrum approach. *Proc. SPIE 9747, Terahertz, RF, Millimeter, and Submillimeter-Wave Technology and Application IX*, 97470E, san Francisco, United States (2016).
- Llopis, O., **Abdallah, Z.**, Auroux, V., Fernandez, A. High spectral purity laser characterization with a self-heterodyne frequency discriminator", *Proc. of the IEEE-International Frequency Control Symposium and European Frequency and Time Forum joint conferences, 2015*, Denver, United States (2015).
- **Abdallah, Z.**, Rumeau, A., Maxin, J., Fernandez, A., Morvan, L., Llopis, O., Cibiel, G. Photodiode nonlinear modeling and its Impact on optical links phase noise. *European Frequency and Time Forum (EFTF), 2014*, Neuchâtel, Switzerland, 48-51 (2014).

National Conferences:

- **Abdallah, Z.**, Boucher, Y. G., Fernandez, A., Balac, S., Llopis, O. Caractérisation spectro-RF d'un résonateur optique fibré. *Journées Nationales de l'Optique Guidée, 2015*, Rennes, France (2015).
- Llopis, O., Saleh, K., **Abdallah, Z.**, Auroux, V., Maxin, J., Fernandez, A., Chembo, Y., Cibiel, G., Pillet, G., Morvan, L. Oscillateurs optoélectroniques : topologies, performances et perspectives. *Horizons de l'optique, 2015*, Rennes, France (2015).
- **Abdallah, Z.**, Fernandez, A., Llopis, O. Oscillateur optoélectronique : modélisation et amélioration des performances. *19ème Journées Nationales Microondes, 2015*, Bordeaux, France (2015).

- Llopis, O., **Abdallah, Z.**, Auroux, V., Ali Slimane, A., Fernandez, A., Maxin, J., Pillet, G., Morvan, L. Oscillateurs micro-ondes à résonateurs optiques : topologies, performances en bruit et perspectives. *Journée du Club Optique Micro-onde, 2014*, Lannion, France (2014).
- **Abdallah, Z.**, Rumeau, A., Fernandez, A., Llopis, O. Modélisation non-Linéaire de photodiodes hyperfréquences. *Journées Nationales du Réseau Doctoral en Micro-Nanoélectronique, 2014*, Lille, France (2014).
- **Abdallah, Z.**, Ali Slimane, A., Auroux, V., Lafleur, G., Fernandez, A., Calvez, S., Lozes, F., Llopis, O. Fibered and integrated approaches for ultra-high Q optical resonators and comb generation; application to microwave and millimeter wave sources. *Workshop Optical Frequency Combs : from sources to applications, 2014*, Toulouse, France (2014).

Résumé

Titre : Sources micro-ondes à base de résonateurs optiques à très fort facteur de qualité; modélisation, stabilisation et métrologie.

Auteur : Zeina ABDALLAH

Directeurs de thèse : Olivier LLOPIS / Arnaud FERNANDEZ

Mots clés : Optique-Hyperfréquence, Résonateurs optiques, Sources micro-ondes, Bruit de phase, Modélisation.

La technologie photonique-RF offre une alternative intéressante à l'approche purement électronique dans différents systèmes micro-ondes pour des applications militaires, spatiales et civiles. Un composant original, l'oscillateur optoélectronique (OEO), permet la génération de signaux RF stables et à haute pureté spectrale. Il est basé sur une liaison photonique micro-onde utilisée comme boucle de rétroaction et comportant soit une fibre longue, soit un résonateur à fort coefficient de qualité. Différentes études ont été menées au cours de cette thèse afin d'optimiser et d'améliorer la performance en termes de stabilité et de bruit de phase pour le cas de l'OEO à résonateur.

La caractérisation fine et la modélisation des résonateurs est une première étape de la conception globale du système. La métrologie du résonateur optique est réalisée par une technique originale, dite de spectroscopie RF. Les résultats expérimentaux ont révélé que cette technique permet d'une part d'identifier le régime de couplage du résonateur et d'autre part de déterminer avec une grande précision tous les paramètres d'un dispositif résonant, comme les facteurs de qualité interne et externe ou les facteurs de couplage.

Une deuxième étude a été orientée vers l'implémentation d'un modèle non-linéaire fiable du dispositif. Dans un tel modèle, la photodiode rapide nécessitait une description plus précise, dans le but de contrôler la conversion du bruit d'amplitude optique en bruit de phase de l'OEO. Un nouveau modèle non-linéaire d'une photodiode hyperfréquence a été développé sous un logiciel commercial: Agilent ADS. Ce nouveau modèle rend effectivement compte de cette conversion de bruit. Une puissance optique optimale à l'entrée de la photodiode a été déterminée, pour laquelle la contribution de RIN du laser au bruit de phase RF pourrait être négligeable.

La performance de l'OEO est affectée par diverses perturbations entrainant un décalage en fréquence entre la fréquence du laser et la fréquence de résonance du résonateur. Il est donc important d'utiliser un système de stabilisation pour contrôler cette différence de fréquence. Des séries d'expériences et de tests ont été menées pour étudier la possibilité, d'une part, de remplacer l'électronique commerciale utilisée auparavant pour le système de verrouillage en fréquence (boucle de Pound-Drever-Hall) par une électronique faible bruit et, d'autre part, d'utiliser un laser à semi-conducteur. Un bilan de ces approches est présenté.

Abstract

Title: Microwave sources based on high quality factor optical resonators; Modeling, optimization and metrology

Author: Zeina ABDALLAH

Supervisors: Olivier LLOPIS / Arnaud FERNANDEZ

Keywords: RF-photonics, Optical resonator, Microwave sources, Phase noise, Modeling.

RF photonics technology offers an attractive alternative to classical electronic approaches in several microwave systems for military, space and civil applications. One specific original architecture dubbed as optoelectronic oscillator (OEO) allows the generation of spectrally pure microwave reference frequencies, when the microwave photonic link is used as a feedback loop. Various studies have been conducted during this thesis on the OEO, especially the one that is based on fiber ring resonators, in order to optimize and improve its phase noise performance and its long-term stability.

Precise characterization and modeling of the optical resonator are the first step towards overall system design. The resonator metrology is performed using an original approach, known as RF spectral characterization. The experimental results have demonstrated that this technique is helpful for the identification of the resonator's coupling regime and the accurate determination of the main resonator parameters such as the intrinsic and extrinsic quality factors or the coupling coefficients.

A second study was directed toward implementing a reliable nonlinear model of the system. In such a model, the fast photodiode require an accurate description, in order to reduce the conversion of the optical amplitude noise into RF noise. A new nonlinear equivalent circuit model of a fast photodiode has been implemented in a microwave circuit simulator: Agilent ADS. This new model is able to describe the conversion of the laser relative intensity noise (RIN) into microwave phase noise at the photodiode output. An optimal optical power at the photodiode's input has been identified, at which the contribution of the laser RIN in RF phase noise is negligible.

When it comes to practical applications, the desired performance of an OEO is threatened by various disturbances that may result in a frequency shift of both the laser frequency and the transmission peak of the resonator, which causes a malfunction of the OEO. Therefore it is desirable to use a stabilization system to control the difference between the laser frequency and the resonator frequency. A series of tests and experiments have been carried out to investigate the possibility, on one hand, to replace the commercial servo controller that was used up until now in the Pound-Drever-Hall loop, with a low noise homemade one and, on the other hand, to use a semiconductor laser to reduce the system size. A detailed review of these approaches is presented.